

On the Role of Convection and Turbulence for Tropospheric Ozone and its Precursors

PROEFSCHRIFT

ter verkrijging van de graad van doctor aan de
Technische Universiteit Eindhoven, op gezag van de
Rector Magnificus, prof.dr. R.A. van Santen, voor een
commissie aangewezen door het College voor
Promoties in het openbaar te verdedigen
op woensdag 30 maart 2005 om 16.00 uur

door

Dirk Jan Leo Olivié

geboren te Sint-Niklaas, België

Dit proefschrift is goedgekeurd door de promotoren :

prof.dr. H.M. Kelder
en
prof.dr.ir. G.J.F. van Heijst

Copromotor :
dr. P.F.J. van Velthoven

Druk : Universiteitsdrukkerij Technische Universiteit Eindhoven

CIP-DATA LIBRARY TECHNISCHE UNIVERSITEIT EINDHOVEN

Olivié, Dirk Jan Leo

On the role of convection and turbulence for tropospheric ozone and its precursors /
door Dirk Jan Leo Olivié. – Eindhoven : Technische Universiteit Eindhoven, 2005. –
Proefschrift.
ISBN 90-386-2161-2

NUR 932

Trefw. : atmosferische ozon / stikstofoxiden / atmosferische chemie / convectie /
turbulentie en diffusie / bliksem
Subject headings : atmospheric ozone / nitrogen oxides / atmospheric chemistry /
convection / turbulence and diffusion / lightning

Contents

| | |
|---|-----------|
| Samenvatting | v |
| 1 Introduction | 1 |
| 1.1 Role of ozone and nitrogen oxides in the troposphere | 1 |
| 1.2 Importance of nitrogen oxides distribution for ozone production | 3 |
| 1.3 Role of transport | 4 |
| 1.4 Global atmospheric models | 6 |
| 1.5 Overview of the thesis | 7 |
| 2 Comparison between archived and off-line diagnosed convective mass fluxes in the chemistry transport model TM3 | 9 |
| 2.1 Introduction | 10 |
| 2.2 Convection and the TM3 model | 11 |
| 2.2.1 The TM3 model | 11 |
| 2.2.2 Convection parameterisation | 12 |
| 2.2.3 222-Radon emission and decay in TM3 | 13 |
| 2.2.4 Chemistry in TM3 | 14 |
| 2.3 Experimental set-up | 15 |
| 2.4 Comparison of convective mass fluxes | 15 |
| 2.5 Effect on 222-Radon, nitrogen oxides and ozone | 18 |
| 2.5.1 Effect on 222-Radon | 18 |
| 2.5.2 Effect on the distribution of nitrogen oxides | 22 |
| 2.5.3 Effect on the distribution of ozone | 24 |
| 2.6 Conclusions and discussion | 25 |
| 3 Evaluation of archived and off-line diagnosed vertical diffusion coefficients from ERA-40 with 222-Radon simulations | 29 |
| 3.1 Introduction | 30 |
| 3.2 Methods | 32 |
| 3.2.1 The TM3 model | 32 |
| 3.2.2 Vertical diffusion data | 33 |
| 3.2.3 222-Radon emission and decay | 36 |
| 3.2.4 Observations | 37 |
| 3.2.5 Experimental set-up | 38 |
| 3.3 Results | 39 |

| | | |
|----------|--|------------|
| 3.3.1 | Comparison of the diffusion coefficients | 39 |
| 3.3.2 | Evaluation of the model simulated atmospheric boundary layer height | 41 |
| 3.3.3 | Comparison with 222-Radon observations in Freiburg and Schauins- land | 44 |
| 3.3.4 | Comparison with 222-Radon observations in Cincinnati and So- corro | 52 |
| 3.3.5 | Global 222-Radon distribution | 54 |
| 3.4 | Conclusions | 57 |
| 4 | Parameterisation of the production of NO_x by lightning for global chemistry transport models | 61 |
| 4.1 | Introduction | 61 |
| 4.2 | Methods | 63 |
| 4.2.1 | The TM4 model | 63 |
| 4.2.2 | Convection | 64 |
| 4.2.3 | LNO _x distribution | 65 |
| 4.2.4 | Observations | 67 |
| 4.2.5 | Experimental set-up | 68 |
| 4.3 | Results | 69 |
| 4.3.1 | Horizontal and seasonal variation | 69 |
| 4.3.2 | Vertical distribution | 71 |
| 4.4 | Comparison of the model results with observations | 75 |
| 4.4.1 | LINOX flights of July 23rd and 24th 1996 | 76 |
| 4.4.2 | EULINOX flight of July 1st 1998 | 76 |
| 4.4.3 | EULINOX flight of July 3rd 1998 | 77 |
| 4.4.4 | Overview of all flights | 78 |
| 4.5 | Conclusions and discussion | 81 |
| 5 | Conclusions and outlook | 83 |
| 5.1 | Introduction | 83 |
| 5.2 | Summary and conclusions | 83 |
| 5.3 | Outlook | 85 |
| 5.3.1 | Radiative forcing | 86 |
| 5.3.2 | Convection | 86 |
| 5.3.3 | Atmospheric boundary layer turbulence | 86 |
| 5.3.4 | Lightning parameterisation | 87 |
| 5.3.5 | Effect of climate change on convection and lightning | 88 |
| | Bibliography | 89 |
| | Dankwoord | 99 |
| | Curriculum vitae | 101 |

Samenvatting

Dit proefschrift gaat over onderzoek naar de beschrijving van turbulentie, convectie en stikstofoxidenproductie door bliksem in het chemie-transportmodel TM. Deze processen zijn van groot belang voor de verdeling van sporengassen en aërosolen in de troposfeer, en worden in mondiale atmosfermodellen beschreven door parametrisaties. We hebben onderzocht hoe gevoelig de resultaten van simulaties met het TM-model zijn voor de keuze van de parametrisatie door het effect van verschillende parametrisaties op de concentratie van een aantal sporengassen te bestuderen. Verder hebben we de sporengasconcentraties uit modelsimulaties vergeleken met waargenomen concentraties.

Motivatie

Ozon (O_3) in de troposfeer¹ is een broeikasgas. Dit betekent dat hogere ozonconcentraties in de troposfeer leiden tot hogere temperaturen aan het aardoppervlak. De intensiteit van dit broeikas effect is sterk afhankelijk van de totale hoeveelheid ozon en zijn verticale verdeling. Het sterkste opwarmend effect wordt verkregen door ozon in de buurt van de tropopauze. Naast het feit dat ozon een broeikasgas is, leiden te hoge concentraties ozon dichtbij het aardoppervlak ook tot negatieve effecten op de gezondheid van flora, fauna en mens. Aan de andere kant absorbeert ozon in de stratosfeer (waar de ozonlaag zich bevindt) schadelijke ultraviolette zonnestraling en is het zo onmisbaar voor het leven op Aarde.

Omwille van de rol van ozon in de troposfeer, is het interessant de hoeveelheid en verticale verdeling van ozon te kennen alsmede de eventuele invloed van de mens daarop. De ozonverdeling in de troposfeer wordt bepaald door verschillende processen. Enerzijds wordt ozon vanuit de stratosfeer, waar de ozonconcentratie hoog is, naar de troposfeer getransporteerd op gematigde en hogere breedtes. In de troposfeer kan ozon vervolgens worden verwijderd door droge depositie of door chemische reacties in aanwezigheid van waterdamp (H_2O) en ultraviolet zonlicht. Anderzijds wordt de concentratie van ozon ook beïnvloed door in situ productie van ozon in de troposfeer. Deze vorming van ozon wordt sterk bepaald door de aanwezigheid van stikstofmonoxide (NO) en stikstofdioxide (NO_2), samen aangeduid als NO_x . In aanwezigheid van koolstofmonoxide (CO), methaan (CH_4) of vluchtige organische koolwaterstoffen

¹De troposfeer is het onderste deel van de aardse atmosfeer. Het strekt zich uit van het aardoppervlak tot ongeveer 8 tot 16 km hoog. In de troposfeer neemt de temperatuur af naarmate men hoger komt : aan de top van de troposfeer, die de tropopauze wordt genoemd, heersen temperaturen tussen -50 en $-70^\circ C$. De troposfeer bevat ongeveer 80% van de totale massa van de atmosfeer.

en in aanwezigheid van voldoende zonlicht, kunnen reacties gekatalyseerd door NO_x immers leiden tot ozonvorming. De efficiëntie van deze reacties is hoger bij een lage NO_x -concentratie : dezelfde hoeveelheid NO_x diffuus verspreid leidt tot meer ozonproductie dan lokaal hoge concentraties. Er zijn verschillende bronnen van NO_x in de troposfeer. Een klein deel is afkomstig uit de stratosfeer. NO_x wordt verder vooral gevormd bij verbranding van fossiele brandstoffen en biomassaverbranding. Tenslotte is naast de oxidatie van ammoniak (NH_3) ook bliksem een bron van NO_x : door de sterke opwarming in de buurt van bliksemflitsen wordt lokaal NO gevormd.

Het is interessant te weten hoe groot de bijdrage van de mens via de uitstoot van NO_x is tot de ozonvorming in de troposfeer. Daarvoor moeten niet alleen de grootte en verdeling van de menselijke bronnen bekend zijn, maar ook de natuurlijke bijdrage, het transport en de verspreiding. Hierbij is verticaal transport een belangrijk onderwerp van studie : het is enerzijds niet eenvoudig te beschrijven, en het heeft anderzijds grote invloed op de concentraties van sporengassen in de vrije troposfeer. De grote onzekerheid over de vorming van NO_x door bliksem bemoeilijkt ook een goede inschatting van de menselijke bijdrage.

Atmosfeermodellen

Mondiale numerieke weermodellen die gebruikt en ontwikkeld worden om het weer tot zowat 10 dagen vooruit te voorspellen, zijn erg afhankelijk van de nauwkeurigheid van de beschrijving van de begintoestand van de atmosfeer. Daarom is een belangrijk onderdeel van het maken van goede weersvoorspellingen een goede beschrijving van de momentane toestand van de atmosfeer. Daarvoor worden grondwaarnemingen, vliegtuig- en scheepswaarnemingen, ballonsonderingen en satellietwaarnemingen van allerlei meteorologische grootheden gebruikt (assimilatie). Bijgevolg is een bijproduct van deze weermodellen dat zij een heel goede momentane beschrijvingen van de mondiale toestand van de atmosfeer geven : temperatuur, druk, neerslag, horizontale en verticale luchtstromingen, vochtigheid, etc.

Sommige fysische processen in de atmosfeer gebeuren op schalen die veel kleiner zijn dan de kleinste schaal van numerieke modellen. Turbulente menging in de atmosferische grenslaag of verticaal convectief transport gebeurt bijvoorbeeld op schalen van enkele meters tot enkele tientallen kilometers. Het stromingspatroon dat hiermee gepaard gaat kan in mondiale modellen met roosterpunten op afstanden van 50 tot 200 km niet worden gerepresenteerd. Dit leidt er noodzakelijkerwijs toe dat turbulente menging en convectie geparametriseerd worden. Het gemiddeld effect van deze processen op langere tijdschaal (uur) en gemiddeld in de ruimte (1 tot 50 km) wordt beschreven. Turbulente diffusie wordt beschreven aan de hand van diffusiecoëfficiënten, convectie vaak door een pluimmodel. Bij deze parametrisaties tracht men het effect te beschrijven uitgaande van grootschalige meteorologische variabelen.

Elke 3 tot 6 uur worden de geassimileerde meteorologische velden van het numerieke weermodel gearchiveerd. Om de hoeveelheid gegevens te beperken, worden de variabelen die het kleinschalig verticaal transport beschrijven vaak niet gearchiveerd. Men gaat er dan van uit dat deze variabelen later met een voldoende nauwkeurigheid opnieuw gegenereerd worden indien de parametrisaties worden toegepast op de variabelen die wel gearchiveerd zijn. In dat geval spreekt men van 'off-line' parametrisaties.

Omdat de modellering van atmosferische processen in weermodellen steeds verbetert en de resolutie constant wordt verhoogt, is de beschrijving van de atmosfeer van de afgelopen jaren geen homogene dataset. Daarom heeft men het idee opgevat om met de hedendaagse modellen en resoluties gebruik makend van alle waarnemingen, nieuwe analyses te maken van de atmosfeer. Hierdoor ontstaan lange consistente tijdreeksen van de mondiale atmosfeer, die zeer geschikt kunnen zijn voor de studie van de samenstelling van de atmosfeer. Bij het Europees Centrum voor Weersvoorspelling op de Middellange Termijn (ECMWF) werd eerder het ERA-15 project succesvol afgerond. Hierbij werd een heranalyse van de periode 1979-1993 gemaakt. Later volgde het ERA-40 project waarbij de periode 1957-2002 opnieuw werd geanalyseerd. In de ERA-40 dataset werd ook de beschrijving van de turbulentie en convectie bijgehouden.

TM-model

Om de samenstelling van de atmosfeer en de interactie tussen de verschillende processen die daarbij een rol spelen te bestuderen, kan gebruik worden gemaakt van mondiale chemie-transportmodellen. Deze modellen gebruiken meteorologische informatie van andere modellen (bijvoorbeeld de ERA-15 of ERA-40 dataset) om de meteorologische toestand van de atmosfeer te beschrijven (temperatuur, neerslagintensiteit, wind, wolken, etc.). De circulatie bepaalt dan het transport van sporengassen en aërosolen, de vochtigheid, temperatuur, wolken en straling beschrijven de omstandigheden waaronder chemische en fysische omzettingen kunnen plaatsvinden. Deze modellen lijden echter onder de onnauwkeurige beschrijving van sommige processen en onder het feit dat de resolutie van het model niet te hoog mag zijn om de rekentijden voldoende laag te houden.

In deze studie is gebruik gemaakt van het TM-model. Dit mondiaal chemie-transportmodel wordt intensief gebruikt in verschillende versies : 3, 4 of 5. TM3 en TM4 verschillen hoofdzakelijk in de horizontale resolutie. Zo wordt TM3 gebruikt op $10^\circ \times 7.5^\circ$, $5^\circ \times 4.5^\circ$ en $2.5^\circ \times 2.5^\circ$, terwijl TM4 een resolutie van $6^\circ \times 4^\circ$ of $3^\circ \times 2^\circ$ gebruikt. Ook verschillen ze in de voorgeschreven emissie van sporengassen en in het gegevensformaat waarin de meteorologische gegevens worden opgeslagen. TM5 gebruikt dezelfde resolutie als TM4 maar is bovendien in staat lokaal de resolutie te verhogen tot $1^\circ \times 1^\circ$. Het TM-model wordt zowel gebruikt voor de studie van de troposfeer als van de stratosfeer.

In deze studie hebben we gebruik gemaakt van de troposferische versie van TM3 en TM4. Daarin wordt de evolutie van 38 sporengassen gemodelleerd waarbij 110 gasfasereacties en 24 fotolysereacties worden beschreven. In dit model wordt de atmosfeer beschreven tot een hoogte van ongeveer 10 hPa, waarbij een 19- en een 31-laags versie van het model zijn gebruikt.

Om de kwaliteit van transport en fysische verwijderingsprocessen in chemie-transportmodellen te onderzoeken, wordt vaak gebruik gemaakt van sporengassen die weliswaar onbelangrijk zijn voor het klimaat of de luchtkwaliteit, maar wel interessante aspecten van atmosferisch transport kunnen blootleggen. Voorbeelden daarvan zijn zwavelhexafluoride (SF_6), radon (^{222}Rn) en lood (^{210}Pb). In dit onderzoek is ^{222}Rn uitgebreid gebruikt. Het heeft een halfwaardetijd van 3.825 dagen en komt vrij uit de bodem. Daarom is het bruikbaar om boven de oceaan te bepalen welke lucht

vrij kort geleden nog in aanraking geweest is met het continent, of om boven land hoger in de atmosfeer aan te geven welke lucht recent van het oppervlak omhoog is gebracht.

Convectie

In hoofdstuk 2 hebben we de invloed van convectie op de sporengassen ^{222}Rn , NO_x en O_3 bestudeerd. Door opwarming van het aardoppervlak door instraling van de zon of door een warme oceaan onder koudere lucht, worden de onderste luchtlagen sterk opgewarmd en kan deze lucht de neiging krijgen te stijgen. Wanneer deze lucht veel vocht bevat kan er bij deze stijging condensatie optreden. Hierdoor komt extra warmte vrij en kan de opwaarts bewegende lucht nog verder stijgen. Zo kan door convectie lucht in korte tijd van dicht bij het aardoppervlak tot hoog in de troposfeer worden gebracht. Afhankelijk van de intensiteit, kan convectie gepaard gaan met de vorming van wolken, neerslag en bliksem. Convectie draagt op die manier bij aan een snelle menging van de troposfeer. Het kan sporengassen die dichtbij het aardoppervlak worden geproduceerd in korte tijd naar grote hoogte transporteren, waar sterkere winden heersen en het kouder is. Daardoor zullen bepaalde sporengassen langer leven en over grote afstanden worden getransporteerd.

We hebben het verschil onderzocht tussen het gebruik van gearcheerde en off-line berekende convectieve data. Om het effect hiervan op sporengassen te bestuderen, hebben we eerst gekeken naar de verdeling van ^{222}Rn , dat, zoals eerder vermeld, alleen aan het aardoppervlak boven de continenten vrijkomt. We hebben simulaties gedaan van de periode november 1990 tot december 1996 met het TM3-model. Door de hogere gearcheerde convectie wordt vooral in de tropen meer ^{222}Rn naar de bovenste troposfeer gebracht, waarna dit zich ook verspreidt naar hogere breedtegraden. De NO_x - en ozonconcentraties blijken erg gevoelig voor de beschrijving van de convectie. Rond de tropopauze worden voor NO_x verschillen van 20 tot 50% gevonden in de zonaal gemiddelde concentratie. Voor O_3 blijkt het hogere transport tot lagere concentraties te leiden boven in de troposfeer, en tot hogere concentraties in de vrije troposfeer.

Om deze twee verschillende datasets te vergelijken hebben we de ^{222}Rn concentraties vergeleken met waarnemingen door vliegtuigen gedurende meetcampagnes. Vergelijkingen met metingen van de TROPOZ-II-campagne, de NARE-campagne, en een campagne vanuit Moffet-Field in 1994, tonen aan dat de verschillen in de onderste 12 km van de atmosfeer niet erg groot zijn. De metingen gedurende de STEP-campagne tussen 13 en 18 km in de tropen geven aan dat de gearcheerde convectie de concentraties in de bovenste troposfeer in de tropen beter beschrijft.

Turbulentie

Door wrijving tussen bewegende lucht en het aardoppervlak of door opwarming van de onderste lagen van de atmosfeer door een aardoppervlak dat is opgewarmd door de instraling van de zon, kunnen kleinschalige bewegingen en wervels ontstaan in de onderste lagen van de atmosfeer. Het gebied waar deze wervels zich bevinden en meer in het algemeen het gebied van de atmosfeer dat rechtstreeks beïnvloed wordt door de aanwezigheid van het aardoppervlak, noemt men de atmosferische

grenslaag. Door de turbulente menging kunnen sporengassen en aërosolen die vaak aan het aardoppervlak worden uitgestoten, zich snel over de hoogte van de grenslaag verplaatsen. Onder bepaalde omstandigheden kan de aanwezigheid van het oppervlak de turbulentie ook onderdrukken. Wanneer het aardoppervlak op een heldere nacht bijvoorbeeld sterk afkoelt, zullen ook de onderste luchtlagen sterk afkoelen wat tot een stabiele gelaagdheid leidt.

Omdat deze turbulente bewegingen gebeuren op schalen die niet gemodelleerd kunnen worden, worden ze ook door parametrisaties beschreven die het effectief resultaat weergeven. Voor deze menging gebruikt men vaak K -diffusie modellen waarbij de verticale diffusiecoëfficiënt aangeeft hoe sterk de menging is.

In hoofdstuk 3 hebben we vier verschillende soorten diffusiecoëfficiënten met elkaar vergeleken : de 3- en 6-uurlijks gearchiveerde coëfficiënten uit de ERA-40 dataset, 3-uurlijkse off-line coëfficiënten volgens een parametrisatie die erg lijkt op de parametrisatie die gebruikt is tijdens het ERA-40 project, en 6-uurlijkse off-line coëfficiënten volgens een lokaal diffusieschema. De laatste twee worden standaard in het TM-model gebruikt. In het laatste locale diffusieschema wordt voor de berekening van de diffusiecoëfficiënt op een bepaalde plaats in de atmosfeer alleen gebruik gemaakt van de meteorologische toestand op die plaats. Bij de andere schema's wordt gebruik gemaakt van profielen van meteorologische informatie. De niet-lokale diffusieschema's berekenen ook de grenslaaghoogte.

We hebben ook een beperkte evaluatie van de grenslaaghoogte van het ECMWF-model (alleen de 6-uurlijkse) en van de 3-uurlijkse TM grenslaaghoogte uitgevoerd, door deze te vergelijken met waarnemingen van Cabauw en de FIFE site.

We hebben ons beperkt tot de bestudering van het effect van de verschillende diffusiecoëfficiënten op ^{222}Rn . Ook voor de validatie van grenslaagmenging is ^{222}Rn een interessant sporengas. Wanneer er weinig turbulente menging is, worden hoge concentraties aangetroffen dicht bij het aardoppervlak en sterk afnemende concentraties op grotere hoogte. Wanneer er wel sterke turbulente menging is, zal de ^{222}Rn concentratie aan het oppervlak niet erg hoog zijn en zal er slechts een zwakke verticale gradiënt zijn. We hebben modelsimulaties vergeleken met uurlijkse ^{222}Rn waarnemingen op twee plaatsen in Duitsland in 1993, met maandelijks gemiddelde dagelijkse cycli in Cincinnati en met maandelijks gemiddelde ochtendwaarden en namiddagwaarden in Socorro.

De vergelijking tussen de waargenomen en gesimuleerde grenslaaghoogte, zowel overdag als 's nachts, toont aan dat de TM en de ERA-40 grenslaaghoogte erg realistisch zijn. De gearchiveerde diffusiecoëfficiënten blijken meer menging te geven dan de off-line diffusiecoëfficiënten. Aan de andere kant blijkt de off-line parametrisatie erg goed de gearchiveerde data te kunnen simuleren. Daar de diffusiecoëfficiënten een heel sterke dagelijkse cyclus hebben, is een hoge tijdsresolutie noodzakelijk.

NO-productie door bliksem

Zoals eerder vermeld, is bliksem een belangrijke bron voor NO_x . Door zijn diffuus karakter (zowel horizontaal als verticaal) kan het grote invloed hebben op het ozonbudget in de troposfeer. De onzekerheid in de totale NO_x -productie is echter zeer groot : schattingen variëren tussen 2 en 20 Tg[N] per jaar. Bliksemflitsen zijn ontladingen die plaatsvinden tussen gebieden met tegengestelde elektrische ladingen.

Deze ladingen worden gevormd door de ladingsscheiding ten gevolge van snelle op- en neerwaartse bewegingen in onweerswolken. Door de energie die vrijkomt bij de ontlading, wordt lucht, die vooral bestaat uit zuurstof (O_2) en stikstof (N_2), in de omgeving van de flits opgewarmd, dissociëren de zuurstof- en stikstofmoleculen en wordt er NO gevormd.

Bliksem en de bijbehorende vorming van NO gebeurt op tijd en ruimtelijke schalen die vele malen kleiner zijn dan de resolutie van een mondiaal chemie-transportmodel. De productie van bliksem is daarom een proces dat ook geparametriseerd dient te worden. Daarbij probeert men het optreden van bliksem en de bijbehorende NO-productie te parametriseren als functie van andere grootschalige meteorologische grootheden zoals convectieve neerslag, intensiteit van de convectieve luchtstroom, hoeveelheid ijs, wolkentophoogte, of top van de opwaartse convectieve luchtstroom.

In het TM-model wordt standaard een parametrisatie gebruikt die het aantal bliksemflitsen laat afhangen van de intensiteit van de neerslag uit convectieve buien. Deze parametrisatie is gebaseerd op metingen gedurende de EULINOX meetcampagne in Europa. We hebben deze parametrisatie vergeleken met een parametrisatie die zich baseert op de hoogte van de opwaartse convectieve luchtstroom en de gemiddelde snelheid daarin. De laatste parametrisatie leidde bij de implementatie in het TM-model tot aanzienlijke problemen. Het model simuleerde lokaal heel intense NO-productie die onrealistisch was. We waren daardoor genoodzaakt tot het invoeren van een bovengrens aan de gesimuleerde bliksemfrequentie.

Naast de horizontale verdeling is ook de verticale verdeling van de NO-productie door bliksem in chemie-transportmodellen erg onzeker. De hoge lokale NO-concentraties in de wolken na ontlading worden door sterke opwaartse en neerwaartse convectieve bewegingen immers herverdeeld waarbij ook snelle chemische omzettingen een rol spelen. Dit maakt de beschrijving niet eenvoudig. In chemie-transportmodellen wordt de verticale verdeling vaak beschreven door een beperkt aantal vast voorgeschreven profielen, die gebaseerd zijn op numerieke simulaties met een hoge resolutie van een beperkt aantal onweersbuien. Om een realistischer beschrijving van de verticale verdeling in het model te realiseren hebben we geprobeerd om het transporteffect (de snelle herverdeling door opgaande en neergaande luchtstromen) van de bliksem-geproduceerde NO afzonderlijk te modelleren door gebruik te maken van de convectieve luchtstromen. Hierbij wordt verondersteld dat NO dichtbij de wolk wordt geproduceerd en daardoor erg beïnvloed wordt door de sterke op- en neergaande luchtstromingen. Deze methode lijkt veelbelovend. Zij blijkt in staat te zijn realistische profielen voor NO op te leveren en ze laat tegelijkertijd meer variatie toe in de verticale verdeling van NO. Een nadeel is dat het succes van deze methode erg samenhangt met de kwaliteit van de profielen van convectieve op- en neerwaartse luchtstromen. De eenvoudige beschrijving van de off-line convectie, en de zwakke neerwaartse luchtstromen in de gearchiveerde convectie bemoeilijken dit.

Om de invloed van de verschillende parametrisaties op de verdeling van NO_x te onderzoeken hebben we gebruik gemaakt van metingen van NO en NO_x door vliegtuigen gedurende vier verschillende meetcampagnes (LINOX, SONEX, PEM-TROPICS A, en EULINOX). De metingen zijn vooral verricht tussen 500 en 200 hPa.

Het werk in dit proefschrift heeft vooral duidelijk gemaakt hoe gevoelig modelresultaten van chemie-transportmodellen zijn voor de beschrijving van convectie, turbulentie en bliksem.

1

Introduction

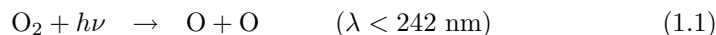
This thesis focuses on the turbulent and convective transport of nitrogen oxides in the troposphere. This chapter starts with explaining some aspects of the photochemical production of ozone in the troposphere, and the role of nitrogen oxides therein. Then the influence of turbulent transport and convection on trace gases is described. This is followed by a short discussion of the tools to model the global atmospheric composition. Finally, we formulate the motivations and scientific aims of this research.

1.1 Role of ozone and nitrogen oxides in the troposphere

Apart from the effect of ozone (O_3) in the stratosphere where it absorbs solar ultraviolet radiation in the range of 240 to 320 nm and protects the Earth's surface from this potentially harmful radiation, ozone also plays an important role in the troposphere. The troposphere is the lowest part of the atmosphere, which extends from the surface up to around 8 km at the poles, and up to around 16 km at the equator. First, tropospheric ozone is the precursor of the hydroxyl radical (OH) and plays therefore a key role in maintaining the oxidizing and cleansing capacity of the troposphere. Many important trace gases are removed from the atmosphere by oxidation : greenhouse gases such as methane (CH_4), anthropogenic non-methane hydrocarbons (NMHCs), or toxic gases as carbon dioxide (CO). Second, high levels of ozone at the surface are a major pollutant because of their harmful effects on human health and plants. Finally, tropospheric ozone also plays an important role because it has a strong absorption band centred at $9.6 \mu m$ within the atmospheric window. This makes it an effective greenhouse gas, particularly in the upper troposphere where the temperature is low [Lacis *et al.*, 1990]. In the 8 to $12 \mu m$ region, called the atmospheric window, terrestrial radiation propagates to space because of the relatively weak absorption in this region of the spectrum. Any gas with strong absorption properties in this spectral region traps relatively efficiently terrestrial radiation. Due to the aforementioned aspects of ozone, one is interested in understanding the impact of anthropogenic activities on the tropospheric ozone distribution.

Ozone is supplied to the troposphere by transport from the stratosphere, and is also produced in the troposphere by cycling of NO_x ($NO_x = NO + NO_2 =$ active nitrogen). In the stratosphere ozone is formed by the photolysis of the oxygen molecule

(O₂) and subsequent combination [*Chapman*, 1930]

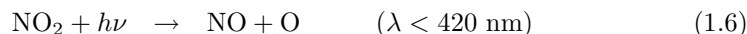


where M is some other molecule. Ozone is transported from the lower stratosphere into the upper troposphere through tropopause foldings and other processes at mid- and high latitudes.

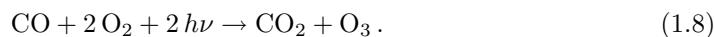
In the troposphere ozone can be formed as a result of chemical reactions involving nitric oxide (NO) and nitrogen dioxide (NO₂). Oxidation of methane (CH₄), non-methane hydrocarbons (NMHCs) and carbon dioxide (CO) in the presence of NO_x can lead to a significant amount of ozone production [*Fishman and Crutzen*, 1978]. Methane, the simplest hydrocarbon, has the highest atmospheric abundance, about 2 ppmv. Because of its long lifetime, methane is almost uniformly distributed throughout the troposphere. Also CO is globally distributed (60-70 ppbv in remote regions in the Southern Hemisphere, 120-180 ppbv in the Northern Hemisphere). NMHCs are more reactive and have lower emission rates making their atmospheric concentration much smaller (except at locations very close to emission sources).

The anthropogenic contribution to methane sources is more than twice the contribution of natural sources. NMHCs are released into the atmosphere from a wide range of anthropogenic and natural sources. Although anthropogenic emissions dominate in urban and industrial areas, natural emissions account for over 75% of the global source. CO is mainly produced by the oxidation of hydrocarbons and by incomplete combustion associated with biomass burning and fossil fuel burning. About 50-60% of the CO emissions results from human activities.

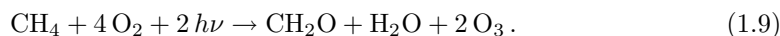
The photochemical formation of O₃ in the presence of NO_x, CH₄, CO and NMHCs is the result of a chain of reactions. As an example the reaction scheme for CO is shown :



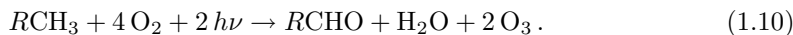
Overall the net effect of these reactions is



In the above reaction chain, CO is consumed, while NO_x works as a catalyst (no net production or destruction of NO_x). The overall result of the cycle involving methane is

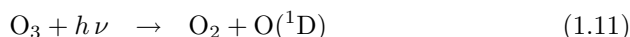


The overall result of the cycle involving NMHCs can be expressed in a similar way. If NMHCs are abbreviated to $R\text{CH}_3$ and carbonyl products are denoted $R\text{CHO}$ where R denotes an organic fragment, then the generalized cycle is

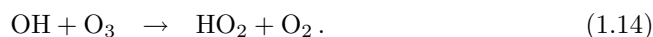
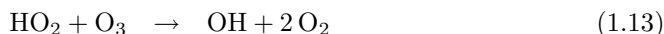


The species NMHCs, CH₄, CO and NO_x are referred to as ozone precursors. In the urban atmosphere, where the emission of NMHCs can be large, the photochemical production of O₃ is dominated by the oxidation of NMHCs. In the free troposphere or remote oceanic boundary layer where the NMHC concentrations are relatively small, the ozone production is dominated by the oxidation of CO and CH₄.

Loss of O₃ from the troposphere takes place by photolysis to O(¹D) followed by the reaction of O(¹D) with H₂O :



Ozone is also consumed by reactions with HO₂ and OH in remote regions of the troposphere :



Additional loss of O₃ takes place by reaction with organic materials at the Earth's surface (dry deposition).

1.2 Importance of nitrogen oxides distribution for ozone production

The catalytic efficiency of NO_x for the production of O₃ is highly non-linear : for each NO_x molecule emitted into the atmosphere, more ozone molecules are produced at low NO_x mixing ratio than at high NO_x mixing ratio [Liu *et al.*, 1987; Lin *et al.*, 1988]. In the limiting case of low NO_x concentrations, the ozone production varies linearly with the NO_x concentration but is independent of hydrocarbons. This is called the NO_x-limited regime. In the other limiting case where NO_x concentrations are high, the ozone production increases linearly with the hydrocarbon concentrations but varies inversely with NO_x concentrations. This is called the hydrocarbon-limited regime. All this implies that for the same emission of NO_x, a spatially diluted source will lead to a significantly greater ozone production rate than a concentrated source. Another implication of this non-linear effect is that the ozone production tends to be increased by transport processes because transport is almost always dispersive and thus dilutes the NO_x mixing ratio.

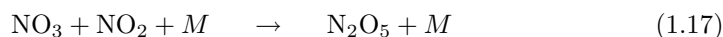
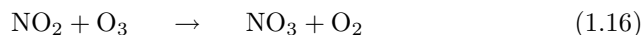
Studies have revealed that the budget of tropospheric ozone is controlled by its production in the free troposphere. Because the free troposphere contains the majority of the tropospheric ozone, the budget and distribution of free tropospheric NO_x is essential. Since NO_x is the rate-limiting precursor of ozone everywhere except in the urban atmosphere, any uncertainty in the budget and distribution of NO_x impacts significantly on that of ozone. The critical question is the identification and quantification of sources of free tropospheric NO_x. The main sources of NO_x in the troposphere are fossil fuel combustion, biomass burning, soil emissions, lightning, NH₃ oxidation, aircraft emissions, and transport from the stratosphere. Human activity is clearly a major source of NO_x in the troposphere, but quantifying the global extent

of human influence on NO_x concentrations is difficult. The uncertainty in the natural source of NO_x production, particularly in the upper troposphere, is a problem for assessing the exact impact of NO_x emissions from anthropogenic activities.

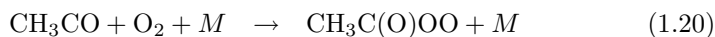
The main sink for NO_x is the conversion to HNO_3 and peroxyacetylenitrate (PAN = $\text{CH}_3\text{C}(\text{O})\text{OONO}_2$). These reservoir species, being longer lived than NO_x , are subject to large-scale redistribution through transport processes. The principal sink of NO_x is oxidation to HNO_3 . The conversion to HNO_3 during daytime is



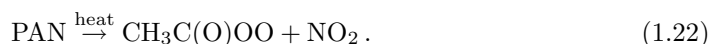
and during night



In the troposphere HNO_3 is scavenged by precipitation due to its high solubility in water, and HNO_3 is therefore an effective sink for NO_x . Apart from its conversion to HNO_3 , NO_x can also be transformed into PAN :



The formation of PAN is generally less important as a sink for NO_x than the formation of HNO_3 . However, in contrast to HNO_3 , PAN is hardly soluble in water and is thus not removed by wet deposition. In the middle and upper troposphere, PAN can be transported over long distances and decomposed to release NO_x far from its source. Its principal loss is by thermal decomposition, regenerating NO_x



In this way it is an efficient mechanism for long-range transport of anthropogenic NO_x to the global troposphere. Although PAN is only one of many organic nitrates produced during oxidation of hydrocarbons in the presence of NO_x , it is by far the most important as a NO_x reservoir.

1.3 Role of transport

Many different scales of motions exist in the atmosphere. The transport in the atmosphere is usually represented by large-scale advective motions (displacements of air masses in the horizontal direction) and by small-scale processes. These small-scale processes include vertical motions produced by thermal instability (often associated with the presence of cloud systems) and mixing associated with turbulence. These motions can have strong implications on the composition of the atmosphere, e.g. : stronger winds at higher altitudes can transport pollution over large distances to remote regions [Kritz *et al.*, 1990]; fast vertical transport can bring surface air to high

altitudes where much colder temperatures prevail which impacts on the chemical lifetime of some trace gases.

Regarding the atmospheric motions, the surface of the Earth is important due to its frictional drag on the atmosphere, and because it is a source or sink of water vapour and heat. The heating of the land surface and the frictional drag excite almost always turbulent motion (eddies), which leads to the formation of an atmospheric boundary layer (ABL) through the depth of the atmosphere most directly influenced by the Earth's surface. Air within the ABL is characterized by horizontal winds that are weak on average but have a high degree of turbulence. The depth of the ABL is related to the atmospheric structure and the surface fluxes of water and heat. For typical conditions the depth of the ABL can range from a few hundred meters to 1 or 2 km and varies strongly with the time of day.

Most pollutants are emitted in the ABL, and therefore the ABL often has relatively high levels of short-lived pollutants. Turbulent mixing by eddies in the ABL is very efficient in transferring chemical constituents away from the surface many orders of magnitude faster than could be done by molecular processes. The result is a rather rapid homogenisation of constituents within the ABL. Above the top of the ABL, vertical mixing is usually significantly smaller than within the ABL as the turbulent eddies are suppressed by the stability of the atmosphere. This slows the transport of chemical species from the boundary layer into the free troposphere above. The rapid mixing time within the ABL, coupled with the slow exchange time between the boundary layer and the free atmosphere, implies that chemical species emitted within the ABL are often trapped there for time periods much longer than the time scale associated with the vertical redistribution of the species within the ABL.

Convection is a class of relatively small-scale, thermally direct circulations that result from the action of gravity upon an unstable vertical distribution of air. Heating at the Earth's surface can lead to convection, in which air from the ABL moves vertically (updrafts) into the free troposphere. The heat released by the condensation of water vapour in rising air parcels, is the main driving force for convective motion. Convection can occur on spatial scales of a few square kilometres to scales of thousands of square kilometres and can extend from the Earth's surface to the tropopause. Associated with convection also downdrafts occur, as large downward buoyancy forces are created by the evaporative cooling of rain as it falls through the atmosphere. Although these localized intense downward motion can occur, a large part of the downward movement occurs much more slowly and over wider horizontal areas (subsidence) than the upward convective motion.

Convective clouds have a large potential for redistributing mass in the troposphere and for transporting trace constituents from the ABL to the overlying atmosphere. An individual convective cloud can move air from the surface to the upper troposphere in a matter of minutes to hours, which can lead to the intermittent presence of short-lived, surface-produced chemical species in the upper troposphere [Ridley *et al.*, 2004]. This provides a mechanism whereby species with sources at the Earth's surface and rather short chemical lifetimes (too short to reach the tropopause diffusively) can interact chemically at the tropopause level.

In addition to the transport effect of convection, it also contributes in other ways to the observed composition of the atmosphere. First, convective precipitation is a very efficient mechanism for removing soluble trace gases from the atmosphere.

Also, the atmospheric chemical content can be changed due to aqueous phase and heterogeneous chemistry in the clouds associated with convection. Finally, the strong updrafts associated with charge separation inside a cloud can lead to lightning. Due to the intense heating by lightning flashes, locally NO is formed [Goldenbaum and Dickerson, 1993].

1.4 Global atmospheric models

To understand and accurately describe the state and evolution of the atmospheric composition, all relevant processes should be described in one numerical model. Chemistry Transport Models (CTMs) model the emissions, chemical and physical transformations, and different transport processes, and simulate thus the spatial distribution and temporal evolution of chemical compounds in the atmosphere. These models are also helpful for the interpretation of field measurements and for testing the sensitivity of calculated quantities to physical or chemical processes.

Very often, CTMs are run 'off-line'. In this case, the dynamical and meteorological variables (wind speed, humidity, temperature, ...) needed to drive the atmospheric transport of trace gases and to describe the atmospheric conditions in which chemical transformations take place, are precalculated in a General Circulation Model (GCM) or in an assimilation model and stored periodically. Models can also be run 'on-line', where the CTM is integrated into a GCM, and both models are run simultaneously so that dynamics and chemistry can be fully coupled. In the troposphere, this type of coupling is weaker, and 'off-line' calculations are sufficient for most applications.

For this study, we made use of the 'off-line' global chemistry transport model TM. The model is adapted from the global tracer model TM2 [Heimann, 1995], and currently 3 different versions are being used (TM3/4/5). It calculates the horizontal and vertical transport, and chemical and physical evolutions based on 3- and 6-hourly meteorological fields of the European Centre for Medium-range Weather Forecasts model (<http://www.ecmwf.int>). The TM models have been applied in many different studies, with different resolutions.

Some atmospheric processes in GCMs or CTMs occur at a geometric scale smaller than the grid size of the model or at a temporal scale smaller than the time step of the model : this is the case for convection and turbulence. Therefore these processes have to be parameterised. It implies that not all the details of the physical processes are described, but only the effect on larger time and spatial scales. It also implies that one wants to describe this effect based on only large-scale variables. Several formulations with different levels of complexity have been used to account for sub grid ABL turbulence and convective transport in the free troposphere. For sub grid ABL turbulence, often first order diffusive models are used, while convection is often described with plume models. Boundary layer turbulence schemes and convective transport parameterisations are a major source of uncertainty in chemical transport models.

Often some fields needed for the CTM calculations are not archived [Rasch *et al.*, 1997]. These fields then have to be diagnosed 'off-line' based on meteorological fields that are archived. Often fields describing convection and turbulence are not archived.

The ECMWF reanalysis project ERA-40 used a variational data assimilation sys-

tem to make a new synthesis of the in situ and remotely sensed measurements made over the period since mid-1957 until 2002 [Simmons and Gibson, 2000]. ERA-40 produced analysed global meteorological fields with 6-hourly frequency throughout the 45-year period, supplemented by intermediate 3-hour forecasts. These fields have a high temporal and spatial resolution with grid spacing close to 125 km in the horizontal and with 60 levels in the vertical located between the surface and a height of about 65 km. What makes the ERA-40 extra valuable for CTM modelling, is that it is one of first long-range data sets containing fields describing convection and turbulent transport.

Because of a lack of knowledge of emissions and a coarse description of the chemical and physical processes in the atmosphere, discrepancies between observations and CTM model results are not always easily interpreted. Therefore, one often measures and models selected tracers that are not relevant for the atmospheric composition itself, but can help in understanding some aspects of the atmosphere. The radio nuclide ^{222}Rn is often used to study atmospheric transport of tracers [Jacob *et al.*, 1997]. ^{222}Rn is emitted from the soil on the continents with a reasonably well-known mean flux (this contrasts with other tracers where the uncertainty in their emissions is much larger). ^{222}Rn is removed from the atmosphere only through radioactive decay (with half-life of 3.825 days). Because it is not removed by precipitation or deposition, uncertainties on the description of such processes do not affect the modelled ^{222}Rn distributions. For example, ^{222}Rn is a useful tracer to assess the performance of models with regard to vertical turbulent mixing and convection [Jacob and Prather, 1990; Feichter and Crutzen, 1990].

1.5 Overview of the thesis

The aim of the work in this thesis is to investigate the convective and diffusive transport in the TM chemistry transport model, and to investigate some aspects of the consequences for NO_x . The large inaccuracy and uncertainty in the description of processes like convection and turbulent diffusion [Mahowald *et al.*, 1995], the strong dependence of the radiative forcing of ozone on its vertical distribution, and the strong dependence of the ozone production on the distribution of NO_x , are the main motivation.

The availability of the ERA-40 data, where convective data and vertical diffusion coefficients are archived, allows a study of the effect of different convective mass flux sets, and different vertical diffusion coefficients on the model-simulated distribution of tracers.

In this thesis the following questions are addressed :

1. How large is the sensitivity of the (model simulated) distribution of ozone and nitrogen oxides on (the) convection (parameterisation)?
2. What requirements should be fulfilled by diffusive transport parameterisations in order to simulate the diurnal cycle in trace gas concentrations?
3. How large are the differences in concentrations between simulations with archived and off-line diagnosed physical parameterisations?

4. How do the results of different parameterisations of nitrogen oxide production by lightning compare?
5. What is the effect of an explicit description of the effect of convective redistribution on the vertical distribution of lightning produced NO_x ?

In Chapter 2, the first question and part of the third question are addressed. Because convection can bring reactive trace gases to the upper troposphere where they can live longer, and possibly are transported to remote regions, it is important to well describe the convective transport. The archival of convective mass fluxes in the ERA-40 data set allows us to drive the convective transport in the TM model. We compare these archived fluxes with the standard off-line diagnosed fluxes used in the TM model. Because the distribution of ^{222}Rn is strongly influenced by convection, ^{222}Rn is a useful tracer to investigate the transport characteristics of CTMs. The model simulated distribution of ^{222}Rn is compared with observations from airborne field campaigns. We will also study the effect of these archived convective fluxes on the global distribution of NO_x and ozone.

In Chapter 3, question 2 and part of question 3 are addressed. The description of vertical diffusion in CTMs is still rather uncertain. Comparison with ground based observations of ^{222}Rn at four continental locations are used to compare the effect of archived and off-line diagnosed vertical diffusion coefficients on the distribution of trace gases in the TM model.

In Chapter 4, questions 4 and 5 are addressed. The parameterisation of NO_x produced by lightning in CTMs is still a subject of much ongoing research. In this chapter, different aspects of the parameterisations of the production of NO_x by lightning are investigated. We separately focus on the horizontal distribution of the lightning flashes, and on the vertical distribution of the produced NO_x . For the horizontal distribution, we compare the effect of the standard TM model parameterisation that uses the convective precipitation as a proxy for the lightning flash frequency [Meijer *et al.*, 2001], and a parameterisation that uses a combination of the updraft top and vertical velocity in the updraft as a proxy for the flash frequency. For the vertical distribution we compare how prescribed emission profiles [Pickering *et al.*, 1998; Zhang *et al.*, 2003] perform opposed to emission profiles that are generated by explicitly describing the transport in lightning clouds. We use these different simulations to perform model simulations in the TM model which are compared with airborne measurements of NO and NO_x .

Chapters 2 and 3 are reviewed papers. Chapter 2 has been published in *Journal of Geophysical Research*, Vol. 109, 2004, and Chapter 3 has been published in *Atmospheric Chemistry and Physics*, Vol. 4, 2004. Chapter 4 will be submitted soon. Chapter 5 presents the main conclusions of this thesis and an outlook to further research.

2

Comparison between archived and off-line diagnosed convective mass fluxes in the chemistry transport model TM3

Abstract

The 40-year reanalysis data set ERA-40 from the European Centre for Medium-range Weather Forecasts includes, unlike ERA-15, archived convective mass fluxes. These convective fluxes are useful for off-line chemistry transport modelling. The impact of using these archived convective mass fluxes (based on a convective parameterisation described in *Gregory et al.* [2000]) instead of off-line diagnosed mass fluxes (based on a convective parameterisation described in *Tiedtke* [1989]) was investigated with the chemistry transport model TM3. At first sight the two types of mass fluxes look similar. However some differences can be noted : the archived updrafts extend higher than the off-line diagnosed ones; they are also less intense below 500 hPa over sea. The archived downdrafts are much weaker than the off-line diagnosed downdrafts. With archived convective mass fluxes, we found slightly higher ^{222}Rn concentrations in the boundary layer, lower ^{222}Rn values in the free troposphere and significantly higher ^{222}Rn values in the upper troposphere and lower stratosphere. The effect on tropospheric chemistry of using archived mass fluxes instead of diagnosed ones is an increase of NO_x and O_3 in the free troposphere, but a decrease in the upper troposphere. The differences amount to up to 20% for O_3 in the zonal and seasonal mean. Our results thus underline the sensitivity of tropospheric ozone chemistry to the description of convective transport. Comparison with ^{222}Rn observations shows that the archived convective mass fluxes give better agreement in the tropical upper troposphere. More comparisons to free tropospheric observations of ^{222}Rn or another tracer of convective transport will be needed to unambiguously identify either of the convective data sets as optimal for use in chemistry transport models.

¹This chapter has been published as : D. J. L. Olivié, P. F. J. van Velthoven, A. C. M. Beljaars and H. M. Kelder, *J. Geophys. Res.*, Vol. 109, D11303, doi: 10.1029/2003JD004036, 2004, [*Olivié et al.*, 2004b]

2.1 Introduction

Convection plays an important role in the transport of trace gases in the troposphere. Within a short period of time, convection can bring boundary layer air with pollutants to the middle and upper troposphere, leading to considerable vertical mixing [Feichter and Crutzen, 1990]. The lifetime of reactive tracers in the boundary layer, can be significantly prolonged if they are transported to the middle and upper troposphere where wet scavenging and photochemical transformations of pollutants are slower. Convective transport is also important for long-range transport of air pollutants. After rapid vertical transport from the boundary layer to the upper troposphere, the strong zonal winds that prevail there, can efficiently transport pollution (and other tracers) from one continent to another and to remote marine locations [Allen *et al.*, 1996; Lin *et al.*, 1996; Zaucker *et al.*, 1996]. Therefore, for studies of the impact of anthropogenic emissions on the atmospheric composition and climate, convective transport is a key process.

In comparison to the synoptic scale processes in the atmosphere, the vertical mixing by convection takes place within small time and spatial scales that are not resolved in global atmospheric models. Three-dimensional General Circulation Models (GCMs) and Numerical Weather Prediction models (NWP) therefore contain parameterisations of convective transport that represent the collective effect of multiple small-scale isolated convective events. However, convection parameterisations are still evolving and still constitute an important source of errors in the results of NWP models and GCMs.

Chemical Transport Models (CTMs) are widely used for calculating the effect of anthropogenic emissions upon the global atmospheric composition. These models use archived data from a parent meteorological model as input to describe the atmospheric transport and atmospheric state. Rasch *et al.* [1997] mention some consequences of the use of meteorological data sets in CTMs. First, because the time interval at which archival takes place is often much larger than the time scale of many atmospheric processes, highly variable processes are averaged out, absent or exaggerated in the input data to CTMs. Secondly, some of the fields needed in a CTM are not available from archived data sets. For instance, these data sets often do not contain convective mass fluxes, three-dimensional precipitation formation rates, or diffusion coefficients. CTMs then usually try to reproduce this information from the archived data by implementing a parameterisation of the missing processes in the CTM, resulting in 'off-line diagnosed data'. It has also been suggested that CTM simulations using archived subgrid-scale parameters are more accurate than those diagnosing those parameters, and also that it is better to use time-averaged archived subgrid-scale parameters than instantaneous values [Rasch *et al.*, 1997]. Finally, these authors suggested that if subgrid-scale parameters are not available, they should be diagnosed internally in the CTM from instantaneous fields rather than from time-averaged fields.

In this paper, we investigate the effect of using archived convective mass fluxes instead of off-line diagnosed convective mass fluxes in the chemistry transport model TM3. The meteorological data set used is the ERA-40 data set from the European Centre for Medium-range Weather Forecasts (ECMWF) [Simmons and Gibson, 2000]. The ERA-40 data set is one of the first multi-decadal reanalyses which includes archival of convective mass fluxes. It also includes archival of three-dimensional pre-

precipitation formation rates and diffusion coefficients but these will not be dealt with here. The convective mass fluxes are stored as values time-averaged over 3 or 6 hours (both are available), while most other fields are stored every 6 hours as instantaneous values, including the fields used to drive the convection parameterisation embedded in TM3 (wind, temperature, evaporation and specific humidity). To generate the diagnosed mass fluxes from these instantaneous fields, a parameterisation is used that mimics to a large extent the convective algorithm used in the ECMWF model itself.

In Section 2.2, the TM3 model and the convective parameterisation are described. In Section 2.3, the experimental set-up is presented. In Section 2.4, the differences between the archived and off-line diagnosed convective mass fluxes are described. In Section 2.5, we describe the impact on the simulated distributions of ^{222}Rn , NO_x and O_3 . In that section we also compare the modelled ^{222}Rn concentration with available measurements. In Section 2.6, we present and discuss our conclusions.

2.2 Convection and the TM3 model

2.2.1 The TM3 model

The chemical tracer model TM3 is a global atmospheric model which is used to evaluate the atmospheric composition and changes herein caused by natural and anthropogenic changes [Dentener *et al.*, 2003b; Lelieveld and Dentener, 2000; Meijer *et al.*, 2000; Dentener *et al.*, 1999; Howeling *et al.*, 1998; van Velthoven and Kelder, 1996]. The TM3 model has a regular longitude-latitude grid and hybrid σ -pressure levels [Simmons and Burridge, 1981] up to 10 hPa. In this study the model is used both with a $7.5^\circ \times 10^\circ$ grid and 19 layers, and with a $2.5^\circ \times 2.5^\circ$ grid and 31 layers.

The meteorological input data from ERA-40 is available for 1957 to 2002. For dynamics calculations ERA-40 used a truncation of T159. The physical calculations were done on a reduced Gaussian grid of 160 nodes. In the vertical, 60 hybrid σ -pressure levels were used, reaching up to 0.1 hPa. To be used in the TM3 model, the meteorological data is interpolated or averaged to the desired TM3 grid cells [Bregman *et al.*, 2003].

TM3 describes the evolution of 38 chemical species, of which 23 are transported, including their emission, chemical formation and destruction, and physical removal. For advection of the tracers, the model uses the slopes scheme developed by Russell and Lerner [1981], which corresponds with the van Leer [1977] III scheme. To describe the effect of convective transport on the tracer concentration, we used either the archived convective mass fluxes from the ERA-40 data set that were kindly stored by ECMWF at our request, or off-line diagnosed convective mass fluxes calculated with a parameterisation that mimics the ECMWF scheme using archived wind speeds, pressures, temperatures, specific humidities and evaporation rates. This diagnosis of the convective mass fluxes is done on the original ERA-40 grid. The parameterisation for diagnosing convection in TM3 and the parameterisation of convection used in the ECMWF model are described in section 2.2.2.

Vertical diffusion, which is another important subgrid-scale process, is also off-line diagnosed using a parameterisation described in Louis [1979].

2.2.2 Convection parameterisation

The parameterisation that is used to calculate the convective mass fluxes off-line is described in *Tiedtke* [1989]. The parameterisation in the ECMWF model used for making the ERA-40 data set, is also based on *Tiedtke* [1989], but has since then evolved [*Gregory et al.*, 2000; *Nordeng*, 1994; *Tiedtke*, 1993].

In the parameterisation described in *Tiedtke* [1989], moist convection is represented by a bulk mass flux scheme. The scheme is based on the supply of moisture by large-scale convergence and boundary layer turbulence (closure). It assumes an entraining plume type cloud (updraft). Entrainment of mass into convective plumes is assumed to occur through turbulent exchange of mass through the cloud edges and through organized inflow. Detrainment is assumed to occur through turbulent exchange and through organized outflow near the cloud top.

This bulk model is applied separately for the various types of convection, i.e. deep penetrative convection, shallow convection and mid-level convection, by varying the entrainment and detrainment parameters. For deep convection and mid-level convection the closure assumption for determining the bulk cloud mass flux is that they are maintained by large-scale moisture convergence and evaporation; shallow convection is driven only by supply of moisture due to surface evaporation.

The scheme assumes downdrafts to occur with a mass flux proportional to the updraft mass fluxes. The downdrafts are associated with convective precipitation from the updrafts and originate from cloud air influenced by the injection of environmental air. As for the updraft, both turbulent and organized entrainment and detrainment are considered.

Large-scale subsidence is introduced to compensate for the imbalance in vertical mass flux between updrafts and downdrafts.

The main differences between the scheme as it is described in *Tiedtke* [1989] and the scheme as it used in the ECMWF model during the production of the ERA-40 data set [*Gregory et al.*, 2000], are twofold. First, the diagnosis of deep or shallow convection is based on different criterions. While in *Tiedtke* [1989] the criterion to distinguish between shallow and deep convection is based on the moisture convergence, it depends in *Gregory et al.* [2000] upon the depth of convection. If the cloud depth exceeds 200 hPa the convection is deemed to be deep. Secondly, in *Tiedtke* [1989] the convective mass flux at cloud base is estimated from the assumption that the integrated moisture (for deep convection) and moist static energy (for shallow convection) of the sub-cloud layer remains constant when convection is active. In *Gregory et al.* [2000] the estimation of cloud base mass flux for shallow convection is as in *Tiedtke* [1989], but the closure for deep convection is based upon the concept that convection acts to reduce convective available potential energy (CAPE) towards zero over a certain time-interval (in *Tiedtke* [1989] a quasi-steady state was assumed for the sub cloud layer moisture content). The impact of these differences has been assessed in several case studies using the ECMWF single-column model, and been shown to lead to improved results [*Gregory et al.*, 2000]. They show that the change in the switch between deep and shallow convection, can lead to the diagnosis of deep convection instead of shallow convection. This implies smaller entrainment rates and less dilution of a parcel during ascent, leading to a larger mass flux in the upper part of the cloud. They mention in addition that this leads to smaller mass fluxes at the

cloud base.

In addition to these two main differences, there is a difference in the description of the organized detrainment in the updrafts. In the ECMWF model, the organized detrainment in the upper part of the cloud is estimated from the variation of the updraft vertical velocity, which is calculated from a budget equation for the updraft kinetic energy. In *Tiedtke* [1989], the organized detrainment all takes place near the level of neutral buoyancy (cloud top).

Yet, another difference concerns the downdrafts. First, while in *Tiedtke* [1989] organized entrainment only happens at the starting layer of the downdraft, in the ECMWF model there might also be organized entrainment through the entire height of the downdraft : it is based on a formulation suggested by *Nordeng* [1994]. Second, organized detrainment can happen wherever the downdraft becomes positively buoyant. In *Tiedtke* [1989], the organized detrainment of the downdrafts is restricted to the region between the cloud base and the surface.

At each horizontal grid point, the updraft plume is described by the entrainment of air from each model layer into the updraft plume and by the detrainment of air from the updraft plume into each model layer. The knowledge of these entrainment and detrainment rates, uniquely determines the upward convective mass flux in the plume at all model levels. This is also true for the downdrafts.

2.2.3 ²²²Rn emission and decay in TM3

²²²Rn is an excellent tracer for evaluating transport parameterisations [*Dentener et al.*, 1999; *Allen et al.*, 1996; *Balkanski and Jacob*, 1990; *Feichter and Crutzen*, 1990; *Jacob and Prather*, 1990; *Kritz et al.*, 1990; *Brost and Chatfield*, 1989; *Polian et al.*, 1986].

²²²Rn is emitted at a relatively uniform rate from the soil on the continents. It is relatively insoluble in water, inert and not efficiently removed by rain. It has a mean lifetime of 5.5 days due to radioactive decay. It is generally accepted that the average flux from the soil lies somewhere between 0.8 and 1.3 atoms cm⁻² s⁻¹ [*Liu et al.*, 1984; *Turekian et al.*, 1977; *Wilkening and Clements*, 1975]. Oceans are also a source for ²²²Rn. However, the mean oceanic flux is estimated to be 100 times weaker than the continental source [*Lambert et al.*, 1982; *Broecker et al.*, 1967].

The fact that ²²²Rn has a lifetime and source characteristics that are similar to the lifetime and source characteristics of air pollutants such as NO, NO₂, propane, butane and other moderately reactive hydrocarbons, makes it even more interesting for evaluation of transport parameterisations.

In the TM3 model we adopted the emission scenario recommended by WCRP [*Jacob et al.*, 1997] : land emission between 60°S and 60°N is 1 atoms cm⁻² s⁻¹; land emission between 70°S and 60°S and between 60°N and 70°N is 0.005 atoms cm⁻² s⁻¹; oceanic emission between 70°S and 70°N is 0.005 atoms cm⁻² s⁻¹. This leads to a global ²²²Rn emission of 16 kg per year. We did not account for any regional or temporal variation in the emission rate.

Table 2.1: NO_x emissions used in the TM3 model.

| Source | (Tg[N] yr ⁻¹) |
|----------------------|---------------------------|
| Microbial production | 7.3 |
| Fossil fuel burning | 27.6 |
| Biomass burning | 5.5 |
| Lightning | 5 |
| Aircraft | 0.65 |

2.2.4 Chemistry in TM3

TM3 contains a tropospheric chemistry module that is a modified CBM-4 scheme [Houweling *et al.*, 1998]. It includes full HO_x-NO_x-SO_x-CO-CH₄-NMHC chemistry. In total 38 gaseous constituents are considered, of which 23 tracers are transported. 110 gas phase reactions and 24 photolysis reactions are taken into account. Dry deposition is accounted for by a resistance chain-based parameterisation [Ganzeveld *et al.*, 1998]. The dry deposition velocity is calculated from the aerodynamic resistance, the quasi-laminar boundary layer resistance, and the surface resistance. The wet deposition is based on a parameterisation of Junge and Gustafson [1957], and Langner and Rodhe [1991]. The heterogeneous removal of N₂O₅ on sulphate aerosols has been accounted for by using a parameterisation by Dentener and Crutzen [1993]. The annual totals and spatial distributions of the emissions of anthropogenic NMHC, anthropogenic CO, isoprene, soil and industrial NO_x are based on 1° × 1° GEIA and EDGAR-V2.0 emission inventories [Benkovitz *et al.*, 1996; Olivier, 1996; Guenther, 1995; Yienger and Levy, 1995].

The lightning parameterisation is based on an empirical linear relation between convective precipitation and lightning intensity [Meijer *et al.*, 2001]. A prescribed profile is used [Pickering *et al.*, 1998] to distribute lightning NO_x in the vertical. In the lightning parameterisation, the height of this profile is determined by the top of the convective updraft. To avoid differences in the vertical distribution of NO_x emissions by lightning between simulations using archived or off-line diagnosed mass fluxes due to differences in the top of the convective updrafts, we used in this study identical lightning NO_x emission scenarios based on the updraft top from the off-line diagnosed convective mass fluxes. The influence of this assumption will be discussed later. The lightning NO_x production is scaled to a global production of 5 Tg[N] per year. Table 2.1 gives an overview of the global NO_x emissions in TM3. Since the chemical scheme cannot adequately describe stratospheric chemistry, a zonally and monthly mean O₃ climatology [Fortuin and Kelder, 1998] scaled with TOMS total O₃ measurements is prescribed above 50 hPa. HNO₃ transport from the stratosphere into the upper level of the TM3 model is accounted for by fixing the O₃/HNO₃ ratio in the model top layer, based on UARS derived O₃/HNO₃ ratios at 10 hPa.

Table 2.2: Overview of the properties of the convective mass fluxes.

| | A-case | D-case |
|--------------------------------|--|--|
| origin | archived in ERA-40 | off-line diagnosed from wind, temperature, evaporation and humidity from ERA-40 |
| convection parameterisation | <i>Tiedtke</i> [1989, 1993], <i>Gregory et al.</i> [2000] | <i>Tiedtke</i> [1989] |
| time | 6-hourly averaged | instantaneous (every 6 hours) |

2.3 Experimental set-up

We have done two sets of simulations with the TM3 model to assess the influence of the type of convective mass flux data. In simulation A we used the archived convective mass fluxes. In simulation D we used the off-line diagnosed convective mass fluxes. We performed simulations for the years 1986 until 1987 and 1991 until 1996. An overview of the essential characteristics of the simulations is shown in Table 2.2.

For the CTM simulations, we ran the model on a $7.5^\circ \times 10^\circ$ grid with 19 layers, both with archived (A-case) and off-line diagnosed (D-case) convective fluxes. To compare with ^{222}Rn measurements, we ran the model on a $2.5^\circ \times 2.5^\circ$ grid with 31 layers.

In the following we will often show comparisons between results from both simulations. The relative difference of the positive quantity x (concentration or air mass flux) between the simulations will be defined as

$$\delta x = \frac{x_A - x_D}{\frac{1}{2}(x_A + x_D + \epsilon)}, \quad (2.1)$$

where x_A and x_D are the values of x in the simulations A and D respectively and ϵ is a small number introduced to avoid singularities. For ease of interpretation, all the differences are shown with the same convention : archived minus off-line diagnosed.

2.4 Comparison of convective mass fluxes

In order to interpret differences in CTM simulations with the different sets of convective mass fluxes we first describe the difference between the convective mass fluxes themselves. Figure 2.1 shows the mean updraft and downdraft profiles for the archived and off-line diagnosed convection over the 6 year long 1991-1996 period during December, January and February (DJF), for 3 latitudinal bands in the northern hemisphere,

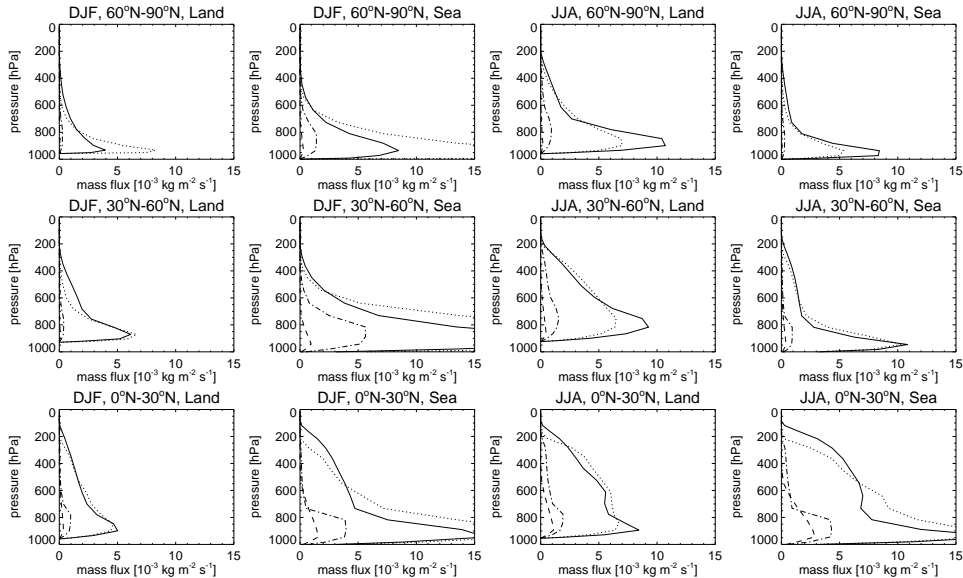


Figure 2.1: Mean convective mass fluxes for DJF (left) and JJA (right) 1991-1996 in the northern hemisphere. The archived updrafts (solid line), off-line diagnosed updrafts (dotted line), archived downdrafts (dashed line), and off-line diagnosed downdrafts (dot-dashed line) are shown. The mass fluxes are expressed in $10^{-3} \text{ kg m}^{-2} \text{ s}^{-1}$. The profiles are given for 3 latitudinal bands, and separately for land and sea.

and separately for land and sea. In spite of the differences in the computation of convective transport, the general characteristics and intensity of the updrafts look quite similar. We note first some of the similarities.

There is a pronounced maximum in the upward mass flux around 850 hPa. This maximum is stronger over sea than over land.

Above 700 hPa, most mass flux profiles decay fast and have a concave shape. However, in the tropics, the mass flux profiles also show strong mass fluxes above 700 hPa, and have a convex shape. This is due to the contribution from deep convection.

The downdrafts are much weaker than the updrafts.

Over sea convection is stronger than over land, except north of 30°N during June, July and August (JJA).

Apart from these similarities, there are also differences. Figure 2.2 shows the relative difference between the archived and off-line diagnosed convective mass fluxes in DJF. From this figure and from the profiles shown in Figure 2.1, the main differences between the archived and off-line diagnosed mass fluxes can be deduced.

The updrafts reach greater heights in the archived case, both over land and over sea. This shows up as stronger mass fluxes in the archived case in the tropics above 300 hPa over land and above 500 hPa over sea, and outside the tropics from 700-500 hPa. Quantitatively, the strongest effect is found in the tropics: the archived fluxes reach about 125 hPa, while the off-line diagnosed mass fluxes end around

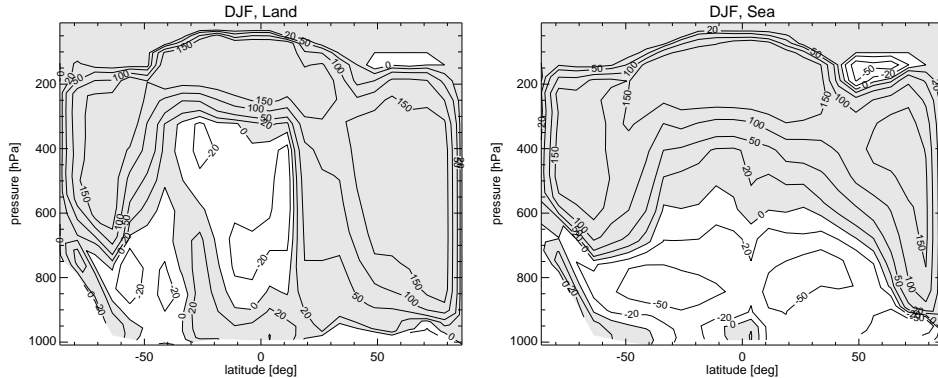


Figure 2.2: Zonal mean relative difference (%) between archived and off-line diagnosed convective upward mass fluxes for DJF 1991-1996, over land (left) and over sea (right). The relative difference is as defined in Equation 2.1.

200 hPa. It is also clearly visible over land in DJF between 30°N and 90°N where much stronger updrafts are found above 700 hPa. Stronger mass fluxes through a certain level of course imply more detrainment above that level.

Between 700 and 300 hPa, the gradient in the upward mass flux is often less steep in the archived case. This implies less detrainment in that region, which will strongly affect the tracer concentrations there.

Over sea, from the surface up to 600 hPa, the archived convection is less intense than the off-line diagnosed convection, except in JJA between 30°N and 90°N .

These differences might be partially attributed to differences in the parameterisation of the convective updrafts. The changes in the convection parameterisation (see Section 2.2.2) indeed lead to higher updrafts with smaller gradients.

Some other differences in the updrafts cannot be attributed directly to differences in the convective parameterisation. One sees that over land, there is in general stronger convection in the archived case between the surface and 800 hPa, except between 30°S and 60°S . This stronger convection even extends up to 500 hPa in DJF between 20°S and 30°S (South-Africa, southern South-America, Australia), and in JJA (not shown) between 20°N and 40°N (northern Africa more than the US).

One can also notice that over land, between 800 and 300 hPa in the tropics and subtropics, and between 800 and 500 hPa in the northern hemisphere at mid-latitudes in JJA (not shown), convection is less intense in case A than in case D. This difference is quite strong in DJF around 400 hPa between 20°S and 30°S and around 500 hPa at 10°N , and in JJA at 10°S around 500 hPa, and around 350 hPa at 30°N . These local minima in the relative mass flux indicate barriers in the vertical transport in the A-case.

The profiles of the downdrafts are quite different (see Figure 2.1). The archived downdrafts are much less intense between the surface and 700 hPa than the diagnosed ones. The pattern of the diagnosed downdrafts closely corresponds to the pattern of the updrafts, including a peak in the tropics. For the archived downdrafts, there is

much less resemblance to the updrafts. In both cases, however, as mentioned earlier, the intensity of downdrafts is many times smaller than the intensity of the updrafts (see Figure 2.1). To a large extent, these big differences between the downdrafts can be attributed to differences in the downdraft parameterisation described above.

2.5 Effect on 222-Radon, nitrogen oxides and ozone

Convection, which is described by updrafts, downdrafts and compensating subsidence, leads to significant vertical mixing of tracers. The resulting net tracer transport by convection is strongly dependent on the vertical concentration gradient. In this section we will discuss the effect of changing convection on the distribution of ^{222}Rn , NO_x and O_3 .

2.5.1 Effect on 222-Radon

Let us first consider the case of a simple radioactive tracer like ^{222}Rn .

222-Radon distribution

Figure 2.3 shows the zonal mean ^{222}Rn concentrations for the archived and off-line diagnosed case in DJF 1991. Figure 2.4 shows the relative difference in ^{222}Rn concentration in DJF between the archived and off-line diagnosed case. There are three main differences between the archived and off-line diagnosed case.

The smaller convective mass flux around 800-700 hPa (see Section 2.4) prevents ^{222}Rn escaping from the boundary layer. As a result, higher concentrations (5 to 10%) are found in the A-case below 800-700 hPa.

The gradient in the convective mass flux is smaller between 700 and 250 hPa (see Section 2.4), hence there is in general less detrainment in that region. This leads to lower concentrations (up to 20-50%) in the A-case between 700 and 250 hPa. The differences are smaller at the poles, which is partially caused by smaller emissions in these regions.

The convective mass fluxes reach higher levels in the A-case (see Section 2.4), bringing up more ^{222}Rn -rich air from the surface, especially in the tropics. This leads to higher concentrations (up to more than 50%) above 250 hPa in the A-case. Although the mass flux is already more intense above 400 hPa in the A-case, the detrainment starts to get more intense above 250 hPa. Only above convectively very active regions over sea (with very low ^{222}Rn concentration values in the boundary layer), one finds lower (50%) ^{222}Rn concentrations in the archived case than in the off-line diagnosed case around 150 hPa (Indian Ocean, West Pacific). Also outside the tropics, stronger convection can lead to increased vertical mixing. Stronger convection in DJF above 700 hPa in the northern hemisphere poleward of 30°N leads to lower concentrations below 700 hPa and higher concentrations above 700 hPa (between 10 and 20% around 500 hPa at 50°N) in the A-case than in the D-case. In JJA over northern Africa (not shown) and in DJF over southern South-America, South Africa and Australia, it leads to higher concentrations around 600-500 hPa. In DJF, between 90°S and 60°S , slightly higher concentrations are found between 400 and 200 hPa.

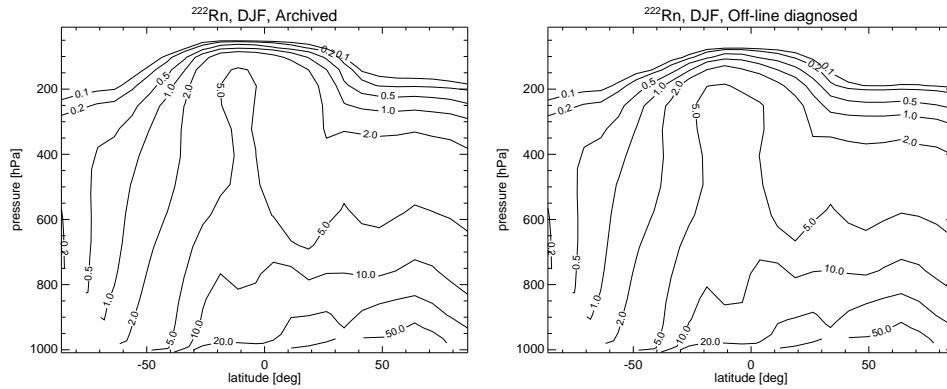


Figure 2.3: Zonal mean ^{222}Rn concentrations in DJF 1991 using archived (left) and off-line diagnosed (right) convective mass fluxes. The ^{222}Rn concentrations are expressed in $10^{-21} \text{ mol mol}^{-1}$.

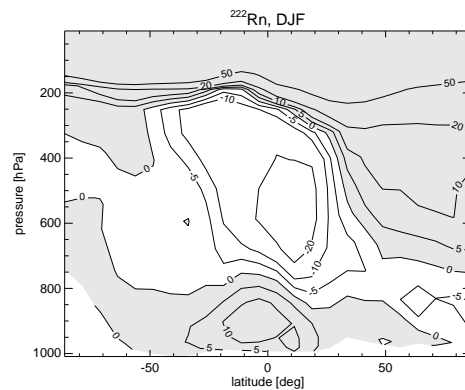


Figure 2.4: Zonal mean relative difference (%) in ^{222}Rn concentrations for DJF 1991 between model simulations using archived and off-line diagnosed convective mass fluxes respectively.

The higher concentrations above 250 hPa in the tropics for the archived case lead to higher concentrations outside the tropics due to meridional transport towards high latitudes.

Finally, over land around 900-800 hPa between 30°S and 90°N in JJA (not shown) and between 60°S and 30°N in DJF, particularly high concentrations are found. This is due to the more intense convection below 800 hPa accompanied by strong detrainment around 800 hPa.

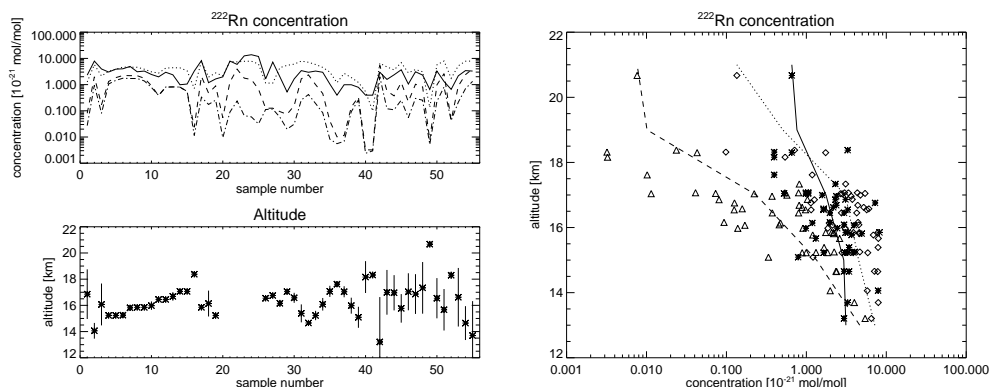


Figure 2.5: Lower left panel : flight altitudes in the STEP campaign for the 55 measurements. The crosses denote the mean height during the measurement, the end points of the vertical bars denote the lowest and highest altitude of the plane during the measurement. The height is expressed in km above sea level. Upper left panel : ^{222}Rn concentrations observed and modelled for the 55 measurements. The measured values (solid line), modelled values using archived mass fluxes (dotted line), using off-line diagnosed mass fluxes (dashed line) and without convection (dot-dashed line) are shown. The ^{222}Rn concentrations are expressed in $10^{-21} \text{ mol mol}^{-1}$. Right panel : the measured and modelled ^{222}Rn concentrations are shown with respect to the altitude. Vertical profiles are computed by averaging all the available data in 2-km bins. Measured values (stars and solid line), and modelled values using archived mass fluxes (diamonds and dotted line) and using off-line diagnosed mass fluxes (triangles and dashed line) are shown. The ^{222}Rn concentrations are expressed in $10^{-21} \text{ mol mol}^{-1}$, the altitude is expressed in km.

Comparison with 222-Radon observations

Many measurements of ^{222}Rn mixing ratios in the troposphere are available, including profiles [Liu *et al.*, 1984], time series in the marine and continental boundary layer and airplane measurements up to the lowermost stratosphere [Kritz *et al.*, 1998; Mahowald *et al.*, 1997; Kritz *et al.*, 1993; Russell *et al.*, 1993; Balkanski *et al.*, 1992; Balkanski and Jacob, 1990; Kritz *et al.*, 1990].

Modelled ^{222}Rn concentrations are compared with measurements from four aircraft campaigns : the STEP campaign in January and February 1987, a campaign performed from Moffet Field (US) in June, July and August 1994, the TROPOZ II campaign in January and February 1991, and the NARE campaign in August 1993. During the STEP campaign ^{222}Rn measurements were made above 12 km altitude, during the three other campaigns the measurements were made below 12 km. For these campaigns simulations were made at a horizontal model resolution of 2.5° by 2.5° and with 31 layers. For each campaign, we performed three simulations, one using archived mass fluxes, one using off-line diagnosed mass fluxes, and one without convective transport.

The measurements of the STEP campaign were made over the tropical western Pacific and over northern Australia in January and February 1987 [Kritz *et al.*, 1993;

Russell et al., 1993]. This is a period of extensive convective activity and rainfall. We used 172 samples, of which 55 showed ^{222}Rn concentrations above the detection limit. The detection limit varied between 0.33 and 0.78×10^{-21} mol mol $^{-1}$. The average sampling time was around 10 minutes. The measurement uncertainty was 35%. For comparison, we only used the 55 samples which have concentrations above the detection limit : most of these samples were obtained between 13 and 18 km height.

For comparison with the STEP data, we applied reduced ^{222}Rn emissions (0.9 atoms cm $^{-2}$ s $^{-1}$) in the model, describing better the local ^{222}Rn emissions over Australia during the southern hemispheric summer [*Schery et al.*, 1989]. Figure 2.1 shows that the convective mass flux profile over land between 250 and 100 hPa in the tropics and subtropics might differ much for the archived and off-line diagnosed convective mass fluxes. This results in large differences in the ^{222}Rn concentration above 200 hPa, as shown in Figure 2.4. The left panels of Figure 2.5 show the modelled and measured ^{222}Rn concentration for the 55 samples and the altitude at which the samples were taken. The modelled ^{222}Rn concentrations for the A-case agree better with the measurements than the modelled ^{222}Rn concentrations for the D-case. The ^{222}Rn concentrations of case A are on the average a little bit larger than the observed values (30%) whereas case D concentrations are about 6 time smaller. The right panel of Figure 2.5 gives the measured and modelled ^{222}Rn concentration as a function of height. It shows that this difference in the mean values can be interpreted as a steeper decrease with height for case D.

The comparison with the measurements from the campaign performed from Moffet Field (US) in June, July and August 1994, the TROPOZ II campaign, and the NARE campaign showed no large differences in ^{222}Rn concentration between the A- and D-case below 12 km altitude.

We used free tropospheric radon profiles that were obtained in the summer of 1994 on flights originating from Moffet Field, California (37.5°N, 122.0°W) [*Kritz et al.*, 1998; *Stockwell et al.*, 1998]. 11 profiles (122 samples) were available, which extend from the surface to 11.5 km and were obtained during flights performed in the period June 3rd to August 16th. The measurement error was around 6%. The sampling time was around 2 minutes. Figure 2.6 gives the measured and modelled ^{222}Rn values for these 11 profiles. From Figure 2.6 one can expect that for the period JJA over land between 30°N and 60°N, below 12 km (200 hPa), there are no big differences in the ^{222}Rn concentration. One might expect slightly higher ^{222}Rn values between 2 and 3 km, and slightly lower values between 3 and 12 km. The effect of convection is mainly visible between 3 and 9 km height. The archived and off-line diagnosed profiles lie very close to each other. The ^{222}Rn concentrations above 3 km are slightly higher (by a factor 1.2) in the off-line diagnosed case, except between 7 and 8 km height. The mean correlation coefficient for the profiles is 0.79 for the A- and D-case, while it is 0.74 for the no convection-case.

The measurements of TROPOZ II were made in January and February 1991 [*Ramonet et al.*, 1996]. 44 samples were obtained, distributed between 55°S and 65°N along the coast of the Atlantic Ocean, and between 1 and 11 km height. The sampling of one sample took at least 15 minutes (about 200 km). The error was estimated to be around 30%. There was a cut-off concentration at 0.18×10^{-21} mol mol $^{-1}$. The archived and off-line diagnosed case give rather similar results.

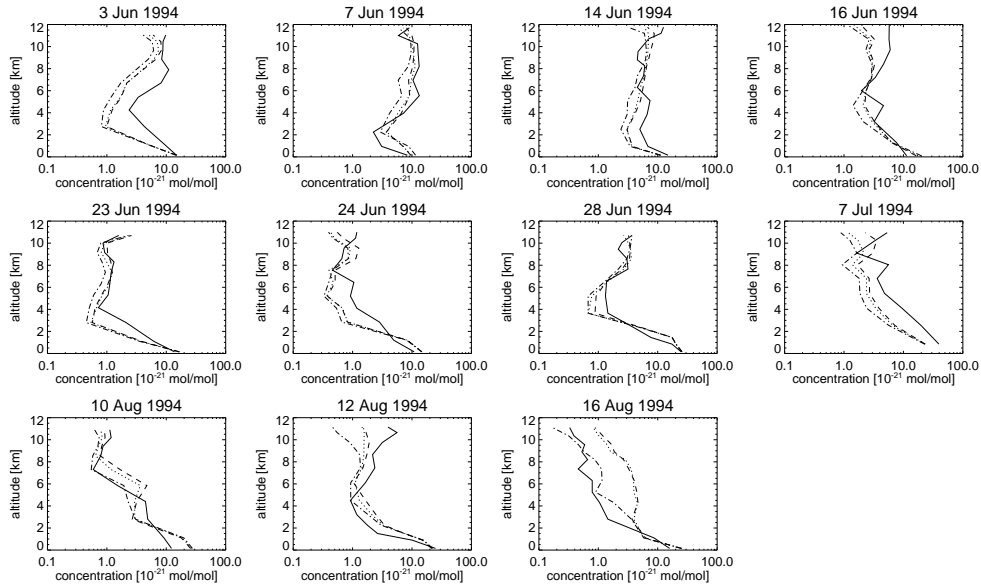


Figure 2.6: ^{222}Rn profiles measured during 11 flights from Moffet Field, in June-July-August 1994 : measured values (solid line), modelled values using archived mass fluxes (dotted line), using off-line diagnosed mass fluxes (dashed line) and without convection (dot-dashed line) are shown. The ^{222}Rn concentrations are expressed in $10^{-21} \text{ mol mol}^{-1}$.

We also used measurements from nine flights of the North Atlantic Regional Experiment (NARE) made over the North Atlantic Ocean and over the continent in the vicinity of Nova Scotia and New Brunswick, Canada [Zaucker *et al.*, 1996]. Samples were taken from the surface up to 5.5 km. The sampling time was less than three minutes. A total of 66 air samples was obtained. The measurement error was estimated around 15%. Comparison between results from an earlier model version of TM3 and these measurements is also described in Dentener *et al.* [1999], who specifically studied the effect of a new diffusion scheme.

From the comparison to the measurements it can be concluded that the archived convective mass fluxes give better agreement with the measurements in the upper troposphere and lower stratosphere. However, from the comparison in the middle troposphere, we do not see large differences between the A- and D-case. It is clear that both simulations agree better with observations than the simulation without convection.

2.5.2 Effect on the distribution of nitrogen oxides

A main objective of this study is to investigate the effect of different convective data sets on tropospheric chemistry simulations. Therefore we performed full chemistry simulations. Figure 2.7 shows the zonal mean NO_x concentration for DJF 1991-1996 for the archived and the off-line diagnosed case. The concentration of NO_x is defined

as the sum of the concentrations of NO and NO₂ :

$$[\text{NO}_x] = [\text{NO}] + [\text{NO}_2]. \quad (2.2)$$

A common feature of both simulations in the tropics is the upward bulge of the isocontours of 500 pptv or higher and the downward bulge of the isocontours of 50-100 pptv. The upward bulge is due to the higher tropopause in the tropics, the downward bulge is due to NO_x production by lightning, mainly over land. A further detail common to both simulations is that the vertical gradient of NO_x is stronger at the tropical tropopause than at mid-latitudes. This is due to leakage of stratospheric air rich in NO_x down to the mid-latitude troposphere.

There are however substantial differences between the two simulations, mainly in the upper tropical troposphere. Figure 2.8 shows the relative difference in mean NO_x concentration in DJF between both simulations for the years 1991 until 1996. In general, stronger convection induces stronger mixing resulting in enrichment in NO_x of clear regions and in a decrease in regions of high concentrations. This can be observed in several places.

Less intense convective mass fluxes around 800 hPa over land in case A result in less mixing of the surface emissions and lead in general to an increase of the concentrations over land below 800 hPa like for ²²²Rn.

Stronger convection and thus stronger mixing, transporting more NO_x-rich surface air upward, leads in the A-case in DJF to higher concentrations over North-America, Europe and Asia between 700 and 300 hPa (see right panel Figure 2.8), and lower values below 700 hPa.

In the tropics, the higher convection also leads to more mixing. On the one hand, the higher updrafts in the A-case give rise to a region of convectively transported low NO_x values between 200 and 100 hPa over the equator (50-100% lower NO_x concentrations). The differences in NO_x concentrations over land are mitigated somewhat due to the lightning NO_x emissions, which are the same in both simulations and much stronger over land than over sea [*Price and Rind, 1992*]. On the other hand, the higher updrafts in the A-case in the tropics lead to more intense subsidence, resulting in higher (20-50%) NO_x values in the tropics between 500 and 200 hPa (see right panel in Figure 2.8). A similar mechanism plays between 90°S and 60°S : there is more NO_x below 500 hPa due to more intense convective transport, bringing NO_x-rich upper troposphere air downward.

In the A-case, more intense convection and thus stronger mixing leads in JJA (not shown) to higher NO_x concentrations over Alaska, Canada and Siberia around 450 hPa (between 600 and 300 hPa).

The lower NO_x values at higher latitudes above 300 hPa are caused by the outflow of convectively transported NO_x-poor air from the tropics to mid-latitudes. The strength of this outflow signal is strongest in DJF in the northern hemisphere, and in JJA in the southern hemisphere, as expected.

One can see interactions with the large-scale vertical motion, which are not present in the ²²²Rn case. Downward transport from the upper troposphere and lower stratosphere (where the concentrations are now lower) in the subtropics consequently leads to lower (up to 20% locally) NO_x concentrations between 700 and 400 hPa in the A-case.

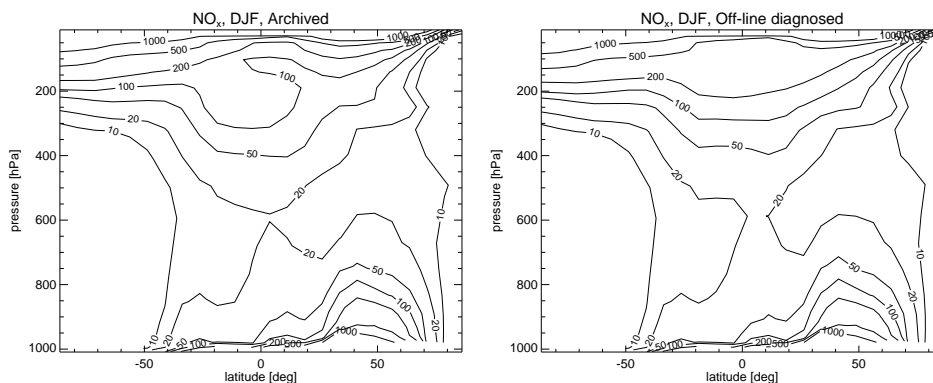


Figure 2.7: Zonal mean NO_x concentrations for DJF 1991-1996 using archived (left) and off-line diagnosed (right) convective mass fluxes. The NO_x concentrations are expressed in pptv.

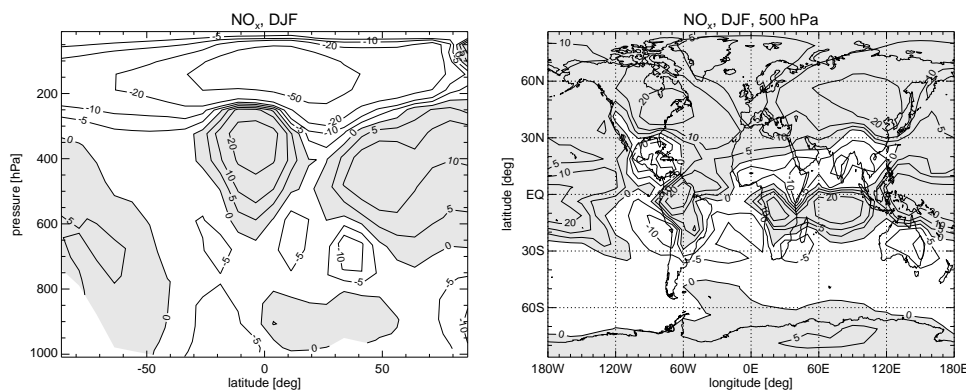


Figure 2.8: Relative difference (%) in NO_x concentrations for DJF 1991-1996 between model simulations using archived and off-line diagnosed convective mass fluxes : zonal mean (left panel) and horizontal cross section at 500 hPa. The relative difference is as defined in Equation 2.1.

2.5.3 Effect on the distribution of ozone

The distribution of O_3 in the troposphere is strongly affected by vertical transport. Differences in convection will therefore also result in differences in the O_3 -distribution. Figure 2.9 shows the zonal mean O_3 concentration for DJF in 1991 until 1996 for the archived and off-line diagnosed cases respectively. Figure 2.10 shows the relative differences in O_3 concentrations in DJF.

The effect on the O_3 distribution is to some extent analogous to the effect on the ^{222}Rn distribution. O_3 and ^{222}Rn both show a marked gradient at the tropopause and a vertical gradient the sign of which does not change with height. The only difference

is the sign of the gradient. As a consequence, the relative difference obtained for O_3 (Figure 2.10) is very similar to that of ^{222}Rn (see Figure 2.4) except for the sign. The difference in magnitude can be partly attributed to the fact that the vertical gradient of O_3 is smaller in the troposphere than that of ^{222}Rn .

The stronger mixing in the tropics leads to lower O_3 concentrations above 250 hPa, and higher O_3 values between 800 and 250 hPa. Around 100 hPa in the tropics, there is a large decrease in O_3 of 20 to 50% locally in the archived case in a broad zonal band. Observations of convective upward transport of O_3 -poor air over the Pacific Ocean have been documented by *Kley et al.* [1996]. The higher O_3 values (10 to 20%) between 800 and 250 hPa in the archived case can be observed in the convectively active regions (not shown) : mid-America (in JJA), South-America (in DJF), Indian Ocean, Indonesia, and West Pacific. This effect is less pronounced over the East Pacific and over the Atlantic.

Less mixing through the 800 hPa level leads to higher O_3 values in the free troposphere between 800 and 500 hPa at higher latitudes. This is clearly visible in DJF around 50°S at 600 hPa and around 40°N at 700 hPa, and in JJA (now shown) around 40°S at 700 hPa and around 60°N at 500 hPa. In a similar way, stronger downward transport due to more intense mixing of upper troposphere O_3 leads in JJA to higher (5%) O_3 values between 700 and 300 hPa over Alaska, Canada and Siberia

Through latitudinal transport, the signal of the lower O_3 values in the tropical upper troposphere is transported to the higher latitudes, leading to lower values outside the tropics above 400-300 hPa. Poleward the differences are smaller : 5-10% lower O_3 values at the poles around 200 hPa.

Further interactions with the large scale flow lead to lower O_3 values over land in the archived case in the subtropical region between 800 and 400 hPa. A similar pattern was observed for NO_x . It is caused on the one hand by the large scale subsidence over land in the subtropics, bringing down the signal from the lower O_3 values in the upper troposphere and lower stratosphere, and on the other hand by less intense convection bringing down less O_3 . One can see in Figure 2.2 minima in the relative convective mass flux over land in DJF at around 400 hPa at 20°S and around 600 hPa at 10°N . In JJA (not shown) similar minima can be found around 600 hPa at 15°S and around 400 hPa at 30°N .

2.6 Conclusions and discussion

We have studied the impact of using two different convective data sets in the chemistry transport model TM3, and investigated the effect on the distribution of ^{222}Rn , NO_x and O_3 . The simulations of the radioactive tracer ^{222}Rn were used to assess the consequences of changing the convective scheme for the distribution of a simple tracer by comparison with measurements, facilitating the interpretation of full chemistry simulations. The effect of convection on the transport of chemically active tracers with lifetimes of the order of days to a week and with sources in the continental boundary layer will be qualitatively similar to that of ^{222}Rn .

The archived and off-line diagnosed convective mass fluxes look quite similar. However, major differences are observed in the tropics where the archived convective updrafts reach greater height. Other major differences are found in DJF over northern

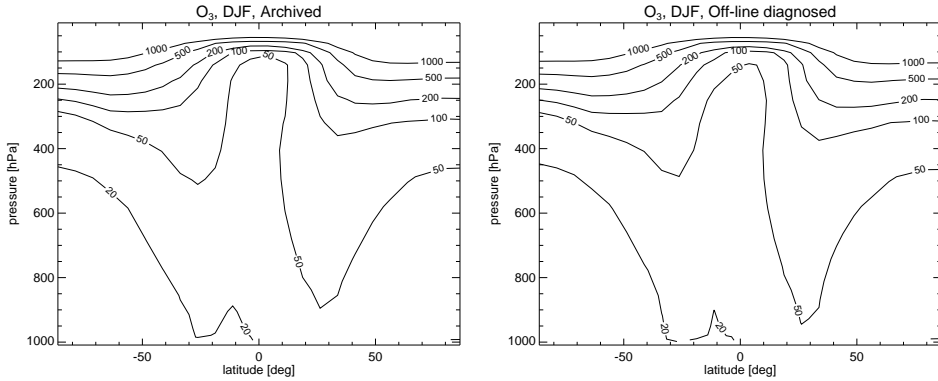


Figure 2.9: Zonal mean O_3 concentrations for DJF 1991-1996 using archived (left) and off-line diagnosed (right) convective mass fluxes. The O_3 concentrations are expressed in ppbv.

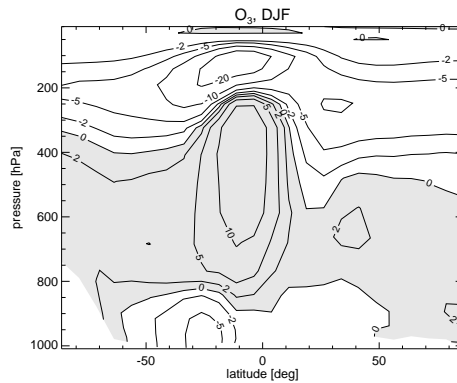


Figure 2.10: Zonal mean relative difference (%) in O_3 concentrations for DJF 1991-1996 between model simulations using archived and off-line diagnosed convective mass fluxes.

America, Europe and Asia, where archived convective mass fluxes are larger above 700 hPa. Also, over sea the archived convection was in general less intense than the off-line diagnosed convection. Finally, the archived downdraft mass flux was much weaker than the off-line diagnosed one. This shows that the differences in the convection parameterisation and the influence of archived instead of off-line diagnosed convection lead to considerable differences in the convective mass flux.

The difference in the convective mass fluxes influences the distribution of ^{222}Rn , NO_x and O_3 . Due to slower vertical mixing due to less transport through the 800 hPa level, we observed in the boundary layer in the archived case higher ^{222}Rn and NO_x concentrations and lower O_3 concentrations. Higher updrafts caused in the tropical upper troposphere and lower stratosphere a significant enhancement in ^{222}Rn concentrations, and a significant decrease in NO_x and O_3 concentration. These signals

were transported poleward, leading also to significantly higher ^{222}Rn and significantly lower NO_x and O_3 in the mid-latitude upper troposphere and lower stratosphere. The detrainment of ^{222}Rn -rich air in the tropics between 700 and 300 hPa was less, leading to lower ^{222}Rn values. At the same time in the tropics, the induced subsidence transported more NO_x and O_3 rich air to the 500-200 hPa region. In the subtropics, the large-scale motion transported the lowered upper troposphere NO_x and O_3 values downward along the subtropical front. At higher latitudes, in the free troposphere more NO_x and O_3 is found due to more convective downward transport. At higher latitudes in northern hemisphere in DJF, for ^{222}Rn and NO_x there are significantly higher values in the free troposphere due to more intense convection increasing the transport from the boundary layer.

Although the large-scale patterns of the archived and off-line diagnosed convective mass fluxes seem similar, the differences have a strong effect on the O_3 concentrations, of up to 20% locally in the seasonal and zonal mean. This demonstrates the sensitivity of tropospheric O_3 -chemistry simulations to the description of convective transport. We were able to explain the main differences in zonal and seasonal NO_x and O_3 by the difference in tracer transport, induced by the difference in convective mass flux. It is clear, however, that, locally and over short time intervals, concentration changes can be larger so that interactions with chemistry might play a role.

The comparison with ^{222}Rn observations in the free troposphere is still a weak base for selecting an optimal set of convective mass fluxes. The comparison with the few available ^{222}Rn observations in the upper troposphere and lower stratosphere showed that using the archived convective mass fluxes gives better agreement with the measurements than using the off-line diagnosed convective mass fluxes. More extensive comparison with ^{222}Rn observations in the free troposphere would be highly useful for further evaluation of the convective data sets.

The difference between the measured and modelled ^{222}Rn concentrations can have many reasons. Temporal and spatial variability in the ^{222}Rn emission rate which is only crudely represented in the model; the resolution, affecting the description of the large scale wind, and the representation of strong gradients in tracer concentrations; the description of the advection of tracers by large scale winds; the parameterisation of subgrid-scale processes like boundary layer diffusion and convection. Using the archived convective mass fluxes, the modelled ^{222}Rn concentrations in the upper troposphere and lower stratosphere were slightly too high. This might be caused by slightly too strong tropical convection induced by too high low-level humidity [Hagemann *et al.*, 2001].

A remaining question is the influence of the dependence of the lightning parameterisation on the convective updraft top. Lightning production is strongly dependent on the convective updraft top [Price and Rind, 1992]. When the total lightning NO_x production is kept at $5 \text{ Tg}[\text{N}] \text{ yr}^{-1}$, but the archived updraft tops are used in the A-simulation, lightning emissions in the tropics extend to greater heights. This would counteract the effect of transport of NO_x -poor air to the upper troposphere by convection. The dipole structure in the tropics in left panel of Figure 2.8 was indeed found to weaken but is still dominant. The minimum around 100 hPa increases by 50%, the maximum around 400 hPa decreases by 10%. The effect of this on the O_3 distribution, is however negligible. The result for O_3 is almost completely similar to Figure 2.10.

Acknowledgement

This work was supported by the Netherlands Organization for Scientific Research (NWO) and by the European Union under contract number EVK2-CT-2002-00170 (RETRO).

3

Evaluation of archived and off-line diagnosed vertical diffusion coefficients from ERA-40 with ^{222}Rn simulations

Abstract

Boundary layer turbulence has a profound influence on the distribution of tracers with sources or sinks at the surface. The 40-year ERA-40 meteorological data set of the European Centre for Medium-range Weather Forecasts contains archived vertical diffusion coefficients. We evaluated the use of these archived diffusion coefficients versus off-line diagnosed coefficients based on other meteorological parameters archived during ERA-40 by examining the influence on the distribution of the radio nuclide ^{222}Rn in the chemistry transport model TM3. In total four different sets of vertical diffusion coefficients are compared : (i) 3-hourly vertical diffusion coefficients archived during the ERA-40 project, (ii) 3-hourly off-line diagnosed coefficients from a non-local scheme based on *Holtslag and Boville* [1993], *Vogelezang and Holtslag* [1996], and *Beljaars and Viterbo* [1999], (iii) 6-hourly coefficients archived during the ERA-40 project, and (iv) 6-hourly off-line diagnosed coefficients based on a local scheme described in *Louis* [1979] and *Louis et al.* [1982]. The diffusion scheme to diagnose the coefficients off-line in (ii) is similar to the diffusion scheme used during the ERA-40 project (i and iii).

The archived diffusion coefficients from the ERA-40 project which are time-averaged cause stronger mixing than the instantaneous off-line diagnosed diffusion coefficients. This can be partially attributed to the effect of instantaneous versus time-averaged coefficients, as well as to differences in the diffusion schemes. The 3-hourly off-line diagnosis of diffusion coefficients can reproduce quite well the 3-hourly archived diffusion coefficients.

Atmospheric boundary layer heights of the sets (ii) and (iii) are also compared. Both were found to be in reasonable agreement with observations of the atmospheric boundary layer height in Cabauw (the Netherlands) and from the FIFE campaign

¹This chapter has been published as : D. J. L. Olivié, P. F. J. van Velthoven and A. C. M. Beljaars, *Atmos. Chem. Phys.*, Vol. 4, 2313-2336, SRef-ID: 1680-7324/acp/2004-4-2313, 2004, [*Olivié et al.*, 2004a]

(United States) during summer.

Simulations of ^{222}Rn with the TM3 model using these four sets of vertical diffusion coefficients are compared to surface measurements of ^{222}Rn at the mid-latitude continental stations Freiburg, Schauinsland, Cincinnati and Socorro in order to evaluate the effect of these different sets of diffusion coefficients on the tracer transport. It is found that the daily cycle of the ^{222}Rn concentration is well represented using 3-hourly diffusion coefficients. Comparison with observations of ^{222}Rn data with the station in Schauinsland which is situated on a hill shows that all considered schemes underestimate the amplitude of the daily cycle of the ^{222}Rn concentration in the upper part of the atmospheric boundary layer.

3.1 Introduction

Boundary layer turbulence is an important transport mechanism in the troposphere [Wang *et al.*, 1999]. In the convective or turbulent atmospheric boundary layer (ABL) tracers can be transported throughout the height range of the ABL in time intervals of tens of minutes. All species emitted at the surface must pass through the ABL in order to reach the free troposphere. Because turbulence acts on spatial scales that are much smaller than the typical size of the grid cells of global atmospheric models, turbulent diffusion must be parameterised in these models.

The European Centre for Medium-range Weather Forecasts (ECMWF) reanalysis project (ERA-40) aims at providing a consistent time series of the state of the global atmosphere for the period 1957-2002 [Simmons and Gibson, 2000]. A wide variety of meteorological fields were archived in ERA-40. In the earlier ERA-15 reanalysis project [Gibson *et al.*, 1997] where the atmosphere for the period 1979-1993 has been reanalysed, meteorological fields describing small-scale transport like convection or boundary layer turbulence were not archived. The more recent ERA-40 data set is one of the first long-term meteorological data sets where vertical diffusion coefficients for heat are archived (available as 3- or 6-hourly averaged values).

Meteorological data sets such as ERA-40 and ERA-15 are commonly used to study the transport and chemical evolution of atmospheric gases and aerosols in chemical transport models (CTMs). The chemical transport model TM3 (Tracer Model Version 3) is a global atmospheric model, which is applied to evaluate the atmospheric composition, and changes herein caused by natural and anthropogenic changes. For describing the turbulent transport, it can use different turbulent diffusion data. Until now, two off-line vertical diffusion schemes have been used in the TM3 model, where the diffusion coefficients are diagnosed off-line based on other regularly (e.g. 6-hourly) archived meteorological fields. The first scheme, based on Louis [1979] and Louis *et al.* [1982], is a local diffusion scheme that describes the vertical diffusion coefficient as a function of a mixing length scale, the local gradient of the wind, and the virtual temperature. However, under convective conditions, when the largest transporting eddies may have sizes similar to the depth of the ABL, local schemes do not perform well [Troen and Mahrt, 1986]: the characteristics of the large eddies are not properly taken into account. The second scheme, based on a combination of Holtslag and Boville [1993], Vogelesang and Holtslag [1996] and Beljaars and Viterbo [1999], is a non-local diffusion scheme. Non-local ABL schemes often contain a term that describes counter

gradient transport by the large eddies [Troen and Mahrt, 1986], and prescribe the shape of the vertical profile of the diffusion coefficient. Apart from the meteorological fields needed for a local scheme, a non-local scheme also uses the surface sensible and latent heat fluxes. The vertical exchange has been shown to be more pronounced with non-local schemes than with local schemes [Holtslag and Boville, 1993; Holtslag et al., 1995]. The 3-hourly off-line scheme [Holtslag and Boville, 1993; Voegelezang and Holtslag, 1996; Beljaars and Viterbo, 1999] is currently most used in the TM3 model. The 6-hourly off-line scheme [Louis, 1979; Louis et al., 1982] was until recently used in the TM3 model for various studies : Dentener et al. [2003a] used meteorological data from the ERA-15 project (which does not provide 3-hourly surface latent heat fluxes) and the 6-hourly off-line scheme [Louis, 1979; Louis et al., 1982]. From now on however, the ERA-40 data set allows the use of archived vertical diffusion data (3-hourly or 6-hourly) in the TM3 model. One of the first to use archived subgrid meteorological parameters was Allen et al. [1996]. They used archived convective mass fluxes and detrainments, as well as the ABL heights. An advantage of the use of archived meteorological fields to describe small-scale transport in CTMs, is the consistency of these fields with the archived fields of cloud cover, temperature, humidity or precipitation.

The effect on the transport of tracers by the diffusion data can be studied by making ^{222}Rn simulations with CTMs. ^{222}Rn is an excellent tracer to study the transport characteristics on short time scales (hours to weeks) because it has an almost uniform emission rate over land and is only lost through radioactive decay with an e-folding lifetime of about 5.5 days [Dentener et al., 1999; Balkanski and Jacob, 1990; Kritz et al., 1990; Brost and Chatfield, 1989; Polian et al., 1986]. Therefore ^{222}Rn has been used extensively to evaluate parameterisations of convective transport [Mahowald et al., 1997; Allen et al., 1996; Feichter and Crutzen, 1990; Jacob and Prather, 1990] and ABL diffusion [Stockwell and Chipperfield, 1999; Stockwell et al., 1998; Jacob et al., 1997; Lee and Larsen, 1997; Mahowald et al., 1997] in atmospheric models.

In this work, we try to answer the following questions : (1) How well is the mid-latitude summer time ABL height reproduced in the ERA-40 data and in an off-line model driven by ERA-40 data? (2a) Can diffusion coefficients be reproduced accurately off-line for use in CTMs? (2b) How do local ABL schemes perform versus non-local ABL schemes when applied off-line? (3a) How crucial is a 3-hourly time resolution for diffusion data for CTM-modelling? (3b) What is the influence of using time-averaged diffusion coefficients on the tracer transport in CTMs?

To answer these questions, we will start with a description of the TM3 model and the diffusion schemes that generate the different sets of vertical diffusion coefficients (Section 3.2). In that section we will also describe the ^{222}Rn emission scenario in the TM3 model, the ^{222}Rn observations, and the ABL height observations. In Section 3.3 we will first compare the vertical diffusion coefficients from the different schemes. Then we will compare the modelled ABL height at two mid-latitude stations with observations. Next we will compare the ^{222}Rn concentration which is modelled in the TM3 model using the different sets of diffusion data, with surface measurements of the ^{222}Rn concentration at four selected surface stations. In Section 3.4 we will formulate the conclusions and formulate some recommendations.

3.2 Methods

3.2.1 The TM3 model

The chemical transport model TM3 (Tracer Model Version 3) is a global atmospheric CTM with a regular longitude-latitude grid and hybrid σ -pressure levels [Lelieveld and Dentener, 2000; Houweling *et al.*, 1998; Heimann, 1995]. The meteorological input data for TM3 from ERA-40 is available for 1957 to 2002. For dynamics calculations ERA-40 used a spectral truncation of T159. The physical calculations were done on a reduced Gaussian grid of 160 nodes (N80). In the vertical, 60 hybrid σ -pressure levels [Simmons and Burridge, 1981] were used, reaching up to 0.1 hPa. To be used in the TM3 model, the meteorological data is interpolated or averaged to the desired TM3 grid cells [Bregman *et al.*, 2003]. For advection of the tracers, the model uses the slopes scheme developed by Russell and Lerner [Russell and Lerner, 1981]. To describe the effect of convective transport on the tracer concentration, we used the archived convective mass fluxes from the ERA-40 data set [Olivié *et al.*, 2004b]. The convection scheme in the ECMWF model used during the ERA-40 project is based on Tiedtke [1989], Gregory *et al.* [2000], and Nordeng [1994].

The vertical diffusion of tracers in the TM3 model is described with a first order closure scheme. The net turbulent tracer flux $\overline{w'\chi'}$ is expressed as

$$-\overline{w'\chi'} = K_z \frac{\partial \chi}{\partial z}, \quad (3.1)$$

where K_z is the vertical diffusion coefficient for heat, w the vertical velocity, χ the tracer concentration, and z the height above the surface. It is assumed that the vertical diffusion coefficient for tracers is equal to the vertical diffusion coefficient for heat. In contrast to Holtslag and Boville [1993] and Wang *et al.* [1999], there is no counter gradient term in the TM3 implementation.

The vertical diffusion coefficients are applied in the TM3 model by converting the vertical diffusion coefficients into upward and downward vertical air mass fluxes of equal magnitude which model the exchange between two model layers. These air mass fluxes are combined with the vertical convective mass fluxes from the convection parameterisation to calculate the subgrid-scale vertical tracer transport with an implicit numerical scheme. This allows the time steps in the TM3 model to be rather large, without introducing stability problems. In the case of very large time steps, the effect of the scheme is that it pushes the tracer concentration at once to its equilibrium distribution. In this study, we used a time step of 1 hour for the small-scale vertical transport.

From Eq. (3.1) one derives that the dimensions of K_z are L^2T^{-1} . Taking the ABL height as a representative length scale for the effect of diffusion gives a relationship between K_z and the time scale of turbulent diffusion. If for example the ABL height is 1000 m and K_z is 300 m^2/s , one finds a time scale of around 1 hour. This means that a tracer initially only present at the surface, will be well mixed throughout the complete ABL on a time scale of 1 hour.

3.2.2 Vertical diffusion data

Different sets of vertical diffusion coefficients are used in the TM3 model. We will briefly describe the schemes that are used to calculate these data sets.

The ERA-40 3-hourly and 6-hourly diffusion coefficients

The scheme as it is used in the ERA-40 project is described in the documentation of the cycle CY23r4 of the ECMWF model, see <http://www.ecmwf.int/research/ifs-docs/CY23r4/>. It is a non-local scheme. The coefficients for vertical diffusion of heat were stored during the ERA-40 project as 3-hourly averaged values. They can also be combined to 6-hourly averaged values.

Different formulations are used based on the stability regime that is determined by the virtual potential temperature flux $(\overline{w'\theta'_v})_0$. If the surface layer is unstable ($(\overline{w'\theta'_v})_0 > 0$), then a method according to *Troen and Mahrt* [1986] is applied. This method determines the ABL height h using a parcel method where the parcel is lifted from the minimum virtual temperature, rather than from the surface. The dimensionless coefficient for the excess of the parcel temperature is reduced from 6.5 [*Troen and Mahrt*, 1986] or 8.5 [*Holtstlag and Boville*, 1993] to 2 (to get a well controlled entrainment rate and a less aggressive erosion of inversions). In the ABL, the vertical profile of diffusion coefficients is predefined [*Troen and Mahrt*, 1986]

$$K_z = \kappa w_h z \left(1 - \frac{z}{h}\right)^2, \quad (3.2)$$

where w_h is a turbulent velocity scale and $\kappa = 0.4$ the Von Karman constant. At the top of the ABL, there is an explicit entrainment formulation in the capping inversion. The virtual heat flux at the top of the ABL is taken proportional to the surface virtual heat flux

$$(\overline{w'\theta'_v})_h = -C (\overline{w'\theta'_v})_0, \quad (3.3)$$

with $C = 0.2$ and θ_v the virtual potential temperature. Knowing the flux, the diffusion coefficient at the top of the ABL can be expressed as

$$K_z = C \frac{(\overline{w'\theta'_v})_0}{\frac{\partial \theta_v}{\partial z}}, \quad (3.4)$$

where $\frac{\partial \theta_v}{\partial z}$ is the virtual potential temperature gradient in the inversion layer.

If the surface layer is stable ($(\overline{w'\theta'_v})_0 < 0$), the diffusion coefficients are determined by the gradient Richardson number Ri which is defined as

$$Ri = \frac{g}{\theta} \frac{\frac{\partial \theta}{\partial z}}{|\frac{\partial \vec{v}}{\partial z}|^2}, \quad (3.5)$$

where \vec{v} is the horizontal wind velocity. When the atmosphere is locally unstable ($Ri < 0$) then

$$K_z = \frac{l_h^2}{\Phi_m \Phi_h} \left| \frac{\partial \vec{v}}{\partial z} \right|, \quad (3.6)$$

where

$$\Phi_m(\zeta) = (1 - 16\zeta)^{-\frac{1}{4}}, \quad (3.7)$$

and where

$$\Phi_h(\zeta) = (1 - 16\zeta)^{-\frac{1}{2}}, \quad (3.8)$$

where ζ is taken equal to Ri . The mixing length l_h is calculated according to

$$\frac{1}{l_h} = \frac{1}{\kappa z} + \frac{1}{\lambda_h}. \quad (3.9)$$

The asymptotic mixing length λ_h [m] is defined as

$$\lambda_h = 30 + \frac{120}{1 + \left(\frac{z}{4000}\right)^2}, \quad (3.10)$$

where z [m] is the height above the surface. The asymptotic mixing length λ_h is a typical length scale in a neutral atmosphere for the vertical exchange of some quantity (momentum, heat, or tracer) due to turbulent eddies. In the lowest layers of the atmosphere, the size of the turbulent eddies is limited by the presence of the earth's surface, which is taken into account in the mixing length l_h in Eq. (3.9).

When the atmosphere is locally stable ($Ri > 0$), ζ is read from a table ($\zeta = \zeta(Ri)$). The diffusion coefficients are calculated with

$$K_z = l_h^2 \left| \frac{\partial \vec{v}}{\partial z} \right| F_h(Ri), \quad (3.11)$$

where the stability function $F_h(Ri)$ is a revised function of the *Louis et al.* [1982] function [*Beljaars and Viterbo*, 1999]

$$F_h(Ri) = \frac{1}{1 + 2b Ri \sqrt{1 + d Ri}}, \quad (3.12)$$

where $b = 5$ and $d = 1$. This formulation has less discrepancy between momentum and heat diffusion : the ratio of momentum and heat diffusion is reduced [*Viterbo et al.*, 1999]. The formulation of K_z in case of a stable surface layer also applies to the formulation of K_z above the ABL in case of an unstable surface layer.

The calculation of the atmospheric boundary layer height stored during the ERA-40 project is also described in the information about the cycle CY23r4. As well in the stable, in the neutral, as in the unstable case, a parcel lifting method proposed by *Troen and Mahrt* [1986] is used. They use a critical bulk Richardson number $Ri_b = 0.25$. The bulk Richardson number is based on the difference between quantities at the level of interest and the lowest model level. This ABL height is available every 3 hours and represents an instantaneous value. We only studied the 6-hourly values. We will refer to these 3-hourly diffusion coefficients as E3, and to these 6-hourly diffusion coefficients and 6-hourly ABL heights as E6.

The TM3 off-line 3-hourly and 6-hourly diffusion coefficients

The first set of off-line diagnosed diffusion coefficients in TM3 is calculated with a scheme that is rather similar to the above-described scheme. It is a non-local scheme based on *Holtstlag and Boville* [1993], *Vogelezang and Holtstlag* [1996], and *Beljaars and Viterbo* [1999]. The diffusion coefficients are calculated every 3 hours, based on 3-hourly latent and sensible heat fluxes and 6-hourly fields of wind, temperature, and humidity. It has been implemented and tested in the TM3 model [*Jeuken, 2000; Jeuken et al., 2001*]. The calculated K_z values are instantaneous values.

Although the scheme is rather similar to the aforementioned E3/E6 scheme, there are some differences : (i) a bulk Richardson criterion instead of a parcel ascent method is used to determine the height of the ABL; (ii) there is no entrainment formulation at the top of the ABL; (iii) the temperature excess of the large eddies under convective conditions is larger; (iv) the prescribed profile of the asymptotic mixing length is different; and (v) the stability functions are different.

If the surface layer is unstable ($(\overline{w'\theta'_v})_0 > 0$), a prescribed profile of the vertical diffusion coefficients as in Equation 3.2 is used. According to *Vogelezang and Holtstlag* [1996] the ABL height h is the layer where the bulk Richardson number

$$Ri_b = \frac{\frac{g}{\theta_{vs}}(\theta_{vh} - \theta_{vs})(h - z_s)}{|\vec{v}_h - \vec{v}_s|^2 + b u_*^2} \quad (3.13)$$

reaches a critical value $Ri_b = 0.3$ (in *Vogelezang and Holtstlag* [1996], the critical value is $Ri_b = 0.25$). The index s refers to values in the lowest model layer, the index h refers to values at the top of the ABL. u_* is the friction velocity. The value for $b = 100$. The exact ABL height is calculated by linear interpolation. The temperature excess under convective conditions is calculated using a coefficient with value 8.5 (versus 2 in the E3/E6 case).

If the surface layer is stable ($(\overline{w'\theta'_v})_0 < 0$), the diffusion coefficients are calculated with Eq. (3.11). When the atmosphere is locally stable ($Ri > 0$), we take

$$F_h(Ri) = \frac{1}{1 + 10 Ri \sqrt{1 + Ri}}, \quad (3.14)$$

while when the atmosphere is locally unstable ($Ri < 0$), we take

$$F_h(Ri) = 1. \quad (3.15)$$

Above the ABL, a formulation according to the *Louis* [1979] scheme is used. In the free atmosphere the stability functions in the unstable case ($Ri < 0$) [*Williamson et al., 1987; Holtstlag and Boville, 1993*] is

$$F_h(Ri) = \sqrt{1 - 18 Ri}, \quad (3.16)$$

and in the stable case ($Ri > 0$) [*Holtstlag and Boville, 1993*]

$$F_h(Ri) = \frac{1}{1 + 10 Ri(1 + 8 Ri)}. \quad (3.17)$$

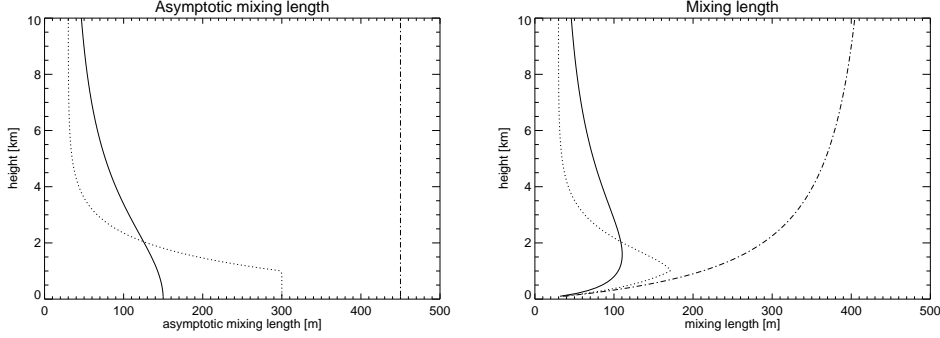


Figure 3.1: Vertical profiles of the asymptotic mixing length (left) and the mixing length (right) for heat in the different diffusion schemes : E3/E6 scheme (solid line), H3 scheme (dotted line), and L6 scheme (dot-dashed line). The mixing length can be derived from the asymptotic mixing length using Equation 3.9.

The asymptotic mixing length λ_h [m] in this scheme is defined as

$$\lambda_h = \begin{cases} 300 & \text{if } z < 1000 \text{ m} \\ 30 + 270 \exp\left(1 - \frac{z}{1000}\right) & \text{if } z \geq 1000 \text{ m} . \end{cases} \quad (3.18)$$

We will refer to the diffusion coefficients calculated with this diffusion scheme as H3.

The second set of diffusion coefficients that are off-line diagnosed in TM3 is based on a local diffusion scheme described in *Louis* [1979] and *Louis et al.* [1982]. These fields of vertical diffusion coefficients are calculated every 6 hours, based on 6-hourly fields of wind, temperature, and humidity. The vertical diffusion coefficients are expressed as in Eq. (3.11). The stability function $F_h(Ri)$ in the stable case ($Ri > 0$) is

$$F_h(Ri) = \frac{1}{1 + 3b Ri \sqrt{1 + d Ri}}, \quad (3.19)$$

where $b = 5$ and $d = 5$, and in the unstable case ($Ri < 0$)

$$F_h(Ri) = 1 - \frac{3b Ri}{1 + 3b c l^2 \sqrt{-\frac{Ri}{2} \left[\frac{\left(1 + \frac{\Delta z}{z}\right)^{\frac{1}{3}} - 1}{\Delta z} \right]^3}}, \quad (3.20)$$

where $c = 5$ and Δz is the height difference between the centres of two model layers. The asymptotic mixing length λ_h is taken to be 450 m. We will refer to this diffusion scheme as L6. A plot of the mixing length and the asymptotic mixing length for heat in the different schemes is shown in Figure 3.1.

3.2.3 ²²²Rn emission and decay

²²²Rn is emitted at a relatively uniform rate from the soil on the continents. It is relatively insoluble in water, inert and not efficiently removed by rain. It has a mean

e-folding lifetime of about 5.5 days due to radioactive decay. It is assumed that the average flux from the soil lies somewhere between 0.8 and 1.3 atoms $\text{cm}^{-2} \text{s}^{-1}$ [Liu *et al.*, 1984; Turekian *et al.*, 1977; Wilkening and Clements, 1975]. Oceans are also a source for ^{222}Rn . However, the mean oceanic flux is estimated to be 100 times weaker than the continental source [Lambert *et al.*, 1982; Broecker *et al.*, 1967]. The fact that ^{222}Rn has a lifetime and source characteristics that are similar to the lifetime and source characteristics of air pollutants such as NO, NO₂, propane, butane and other moderately reactive hydrocarbons, makes it interesting for evaluation of transport parameterisations.

We adopted the ^{222}Rn emission scenario recommended by WCRP [Jacob *et al.*, 1997]: land emission between 60°S and 60°N is 1 atoms $\text{cm}^{-2} \text{s}^{-1}$; land emission between 70°S and 60°S and between 60°N and 70°N is 0.005 atoms $\text{cm}^{-2} \text{s}^{-1}$; oceanic emission between 70°S and 70°N is 0.005 atoms $\text{cm}^{-2} \text{s}^{-1}$. This leads to a global ^{222}Rn emission of 16 kg per year. We did not account for any regional or temporal variation in the emission rate.

3.2.4 Observations

ABL height observations

ABL height observations from two mid-latitude sites are used in this study. They are made in Cabauw (the Netherlands) and during the FIFE campaign in Manhattan (Kansas, United States). The ABL height in Cabauw (52.0°N, 4.9°E) is derived from measurements with a wind profiler during the day, and with a SODAR (Sound Doppler Acoustic Radar) during the night. The wind profiler is a pulsed Doppler radar. The strength of the echo from the radar pulse depends on the turbulence intensity. In the clear air case (no clouds or rain drops), the strength of the echo is directly proportional to the eddy dissipation velocity, and ABL heights can be derived from it in a straightforward manner. ABL heights below 2 km are measured with a resolution of 100 meter and ABL heights above 2 km with a resolution of 400 meter. The SODAR measures wind velocities and wind directions between 20 and 500 m by emitting sound pulses and measuring the reflection of this pulse by the atmosphere. The ABL height is available as 30-minute averages. The Cabauw observations that are available to us were performed during 12 days in the summer of 1996.

The second set of ABL height measurements was made during the field experiments of the First ISLSCP Field Experiment (FIFE) [Sellers *et al.*, 1988], which were performed in 1987 and 1989 near Manhattan. Measurements of ABL height were done with a Volume Imaging LIDAR [Eloranta, 1994] and with a SODAR [Wesely, 1994]. The Volume Imaging LIDAR is an elastic backscatter LIDAR that uses atmospheric light-scattering particles as tracers. It measures the radial component of the air velocity, and operates at a wavelength of 106.4 nm. Measurements are available for 22 days in the summer of 1987 and 1989. The time resolution of the data is about 30 minutes. The SODAR in Manhattan [Wesely, 1994] measured during day as well as night and gave estimates of the height of the mixed layer and the vertical dimensions of inversions within the lowest kilometre of the atmosphere. It worked at a frequency of 1500 Hz. It has measured during 42 days in summer of 1987. The data is available as 30-minute averages, and the vertical resolution is approximately 25 m.

222-Radon observations

^{222}Rn observations from four stations are used in this study. Hourly measurements of ^{222}Rn at Freiburg and Schauinsland (both at 48°N , 8°E) for the year 1993 are used. These data have also been used in a study by *Dentener et al.* [1999]. Freiburg and Schauinsland are located at heights of 300 and 1200 m above sea level respectively. Schauinsland is located approximately 12 km south of Freiburg. Because the orography on horizontal scales smaller than 150 km is not resolved in the TM3 model at mid-latitudes, the observations at the Schauinsland station are not compared with the concentrations from the lowest model layer, but with the concentrations from the model layer at 900 m above the surface.

^{222}Rn measurements were made in Cincinnati (40°N , 84°W) at 8h00 and 15h00 LT from January 1959 until February 1963. The monthly mean ^{222}Rn concentrations at these two times of the day have been taken from the literature [*Gold et al.*, 1964]. The measurements in Cincinnati were in the past extensively used in tracer transport models but never allowed a direct comparison. The ERA-40 reanalysis, which starts from the year 1957, now allows a month-to-month comparison of these measurements.

In Socorro (34°N , 107°W) measurements of ^{222}Rn in the atmosphere over a 6-year period have been made between 1951 and 1957. Monthly mean daily cycles over this period of the ^{222}Rn concentration in Socorro (34°N , 107°W) are published in *Wilkening* [1959]. Although the measurements were not continuous (only 692 days were sampled during this period), they give a good indication of the average monthly mean daily cycle of the ^{222}Rn concentration in Socorro.

3.2.5 Experimental set-up

We have performed model simulations with the TM3 model separately for each of the available sets of vertical diffusion coefficients. We performed 5 simulations, each with different vertical diffusion coefficients. The 5 model set-ups are (as described in Section 3.2.2) : (E3) using 3-hourly averaged fields archived during the ERA-40 project; (H3) using 3-hourly instantaneous off-line diagnosed fields; (E6) as E3 but with 6-hourly averaged fields; (L6) using 6-hourly instantaneous off-line diagnosed fields with a local diffusion scheme; and (N) using no diffusion. Table 3.1 gives an overview of the different model simulations. The model is used with a horizontal resolution of $2.5^\circ \times 2.5^\circ$ and 31 layers up to 10 hPa. The lowest layer has a thickness of about 60 m, the second layer of about 150 m.

For comparison with the ^{222}Rn observations in Freiburg and Schauinsland, we performed model simulations from November 1992 until December 1993. November and December 1992 are included as a spin up period, and the analysis is restricted to the year 1993. To allow comparisons with ^{222}Rn measurements in Socorro and Cincinnati, we made model simulations from November 1958 until February 1963. We analysed the period from January 1959 until February 1963 and used November and December 1958 as a spin up period. For this period we did not perform an E3 simulation.

Table 3.1: Overview of the diffusion schemes.

| code | scheme | time step | data origin | K_z | ABL height |
|------|--------------|-----------|--------------------|---------------|---------------|
| E3 | non-local | 3 hours | archived | averaged | |
| H3 | non-local | 3 hours | off-line diagnosed | instantaneous | instantaneous |
| E6 | non-local | 6 hours | archived | averaged | instantaneous |
| L6 | local | 6 hours | off-line diagnosed | instantaneous | |
| N | no diffusion | | | | |

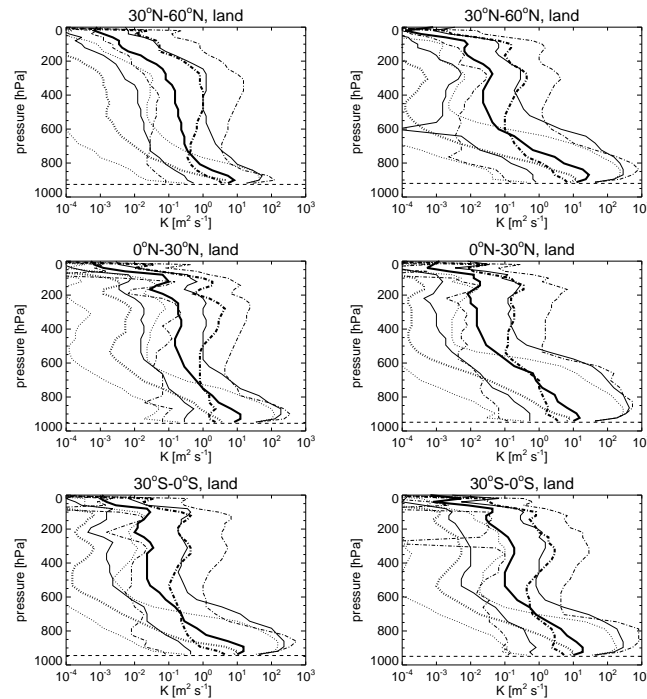


Figure 3.2: Profiles of K_z [m^2/s] in January (left) and July (right) 1993 over land as a function of pressure level. Profiles are given separately for 3 latitude bands. The solid line denotes the E3/E6 case, the dotted line the H3 case, and the dot-dashed line the L6 case. The thick lines denote the median, the thin lines denote the 10- and 90-percentile. The mean surface pressure level is indicated as the horizontal dashed line. For an overview of the different cases, see Table 3.1.

3.3 Results

3.3.1 Comparison of the diffusion coefficients

Zonally averaged K_z profiles from the E3/E6 scheme, the H3 scheme, and the L6 scheme are shown in Figure 3.2 for January and July 1993. High values between the

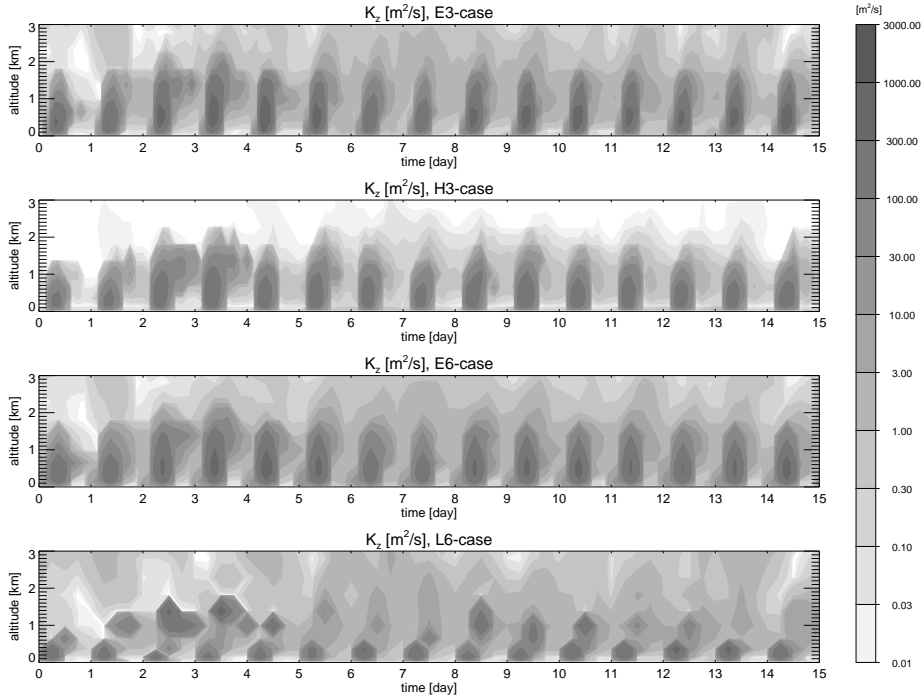


Figure 3.3: Time series of K_z profile [m^2/s] in lowest 3 km of the atmosphere at 80°E and 20°N (India) from 1 until 15 January 1993.

surface and 600 hPa correspond to the presence of an ABL, a local maximum around 300 hPa corresponds to strong vertical wind gradients in the upper troposphere. Between 900 and 600 hPa over land, the 90-percentile K_z value is almost a factor 10 smaller in winter than during summer. The largest differences between the data sets can be found above the ABL. In the free atmosphere the L6 diffusion coefficients are 2 to 3 orders of magnitude larger than the H3 diffusion coefficients. This is mainly due to the difference in the asymptotic mixing length : 450 m in the L6 case, 30 m in the H3 case. The E3/E6 coefficients in the free atmosphere have values between the L6 and H3 case.

We studied time series of K_z at many different sites. As an example, Figures 3.3, 3.4 and 3.5 give time series of the K_z profile in the lowest 3 km of the atmosphere at 3 different locations : at 80°E and 20°N (India) in January 1993, at 140°E and 20°S (Australia) in January 1993, and at 150°W and 30°N (Pacific Ocean) in July 1993. In the ABL, the profile of K_z in the H3 case is very similar to the E3/E6 case. The vertical extent of the intense K_z values is a bit smaller than in the E3/E6 case. In the H3 case, the values are also slightly less intense, except in the winter over the continent at mid-latitudes. Also in these time series, one can observe the very low values in the free troposphere in the H3 case. There is a slightly higher variability in the E3 than in the H3 case (see Figure 3.5), which might be due to the archival of K_z (E3) versus off-line diagnosis of K_z (H3) : only every 6 hours, new profiles of

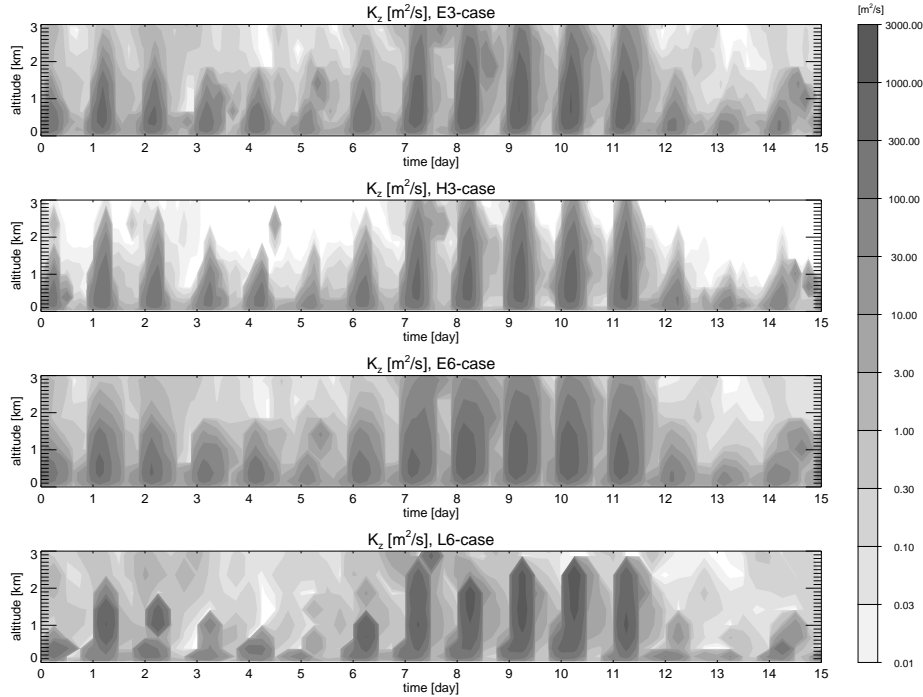


Figure 3.4: Time series of K_z profile [m^2/s] in lowest 3 km of the atmosphere at 140°E and 20°S (Australia) from 1 until 15 January 1993.

temperature, humidity and wind are used in the H3 case.

The K_z value in the L6 case differs often strongly from the other data sets. At mid-latitudes, E6 is much stronger in winter. Above sea, the vertical extent of the ABL is much smaller (see Figure 3.5). Also the profile of K_z is sometimes very different, because one finds locally sometimes very high K_z values in the L6 profile : above sea (see Figure 3.5), in the subtropics over land in the upper part of the ABL (see Figure 3.4), or as disconnected spots in Figure 3.3. Although the strong deviation for the L6 case which is caused by the local nature of the scheme, there is still a strong similarity with the other K_z profiles. This is due to the fact that the L6 K_z values are based on atmospheric profiles of temperature, humidity and wind, which carry the imprint of the ABL scheme used during ERA-40.

3.3.2 Evaluation of the model simulated atmospheric boundary layer height

We compared the 6-hourly ABL height from the ERA-40 data (E6), and the 3-hourly ABL height diagnosed in the H3 scheme with ABL heights observed in Cabauw and during the FIFE campaign. The calculated and measured ABL heights during the FIFE campaign are shown in Figure 3.6 (only a subset of the data is shown); for Cabauw they are shown in Figure 3.7 (all data is shown). The maximum value of the

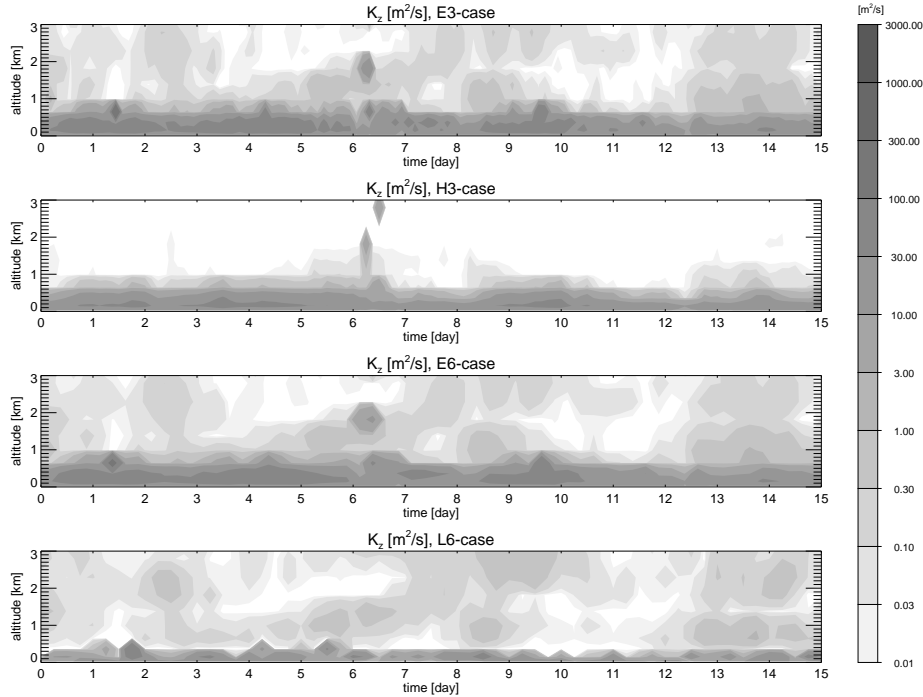


Figure 3.5: Time series of K_z profile [m^2/s] in lowest 3 km of the atmosphere at 150°W and 30°N (Pacific Ocean) from 1 until 15 July 1993.

height of the ABL is quite well represented both for the E6 and H3 case. Also the time of strongest growth and decrease is well represented.

Figure 3.8 gives a scatter plots of the measured ABL height during the FIFE campaign versus the modelled ABL height for the cases E6 and H3 separately. A distinction is made between measurements made during daytime and measurements made during nighttime. At the end of the day (observations before 21h00 LT) we see that the observations and measurements do not correspond very well (the model ABL height is much larger). At this time of the day, the ABL is hard to define anyway : a stable inversion layer is building up below the residual layer. Later during the night we see that the agreement between the observations and model is much better. It is clearly visible in Figure 3.8 that the ABL height with low as well as with high wind speeds corresponds well between model and observations. The H3 case gives a better agreement than the L6 case.

Also during daytime there is a good agreement. For both cases (E6 and H3), the modelled ABL height is larger than observed : the H3 ABL height corresponds however slightly better with the observations. The higher ABL height in the E6 case can be caused by the smaller coefficient for the excess of the parcel temperature under unstable conditions. It also shows that a 6-hourly resolution is rather coarse for describing the ABL height evolution.

Due to the limited amount of data in Cabauw, we only look at the time evolu-

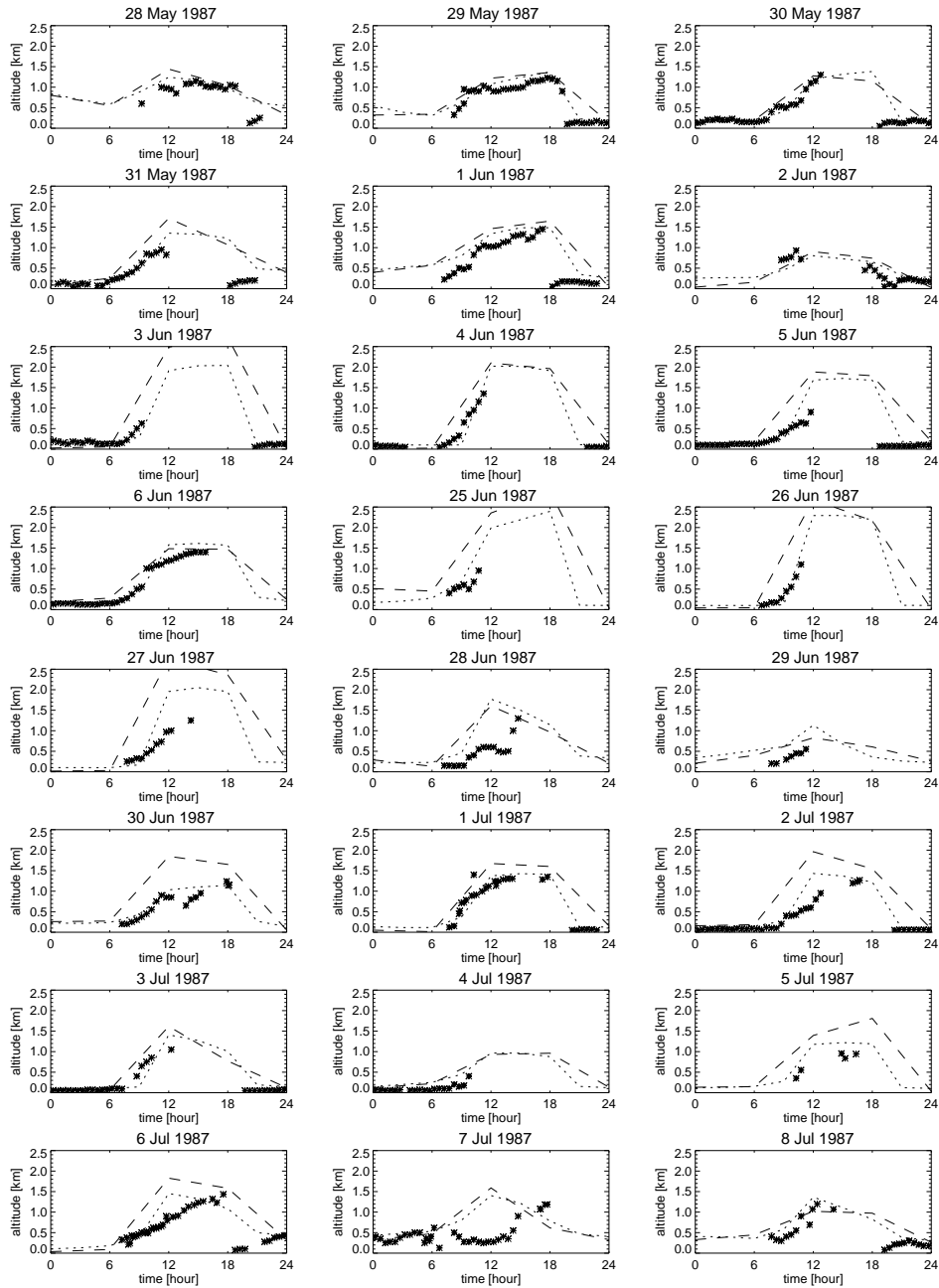


Figure 3.6: Time evolution of the ABL height during the FIFE campaign in 1987 and 1989 in the US. The stars denote the observed ABL height, the dashed line denotes the ABL height archived in the ERA-40 data (E6), the dotted line denotes the ABL height calculated in the H3 scheme. The time is expressed in GMT-6h.

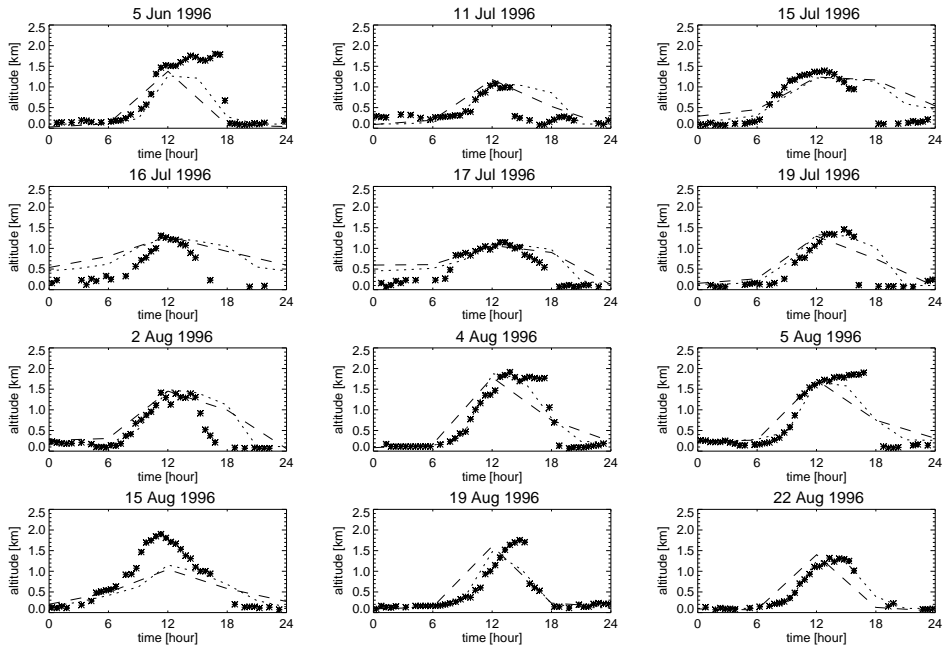


Figure 3.7: Time evolution of the ABL height during some days in June, July and August 1996 in Cabauw, the Netherlands. Symbol and line code as in Figure 3.6. The time is expressed in GMT.

tion of the ABL height in Figure 3.7. We see that the quality of the ERA-40 ABL height and the H3 ABL height are similar : for both schemes, the ABL height in the afternoon falls off in the model sometimes too fast, and is at night sometimes too high. Comparison of the ABL height between model and observations is hampered by representation errors in modelled fluxes, the presence of clouds during daytime, and limited space and time resolution of the model. *Bosveld et al.* [1999] have compared observed heat fluxes with modelled heat fluxes from ERA-15 at Cabauw. They found that the ECMWF model underestimates the amount of clouds at Cabauw, which leads to excessive surface heating, resulting in too large surface heat fluxes. Similar deficiencies seem to be present in the ERA-40 data.

Despite the rather limited comparison with measurements, we can conclude that the ABL heights as calculated during the ERA-40 project (E6) and with the H3 scheme, agree reasonably with the measurements during summer in mid-latitudes.

3.3.3 Comparison with ^{222}Rn observations in Freiburg and Schauinsland

We compared the simulated ^{222}Rn concentrations from the TM3 model with surface observations from Freiburg and Schauinsland. Time series of modelled and observed ^{222}Rn concentrations are shown in Figure 3.9 for the first 15 days of September 1993.

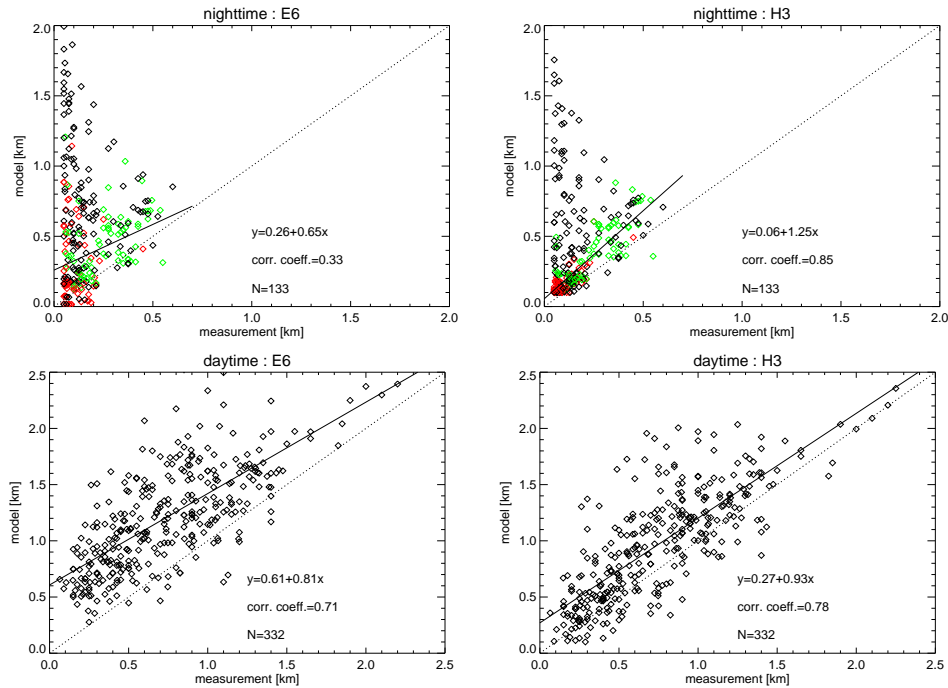


Figure 3.8: Scatter plot of the measured ABL height during the FIFE campaign versus the modelled ABL height for E6 (left) and H3 (right). In the upper panel the nighttime observations are shown : black signs refer to measurements before 21h00 LT, green signs (wind speed > 3 m/s) and red signs (wind speed < 3 m/s) refer to measurements after 21h00 LT. The regression line for the nighttime is only based on the observations after 21h00 LT. In the lower panel the daytime observations are shown.

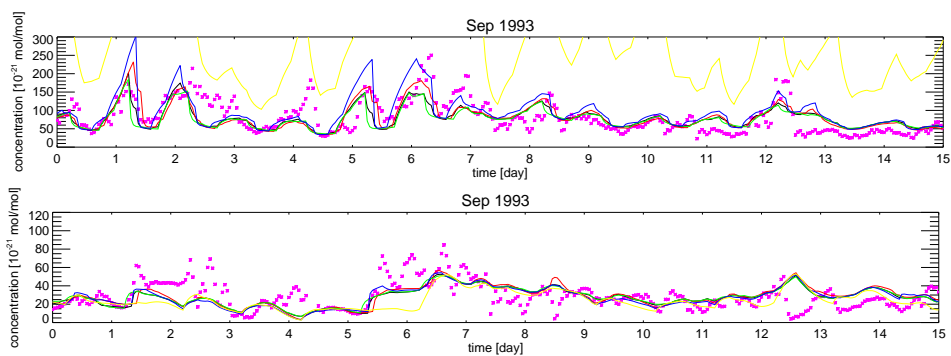


Figure 3.9: Time series of ^{222}Rn concentration [10^{-21} mol/mol] in first 15 days of September 1993 for Freiburg (upper panel) and Schauinsland (lower panel). The pink stars denote the observations, the lines denote the results from the model runs : using E3 data (black line), using H3 data (red line), using E6 data (green line), using L6 data (blue line), and using no diffusion (yellow line).

Table 3.2: Mean value of the ^{222}Rn concentration [10^{-21} mol/mol] in 1993 in Freiburg and Schauinsland.

| diffusion | Freiburg | Schauinsland |
|-----------|---------------|--------------|
| E3 | 102 ± 45 | 33 ± 15 |
| H3 | 110 ± 59 | 33 ± 16 |
| E6 | 98 ± 41 | 34 ± 15 |
| L6 | 125 ± 68 | 32 ± 16 |
| N | 501 ± 113 | 26 ± 17 |
| observed | 113 ± 70 | 37 ± 19 |

Table 3.3: Correlation of the modelled with the observed ^{222}Rn concentration in 1993 in Freiburg and Schauinsland. In column (a) the correlation of the modelled with the observed daily mean is given, in column (b) the correlation of the modelled with the observed hourly value, and in column (c) the correlation of the modelled with the observed residue (the residue is defined as the hourly concentration minus the daily mean concentration).

| diffusion | Freiburg | | | Schauinsland | | |
|-----------|----------------|-----------------|-----------------|----------------|-----------------|-----------------|
| | (a) (N=306) | (b) (N=7731) | (c) (N=7344) | (a) (N=243) | (b) (N=7250) | (c) (N=5832) |
| E3 | 0.870 | 0.773 | 0.498 | 0.589 | 0.508 | 0.282 |
| H3 | 0.871 | 0.790 | 0.522 | 0.528 | 0.455 | 0.242 |
| E6 | 0.871 | 0.759 | 0.449 | 0.596 | 0.509 | 0.262 |
| L6 | 0.844 | 0.735 | 0.484 | 0.538 | 0.477 | 0.286 |
| N | 0.704 | 0.648 | 0.364 | 0.400 | 0.347 | 0.125 |

Seasonal cycle of the modelled and measured ^{222}Rn -Radon concentration

The monthly mean values of the ^{222}Rn concentration, the correlation of the modelled with the observed daily mean values, and the correlation of the residues for the year 1993 in Freiburg and Schauinsland are shown in Figure 3.10 (the residue is defined as the hourly concentration minus the daily mean concentration). Table 3.2 gives the 1993 yearly mean ^{222}Rn concentration. All schemes reproduce the monthly mean values quite well, both in Freiburg and in Schauinsland. In Freiburg, the spread in mean concentration between the different diffusion schemes is about 20%. The L6 scheme results in the highest mean concentrations, the E6 scheme in the lowest mean concentrations. The E3 case gives almost similar results as the E6 scheme. In Schauinsland, the spread in the modelled result is much smaller (except in February), but the agreement with the measurements is smaller. For both stations, the correlation of the modelled with the observed mean daily value is higher than the correlation of the modelled with the observed hourly value (not shown), and the correlation of the modelled with the observed residue is smallest. It clearly shows that the variation of the ^{222}Rn concentration by large scale synoptic variability is well modelled, and that the variation of the ^{222}Rn concentration due to local and short time scale phenomena

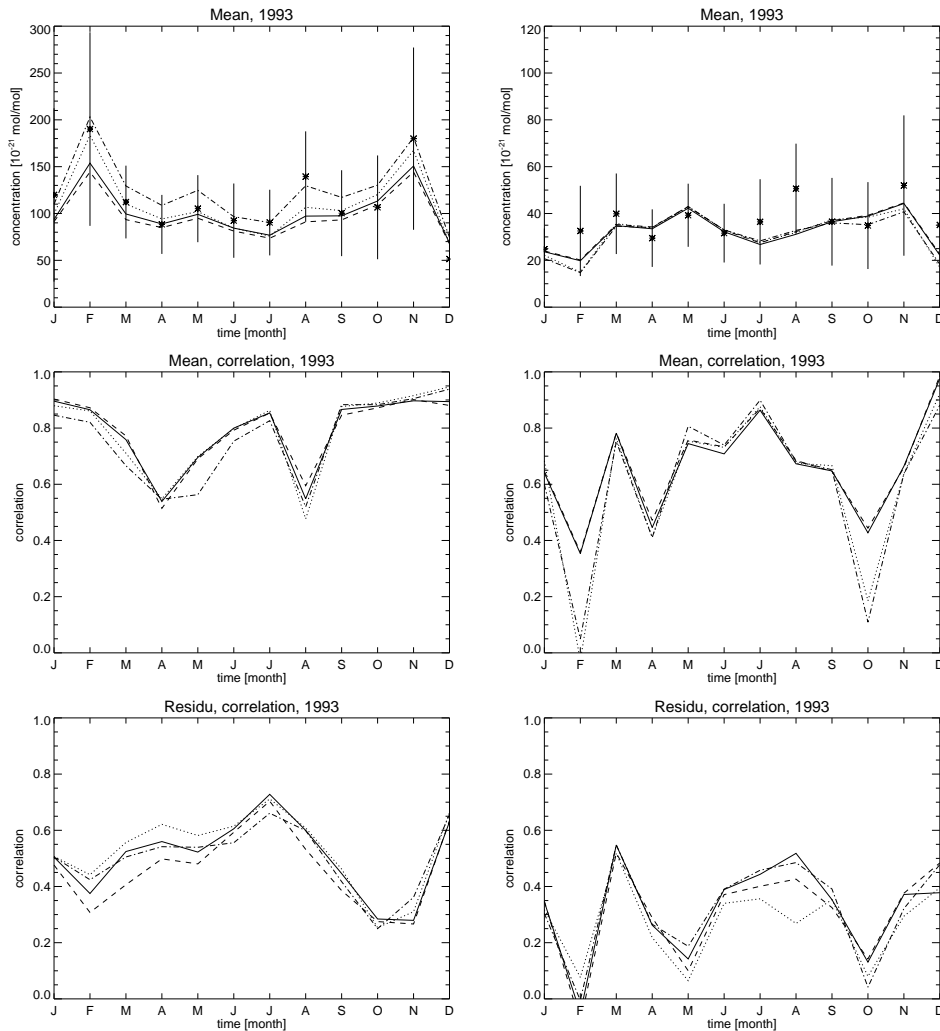


Figure 3.10: Monthly mean ^{222}Rn concentration (upper panels), correlation of the modelled with the observed mean daily value (middle panels), and correlation of the observed with the modelled deviation (lower panels), for Freiburg (left) and Schauinsland (right) in 1993. The stars denote the mean observations, the lines denote the results from the model runs : using E3 data (solid line), using H3 data (dotted line), using E6 data (dashed line), and using L6 data (dot-dashed line). The error bars (upper panels) show the 1σ standard deviation of the observations.

(like diffusion) is harder to describe. There is also a remarkable difference between the correlation of the modelled with the observed residue between the E6 and the E3 case, as well in Freiburg as Schauinsland. Table 3.3 gives the correlations between the observed and modelled ^{222}Rn concentration during 1993.

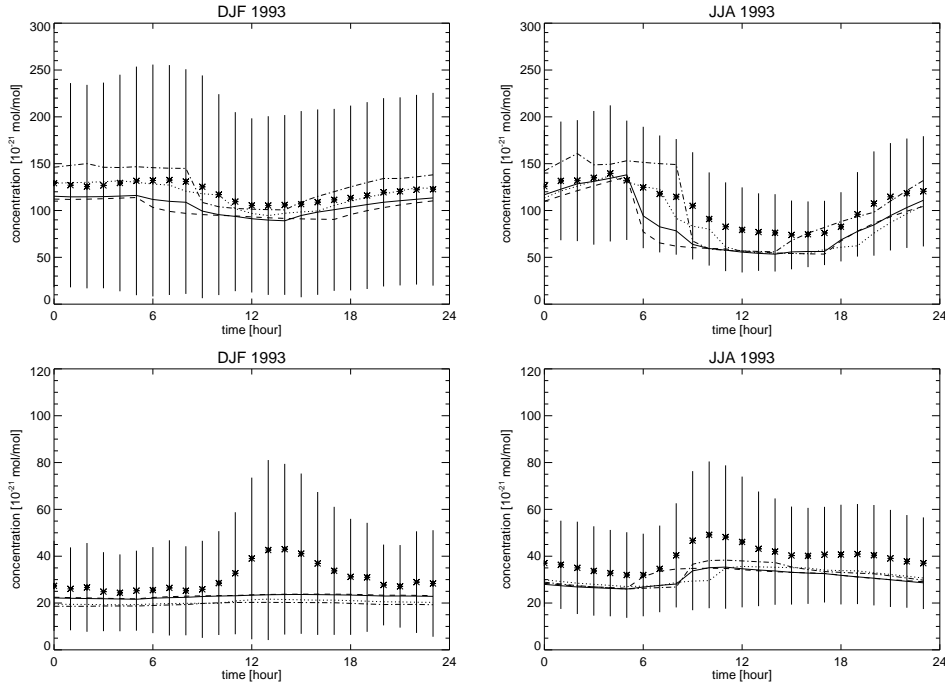


Figure 3.11: Daily cycle of observed and modelled ^{222}Rn concentration in Freiburg in DJF (upper left) and JJA (upper right) and in Schauinsland in DJF (lower left) and JJA (lower right) 1993. The stars denote the observed value, the lines denote the modelled values (line code is as in Figure 3.10). The error bars show the 1σ standard deviation of the observations.

Daily cycle

The mean daily cycle of the ^{222}Rn concentration in Freiburg and Schauinsland for December, January and February (DJF) and for June, July and August (JJA) are shown in Figure 3.11. In Freiburg, the daily cycle of the L6 case is largest. The E3 and E6 cases are very similar, except for the periods 6h00-9h00 and 15h00-21h00 (only in DJF) where the E6 case results in lower ^{222}Rn values. For all schemes the daytime concentrations are almost the same in JJA, while differences persist in DJF.

The daily cycle in the model simulations in Schauinsland is clearly not as strong as in the measurements. The deviation is quite large in DJF. In JJA, the simulations reproduce an increase in the concentration in the morning, but not large enough. The schemes differ in the time positioning of this increase. The second maximum in the measurements in JJA in Schauinsland is clearly not present in the model simulations (except for the H3 case). In Figure 3.11, one can clearly identify the times when the meteorological fields are updated.

The daily minimum, daily maximum and daily amplitude of the ^{222}Rn concentration are closely related to the daily cycle of the ABL turbulence. In Figure 3.12 the monthly mean value of the daily minimum, maximum and amplitude are shown.

It can be seen that in Freiburg these values correspond quite well with the measurements. The amplitude is slightly overestimated by the L6 scheme, while it is underestimated by the E3, H3 and E6 scheme. At the same time the correlation (not shown) of the modelled with the observed daily amplitude is considerably smaller than the correlation of the modelled with the observed daily minimum or daily maximum. In Schauinsland, we see that the minimum values in the model are in general higher than the observed minimum values, that the maximum values are in general smaller than the observed values, and that the modelled amplitude is therefore much smaller than the observed amplitude. The amplitude in the L6 case is largest. In Schauinsland, the variation between the schemes is much smaller than in Freiburg. All this shows that the coarse time and spatial resolution of the model limit its ability to reproduce variations on short time scales.

Ratio between ^{222}Rn concentration in Freiburg and Schauinsland

Because the stations at Freiburg and Schauinsland are close to each other (12 km), and the station at Schauinsland lies on a hill 900 m higher than Freiburg, these stations are quite well suited to study vertical concentration gradients in the model. Ideally we would prefer to use co-located observations, however tower measurements were not available to us.

The ratio of the ^{222}Rn concentration in Freiburg (300 m above sea level) and Schauinsland (1200 m above sea level) is assumed to be less sensitive to errors in the ^{222}Rn emission and to influences of large-scale transport (synoptic variability). In Figure 3.13 and Table 3.4 the correlation between the ratio in the model and the ratio in the measurements is given. This value of the correlation lies close to the correlation of the hourly value in Freiburg, and is significantly higher than the correlation of the hourly concentration in Schauinsland (see Table 3.3).

Because we expect a strong dependence of the aforementioned ratio on the ABL height, we have grouped the measured and modelled ratios as a function of the height of the ABL. For the height of the ABL we took the values as they are calculated in the H3 scheme : they are calculated every 3 hours and correspond well with observations (see Section 3.3.2). Because the ^{222}Rn data are available hourly, we interpolated the ABL height to an hourly resolution. (We also tried this with the 6-hourly ABL heights from the ERA-40 data set. We noticed however that this gave more noisy relationships due to the coarser time resolution of the E6 ABL height.)

In Figure 3.13 one can observe that the ratio becomes smaller as a function of the height of the ABL. We would expect the ratio to go to one when the ABL height reaches higher than the station in Schauinsland : one expects hyperbolic behaviour for ABL heights below 800-1000 m, and a sharp drop in the ratio around 800-1000 m. We see however that as well for the observed ratio as for the modelled ratio, the transition point is around 500 m, and not around 800-1000 m. This can be related to the coarse vertical resolution between 500 and 1000 m, the large scatter of the data, and the use of a modelled ABL height to deduce these curves. The E3/E6 scheme shows the strongest correspondence with the measurement, the H3 and L6 scheme show the worst correspondence. Also from this graph it is clear that the E3 and E6 case cause stronger mixing than the H3 and L6 case. In general this Figure 3.13 shows that, despite of the failure of the schemes to reproduce all the short time scale

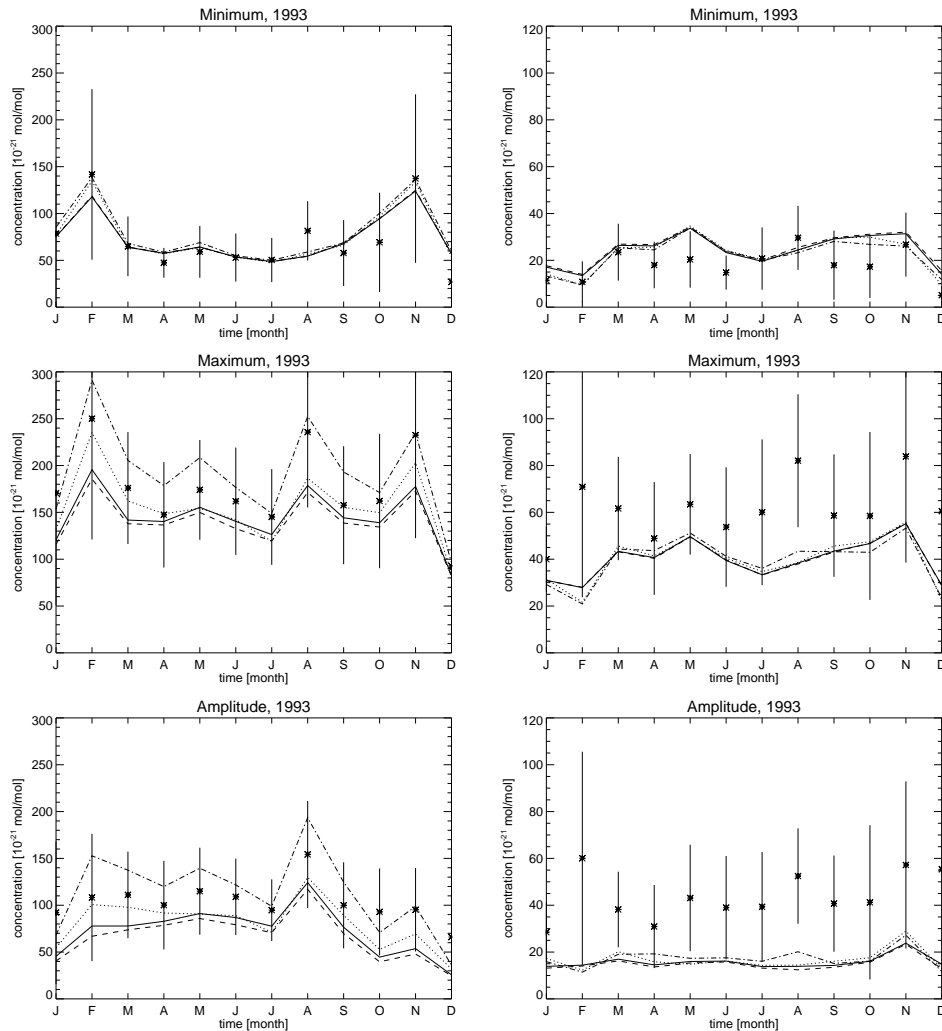


Figure 3.12: Monthly mean of the daily minimum (upper panels), daily maximum (middle panels) and daily amplitude (lower panels) in the ^{222}Rn concentration in Freiburg (left) and Schauinsland (right) in 1993. The stars denote the measurements, the lines denote the results from the model runs (line code as in Figure 3.10). The error bars show the 1σ standard deviation of the observations.

variations, the mean variations in the ratio are reasonably captured.

Time shift

The diffusive and convective mass fluxes are updated in the TM3 model every 3 or 6 hours. The updates have a strong influence on the modelled ^{222}Rn distribution (see Figure 3.11). The simulations show that the more frequent the updates are, the

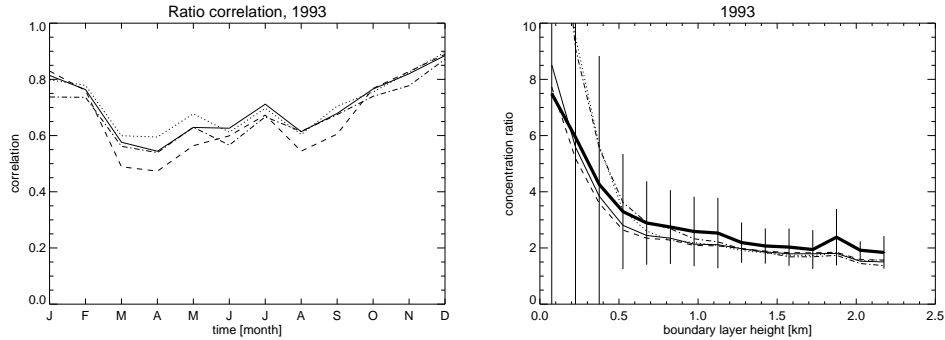


Figure 3.13: Left panel : correlation of the modelled with the observed ratio of the concentration in Freiburg and the concentration in Schauinsland. Right panel : mean ratio between the ^{222}Rn concentration in Freiburg and the concentration in Schauinsland as a function of the ABL height (calculated with the H3 scheme) for the year 1993. The thick line denotes the ratio derived from the observed concentrations, the other lines denote the ratios derived from the modelled concentrations using E3 data (solid line), using H3 data (dotted line), using E6 data (dashed line), and using L6 data (dot-dashed line). To calculate these curves, we binned all the hourly ABL height data in 15 bins with a width of 150 m, ranging from 0 up to 2250 m. The ABL height is taken from the H3 scheme. The error bars denote the 1σ standard deviation of the ratio derived from the observed concentrations.

Table 3.4: Correlation between the observed and modelled ratio of the ^{222}Rn concentration in Freiburg and in Schauinsland in 1993.

| diffusion | Freiburg/Schauinsland (N=6531) |
|-----------|-----------------------------------|
| E3 | 0.758 |
| H3 | 0.772 |
| E6 | 0.741 |
| L6 | 0.717 |
| N | 0.575 |

better the correspondence with the measurements is : E3 performs better than E6, H3 performs better than L6.

Averaging of diffusion coefficients over a certain time interval leads to a strong influence of the large diffusion coefficients during a part of this interval on the time-averaged diffusion coefficient, and thus on the concentration and transport in the tracer transport model. If one compares the E6 and E3 case, it shows up as an earlier start and a sustained prolongation of the low daytime ^{222}Rn values in Freiburg (see again Figure 3.11). Using instantaneous diffusion coefficients can maximally lead to a time shift of half the time step, while using a time-averaged value can lead in the extreme case to a time shift of almost the whole time step. This has a considerable influence in case of time steps of 6 hours. This might also play an important role for

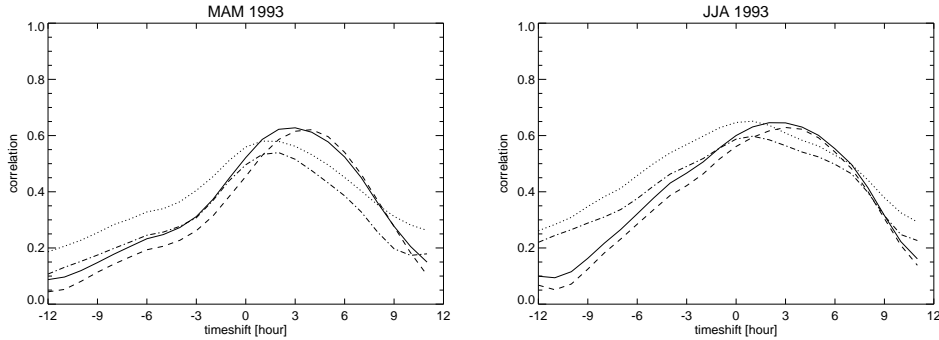


Figure 3.14: The correlation of the hourly modelled with the hourly observed ^{222}Rn concentration in Freiburg in MAM (left) and JJA (right) as a function of the time shift. Only the modelled concentration between 0h00 and 12h00 GMT is used. Values in the right hand part of the figure (positive time shifts) give the correlation of model concentrations with a later observation, values in the left part of the figure (negative time shifts) give the correlation of model concentrations with an earlier observation. Line code : using E3 data (solid line), using H3 data (dotted line), using E6 data (dashed line), and using L6 data (dot-dashed line).

other tracers than ^{222}Rn where chemistry and dry deposition come into play.

We have investigated this effect by correlating the modelled morning concentrations (from 0h00 until 12h00 GMT) with time-shifted observed concentrations. The correlation as a function of the applied time shift is shown in Figure 3.14 for the periods March-April-May (MAM) and JJA. The strongest time shift is found for the E6 and E3 case (E6 stronger than E3), which both use time-averaged diffusion coefficients. The time shift is smallest for the L6 and H3 case (instantaneous values). With an applied time shift for the morning concentrations of 3 hours for the E3 case, and up to 4 or 5 hours in the E6 case, the E3 and E6 case perform equally good (JJA) or better (MAM) than the H3 scheme. We have also correlated the modelled afternoon concentrations (from 12h00 until 24h00) with time-shifted observed concentrations. This resulted in slightly smaller time shifts with the highest correlation for shifts back in time in the E6 and E3 case (corresponding to persistent low ^{222}Rn concentrations at the end of the day). Due to the opposite sign of the shifts between morning and afternoon, and due to a probable geographical dependence of this shift, it is not easy to implement a remedy. It shows the necessity of high sampling frequency of data.

3.3.4 Comparison with 222-Radon observations in Cincinnati and Socorro

Figure 3.15 gives the observed and modelled monthly mean surface concentration in Cincinnati for 8h00 and 15h00 LT from January 1959 until February 1963. The seasonal variation in the observations is much larger than in the model. *Gold et al.* [1964] attribute this to freezing minimizing the emission in winter, and to an increasing emanation rate of ^{222}Rn due to the decrease of the moisture content of the soil

Table 3.5: Correlation of the observed with the modelled ^{222}Rn concentration in Cincinnati and Socorro.

| diffusion | Cincinnati | | Socorro |
|-----------|-------------------|---------------------|------------------------|
| | morning (N=48) | afternoon (N=48) | daily cycle (N=288) |
| H3 | 0.523 | 0.388 | 0.823 |
| E6 | 0.639 | 0.399 | 0.714 |
| L6 | 0.711 | 0.421 | 0.759 |

Table 3.6: Mean observed and modelled ^{222}Rn concentration [10^{-21} mol/mol] at Socorro. The observations have been made between November 1951 and June 1957. The modelled concentrations are mean values for the period January 1959 until December 1962.

| diffusion | Socorro |
|-----------|--------------|
| H3 | 113 ± 44 |
| E6 | 91 ± 44 |
| L6 | 121 ± 44 |
| observed | 158 |

with increase of temperature in summer. This dependence of the emanation of ^{222}Rn on meteorological conditions is not included in the TM3 model. The poor correspondence of the morning data is probably also caused by a bad representation of the night and morning ^{222}Rn profiles in the global model due to the large thickness of the lowest model layer (about 60 m), resulting in lower modelled ^{222}Rn concentrations under very stable meteorological conditions. Another main reason for discrepancy is that the morning measurements represent more local conditions, which may not fulfil the $1 \text{ atoms cm}^{-2} \text{ s}^{-1}$ emission rate. Although the observed morning concentration is quite different from the modelled morning concentration, the afternoon concentrations agree quite well with the observations (see Figure 3.15). As for the ^{222}Rn concentrations in Freiburg, we see that the L6 scheme leads to the highest morning concentrations, while the E6 case gives the lowest values. The H3 case gives intermediate values.

Measurements of ^{222}Rn have been made at Socorro from November 1951 until June 1957. These data were used to generate monthly mean daily cycles of the ^{222}Rn concentration [Wilkening, 1959]. We have compared the monthly mean daily cycles from January 1959 until February 1963 with these data. The result can be seen in Figure 3.16. The afternoon values for E6, L6 and H3 are very similar. The mean values are given in Table 3.6.

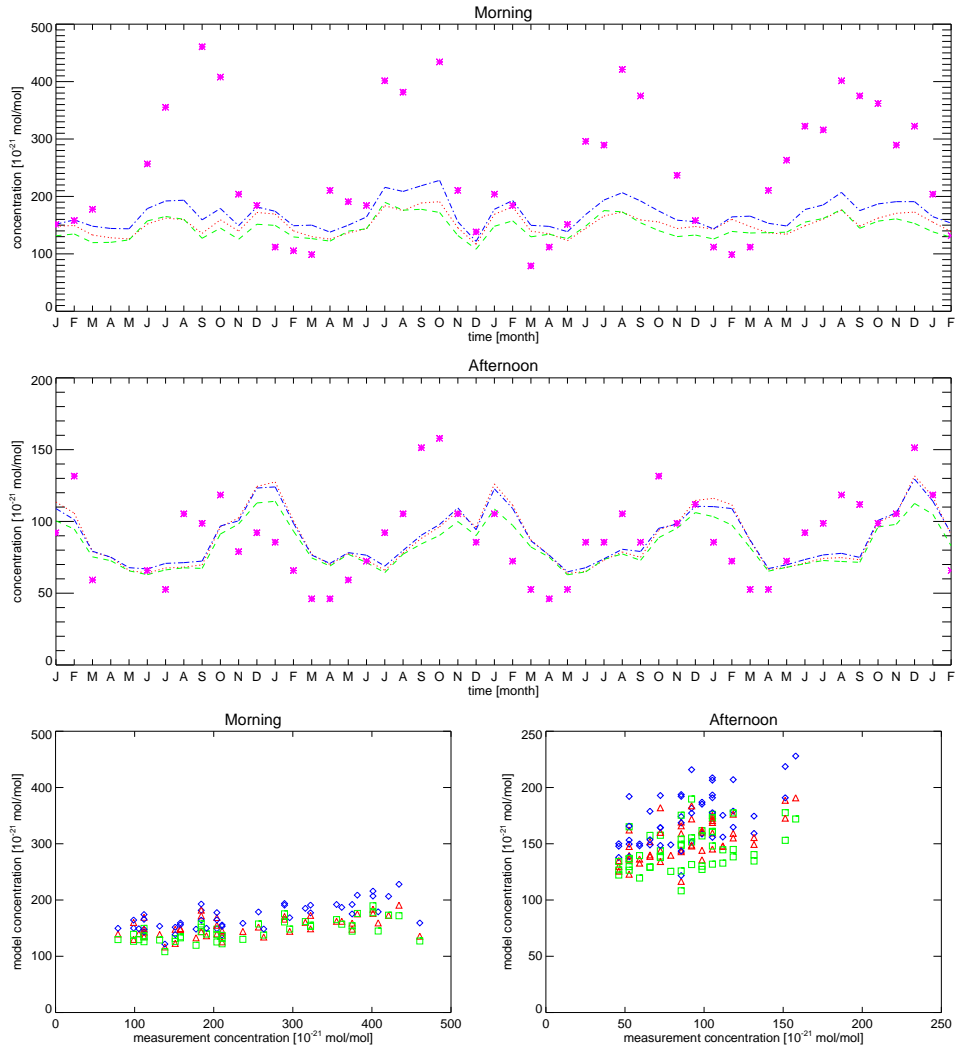


Figure 3.15: Monthly mean morning (upper panel) and afternoon (middle panel) ^{222}Rn concentration from January 1959 until February 1963 at Cincinnati. Observed concentrations (pink stars) and modelled concentrations using H3 data (dotted red line), E6 data (dashed green line), and L6 (dot-dashed blue line) are shown. Scatter plots of the monthly mean morning (lower left) and afternoon (lower right) ^{222}Rn concentration are shown using H3 data (red triangles), using E6 data (green squares), and using L6 data (blue diamonds).

3.3.5 Global ^{222}Rn distribution

In order to see the effect of diffusive transport on the free troposphere concentrations of tracers, we now consider the budgets and transport of ^{222}Rn . Diffusion leads in general to differences of up to 30% in the zonal mean ^{222}Rn concentration compared to

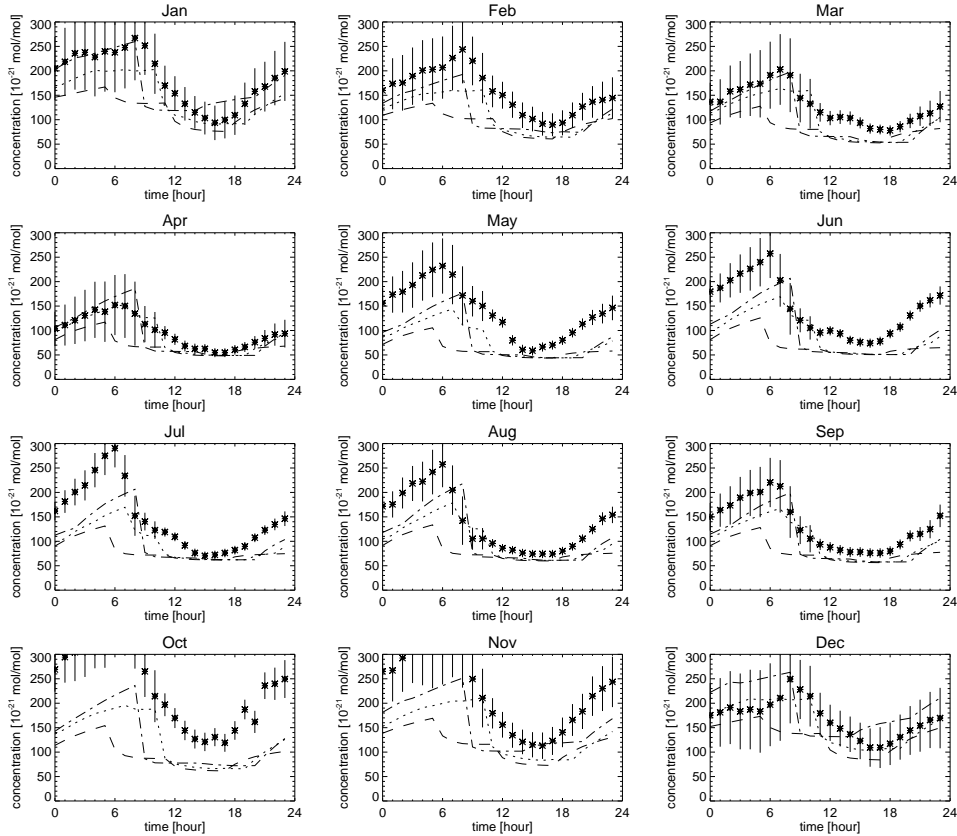


Figure 3.16: Monthly mean daily cycle of ^{222}Rn concentration from January 1959 until February 1963 in Socorro : measured (stars) and modelled using H3 (dotted line), using E6 (dashed line) and using L6 (dot-dashed line). The observed monthly mean daily cycles are based on measurements from November 1951 until June 1957. The error bars denote the 1σ standard deviation of the modelled concentration.

the case where no diffusion is applied in the TM3 model. Smaller diffusion coefficients lead to higher ^{222}Rn concentration in the lowest layers and higher concentrations higher up in the atmosphere. The influence of diffusion is strongest in the parts of the atmosphere with strong downward large-scale motion like the subtropics, and/or where there is no vertical mixing by convection. In Figure 3.17, the relative difference in the zonal mean ^{222}Rn concentration between the E3 and H3 case and between the E3 and L6 case is shown for DJF 1993. In Figure 3.18, the relative difference in ^{222}Rn concentrations at 700 hPa between the E3 and H3 case and between the E3 and L6 case is shown for JJA 1993.

If we compare the E6 and E3 case, the zonal mean differences are everywhere smaller than 1% (not shown).

If we compare H3 and L6 with E3, we always see that the ^{222}Rn concentration in the lowest 500-1000 m is lower for E3, while above 1 km it is higher for E3. This

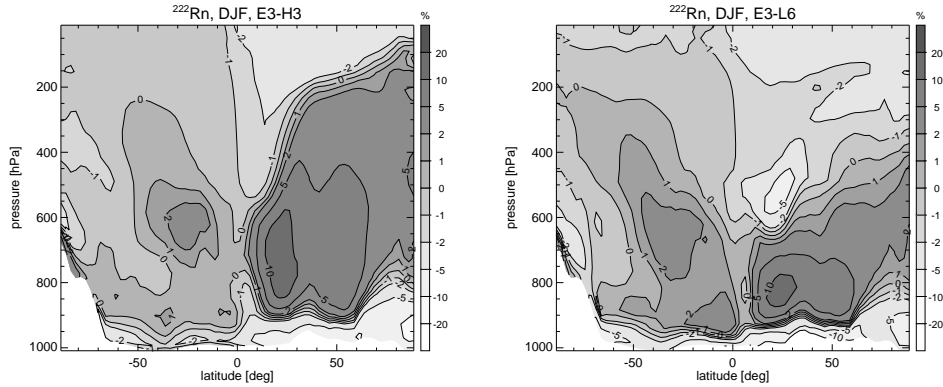


Figure 3.17: Zonal mean relative difference (%) in ^{222}Rn concentration between E3 and H3 (left panel) and between E3 and L6 (right panel) for DJF 1993.

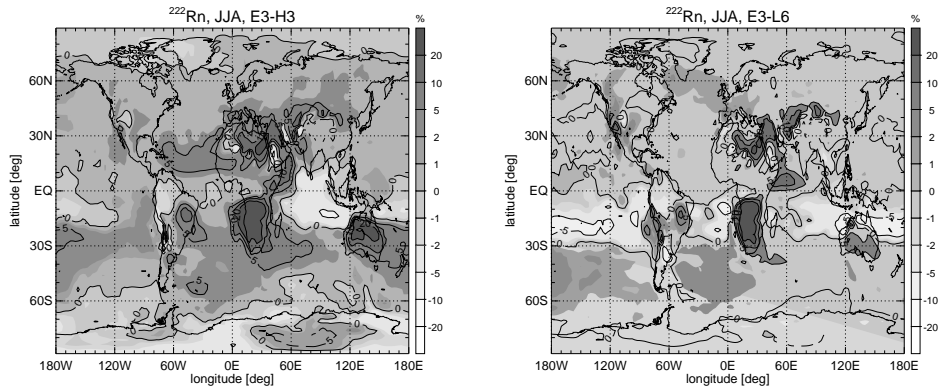


Figure 3.18: The relative difference (%) in ^{222}Rn concentration at 700 hPa between E3 and H3 (upper panel) and between E3 and L6 (lower panel) for JJA 1993.

higher concentration for H3 and L6 in the lowest layers of the atmosphere, leads to higher ^{222}Rn concentrations in the upper troposphere by convection, which transports the surface air to high altitudes in the tropics. We see in JJA around the North Pole higher concentrations in the lowest kilometre in the E3 case. Because there is almost no ^{222}Rn emission north of 60°N , the concentration is higher in the free troposphere than at the surface (via long range transport). The increased mixing in the E3 case will then transport this ^{222}Rn downward.

If we compare the H3 and E3 case, we see much higher concentrations in the E3 case in almost the whole troposphere (except the lowest layers). The stronger diffusion gives more mixing. Large differences can be found around 700 hPa in the winter subtropics, i.e. around 20°N in DJF and around 20°S in JJA.

If we compare L6 and E3, we see the effect of stronger diffusion in the free troposphere in the winter subtropics for L6. Through more intense and higher mixing, the ^{222}Rn concentrations are 5 to 10% higher around 500 hPa and 15% lower around 800 hPa in DJF around 20°N and in JJA around 20°S.

Because ^{222}Rn has a short lifetime (about 5.5 days), we can deduce the global mean net vertical ^{222}Rn transport and changes therein due to differences in the diffusion schemes from its mean distribution. The net flux profile of ^{222}Rn is an indication of how the vertical diffusion will affect other tracers. This flux strongly depends on the source characteristics of the tracer (which are uniform on the continent for ^{222}Rn), and it is also strongly dependent on the sinks and the lifetime. In Figure 3.19, we show the net global vertical ^{222}Rn fluxes. All fluxes are expressed relative to the E3 case. The differences in net global transport are maximally 4%. The difference is largest around 900 hPa. The difference between E3 and E6 are less than 1%. The net transport for the H3 case is stronger than the E3 case above 500 hPa, and stronger for the L6 case than the E3 case above 700 hPa. The interaction between the convection and the ABL turbulence is clearly visible. One can observe the following pattern : weaker transport in the lower troposphere leads to stronger transport in and into the upper troposphere. As mentioned before, if the turbulent transport is weaker, more ^{222}Rn remains in the lowest atmospheric levels, which can then be transported to the upper troposphere via fast convective transport. Higher concentrations at the surface (due to less turbulent transport) thus lead to higher concentrations in the upper troposphere.

In general, one can see in Figure 3.19 that the differences in concentration and transport are quite small. This can partly be attributed to the fact that diffusion is not the only way of vertical transport. If the diffusive transport changes, it will be partly compensated by convective or large-scale vertical transport.

3.4 Conclusions

We have studied the application of archived and off-line diagnosed vertical diffusion coefficient from the ERA-40 project for making simulations with chemistry transport models. We compared 4 sets of vertical diffusion coefficients : (E3) 3-hourly archived coefficients based on a non-local scheme, (H3) 3-hourly off-line diagnosed coefficients based on a non-local scheme, (E6) as E3 but 6-hourly values, and (L6) 6-hourly off-line diagnosed coefficients based on a local diffusion scheme. We also compared the ABL height of the sets E6 and H3.

With the results of these comparisons in mind, we want to return to our research questions formulated in Section 3.1. Comparison with ABL height measurements shows that the ABL height (question 1) archived in ERA-40 (E6) and the ABL height from the 3-hourly off-line non-local scheme (H3) are in reasonable agreement with the ABL height observations performed in Cabauw and during the FIFE campaign. The time resolution of 3 hours makes the H3 ABL height more valuable than the 6-hourly E6 ABL height.

Vertical diffusion coefficients can be calculated accurately off-line (question 2a). The off-line diagnosed set of non-local diffusion coefficients (H3) is based on a parameterisation that is very similar to the parameterisation used in the ECMWF model

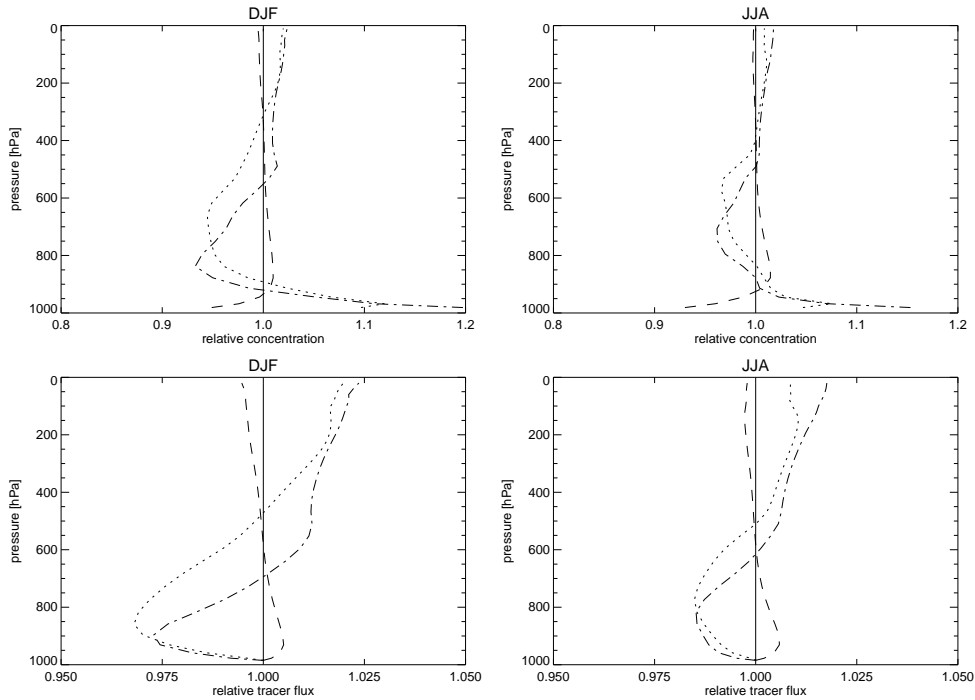


Figure 3.19: Profiles of the global mean ^{222}Rn concentration (upper panels) and profiles of the global mean net upward ^{222}Rn flux (lower panels) are shown for DJF and JJA 1993. The concentration and flux of E3 (solid), H3 (dotted), E6 (dashed), L6 (dot-dashed) are expressed with respect to the flux of E3.

to generate the archived diffusion coefficients (E3/E6). We find that the results are quite similar between the E3 and H3 case (both with 3-hourly time resolution), and that the apparent difference can be attributed to small differences in the implementation of the parameterisation (different asymptotic mixing length, different stability functions, present or absent detrainment formulation). Hence the off-line diagnosis of diffusion coefficients reproduces quite well the archived diffusion coefficients.

The K_z values from the local scheme in the L6 case (question 2b) were sometimes quite different from the non-local scheme E6. Although the mean values of the diffusion coefficients in the lower troposphere were larger for the L6 case than for the E6 case, the instantaneous values led to smaller ABL transport. This could be attributed to the fact that the daytime ^{222}Rn concentrations are not very sensitive to the much larger daytime L6 diffusion coefficients, while the smaller night time diffusion coefficients have a strong impact on the night concentration. Sometimes the K_z values of L6 and E6 were still surprisingly similar. This is due to the fact that the underlying profiles of temperature, humidity and wind to drive the off-line L6 scheme are taken from the ECMWF model.

Comparison of ^{222}Rn simulations from the TM3 model with surface ^{222}Rn observations in Freiburg, Schauinsland, Cincinnati, and Socorro shows that the 3-hourly E3

and H3 (question 3a) schemes perform better than the 6-hourly E6 and L6 schemes. Using the 3-hourly coefficients results in a better description of the daily cycle of the ^{222}Rn concentration. This might have an impact on tracers that undergo fast photochemistry or are affected by dry deposition or vegetation.

It is also shown that using time-averaged diffusion coefficients (question 3b) can lead to time shifts of the daily cycle of tracer concentrations and stronger vertical transport than instantaneous diffusion coefficients.

Finally, some recommendations can be formulated. First, using the E3 scheme resulted in higher ^{222}Rn concentrations in the free troposphere than using the H3 scheme. The seasonal zonal and monthly mean ^{222}Rn concentration can differ up to 10%. Earlier studies with the TM3 model suggested that vertical mixing was underestimated. As mentioned before, this difference can be partially attributed to the use of the detrainment formulation at the top of the ABL for the E3 case, a larger asymptotic mixing length, and differences in the stability functions. It would be therefore worthwhile making these changes in the off-line H3 scheme.

Secondly, the non-local schemes that are used here, do not contain a counter gradient term. Also here, it could be interesting to investigate whether including the counter gradient term could further improve the agreement with measurements.

Finally, the large discrepancy in ^{222}Rn concentration between model and observations at some sites suggests that a more physical based emanation rate of ^{222}Rn and perhaps a higher spatial resolution should be used.

Acknowledgements

This evaluation of diffusion coefficients would not have been possible without the atmospheric monitoring work of H. Sartorius from the Federal Office for Radiation Protection in Freiburg, Germany, who provided ^{222}Rn data from the locations Freiburg and Schauinsland. We thank H. Klein Baltink for the ABL height measurement data from Cabauw. ECMWF ERA-40 data used in this study have been provided by ECMWF. This work was supported by the Netherlands Organization for Scientific Research (NWO) and by the European Union under contract number EVK2-CT-2002-00170 (RETRO).

Parameterisation of the production of NO_x by lightning for global chemistry transport models

Abstract

The temporal and spatial variability of NO_x production by lightning is notoriously difficult to simulate in 3-dimensional global atmospheric chemistry models. Lightning therefore leads to large uncertainties in the free tropospheric NO_x budget. We have compared several descriptions of the horizontal and vertical distribution of this NO_x source and evaluated them against observations of the LINOX, SONEX, PEM-TROPICS A and EULINOX campaigns performed in the period 1996-1998.

The ECMWF 45-year reanalysis (ERA-40) data set contains archived convective mass fluxes that allow the comparison of archived and off-line diagnosed convective mass fluxes for NO_x production by lightning. We found that using archived fluxes in the lightning parameterisations gives a better description of lightning.

We also compared the standard TM lightning parameterisation where the flash frequency scales linearly with the convective precipitation, and a more recently developed parameterisation where the lightning flash frequency depends non-linearly on the updraft velocity and the cloud top height. The latter parameterisation appeared to be rather sensitive to the vertical wind speed in the updrafts in the model, which forced us to introduce a slightly modified parameterisation.

Finally, we have studied the vertical redistribution of NO_x produced by lightning. We have compared the use of prescribed profiles to describe the lightning source, versus a simple explicit description of the vertical redistribution that depends on the convective mass flux profile. This latter description was found to be able to reproduce the typical C-shaped profiles observed in thunderstorms.

4.1 Introduction

Nitrogen oxides ($\text{NO}_x = \text{NO} + \text{NO}_2$) play a pivotal role in the reactions that determine the O_3 concentration in the atmosphere [*Fishman and Crutzen, 1978*]. Many different sources contribute to the NO_x distribution in the troposphere. Fossil fuel burning, biomass burning, aircraft emissions, stratosphere-troposphere exchange, soil emissions, NH_3 -oxidation and lightning are the main sources of NO_x in the tropo-

sphere. Lightning is probably the largest free tropospheric source of NO_x. The uncertainties in the production of NO_x by lightning (LNO_x) are very large. Estimates of LNO_x vary roughly between 2 and 20 Tg[N]/y.

Because O₃ is a greenhouse gas [*Ramanathan and Dickinson, 1979*], the knowledge of NO_x concentrations is important for global climate studies. Since the radiative forcing of O₃ is rather sensitive to its vertical distribution [*Lacis et al., 1990*], and since the lifetime of NO_x is very sensitive to temperature and altitude [*Ridley et al., 1996*], it is crucial to understand the vertical distribution of NO_x production in the troposphere, especially in the tropics.

Lightning is produced in thunderstorms where strong updrafts and the presence of hydrometeors, lead to charge separation [*Williams, 1985*]. Therefore, most lightning parameterisations in chemistry transport models (CTMs) are based on meteorological variables related to convection : convective precipitation, convective mass flux (profile), cloud top height, cloud cover, updraft top height, or a combination of these. Both the horizontal and vertical distribution correlate to some extent with these parameters. Often, some of these parameters are not archived in meteorological data sets, and therefore have to be diagnosed off-line in order to apply a certain parameterisation of LNO_x. The European Centre for Medium-range Weather Forecasts (ECMWF) reanalysis project (ERA-40) aimed at providing a consistent time series of the state of the global atmosphere for the period 1957-2002 [*Simmons and Gibson, 2000*]. This data set also contains archived convective mass fluxes, which can be used in the parameterisation for the LNO_x production.

In lightning parameterisations, the horizontal distribution of LNO_x depends to a large extent on the lightning flash frequency. Here, we will on the one hand use the standard TM lightning parameterisation where the flash frequency is based on a linear relation between flash frequency and convective precipitation [*Meijer et al., 2001*]. This parameterisation is based on observations performed during the EULINOX campaign in July 1998 over central Europe. From cloud top height, convective precipitation and total ice cloud content, *Meijer et al.* [2001] have shown the convective precipitation to be the best proxy for the lightning flash frequency. On the other hand, we will use a parameterisation that uses the mean convective upward wind speed and the height of the convective cloud to calculate the lightning frequency [*Grewe et al., 2001*]. These two parameterisations have not been closely compared yet.

Cloud resolving models have been used to calculate the lightning flash frequency and LNO_x production by thunderstorms at high spatial resolution [*Pickering et al., 1998; Zhang et al., 2003*]. However, including cloud-resolving models in global atmospheric models would be very computationally expensive. Therefore the three profiles calculated by *Pickering et al.* [1998] for typical atmospheric conditions (continental mid-latitude, continental tropical and ocean tropical) are often used in global models to give the vertical distribution of the LNO_x production (where one usually scales the prescribed profiles with the model cloud top). These profiles describe the effect of the production of LNO_x in a cloud including its rapid up- and downward transport by convection in the cloud. Using these 3 profiles in global atmospheric models implies that one allows only very limited variability of the vertical distribution of LNO_x. Alternatively, one might ask the question if the information in convective mass flux profiles cannot be used to describe the effect of vertical redistribution by

updrafts and downdraft on produced LNO_x. Convective parameterisations in global models aim to describe the large-scale effect of convection on momentum, energy, temperature, water vapour and other tracers. From the point of view of atmospheric composition, convection is important because it can very rapidly transport pollutants from the boundary layer into the free and upper troposphere, where their lifetime is usually substantially longer. When tracers are horizontally quite well homogeneously distributed, the effect of this transport is reasonably well described by applying convective parameterisations on the whole content of the grid cells. However, to describe the effect of convection on LNO_x, another approach is needed. NO_x production by lightning is not homogeneous over the grid cells of global models, but concentrated at certain locations within the storm cells. Lightning flashes originate from the electric charge centre, which is often near the centre of the cloud, where strong ascending winds are present. Therefore, the LNO_x is more strongly influenced by convection than the tracers in the environmental air. Here we try to model this by using the available information about convection to redistribute the LNO_x in the vertical. In a first step, the production of NO_x is calculated and inserted only in those parts of the model cells occupied by convective clouds, exactly at the height where it is produced. In a second step this LNO_x is redistributed in the vertical using the convective meteorological information. This finally gives an effective vertical distribution of the LNO_x.

The scientific questions we will address here are : (i) Do archived convective fluxes give a better description of lightning? (ii) Does the recently developed updraft velocity approach for the lightning flash frequency performs better than the convective precipitation approach? (iii) Can the convective mass fluxes themselves be used to redistribute the produced NO_x in the vertical?

In Section 4.2 the TM4 model and the different lightning parameterisations are described briefly. In Section 4.3 we will compare the horizontal and vertical distributions of LNO_x production resulting from the different parameterisations. In Section 4.4 we will compare the results from the parameterisations in the TM4 model with aircraft measurements. In Section 4.5 we present our conclusions and offer some discussion.

4.2 Methods

4.2.1 The TM4 model

The chemistry transport model TM4 (Tracer Model Version 4) is a global atmospheric model which is used to evaluate the atmospheric composition and changes herein caused by natural and anthropogenic changes [*van Noije et al.*, 2004; *Dentener et al.*, 2003a,b; *Lelieveld and Dentener*, 2000; *Meijer et al.*, 2000; *Dentener et al.*, 1999; *Houweling et al.*, 1998; *van Velthoven and Kelder*, 1996]. The TM4 model has a regular longitude-latitude grid and hybrid σ -pressure levels.

The meteorological state of the atmosphere is described by data from the ECMWF, which is available as 3- or 6 hourly fields, either from the operational model or from the ERA-40 project. The ECMWF model presently has 60 hybrid σ -levels from the surface up to 0.1 hPa. For application in the TM4 model the meteorological data is interpolated or averaged from the original horizontal resolution (e.g. for the ERA-40

data from either T159 spherical harmonics truncation or an N80 reduced Gaussian grid, which corresponds to a resolution of about $1.125^\circ \times 1.125^\circ$) and 60 layers to the desired TM4 grid cells [Bregman *et al.*, 2003] with a horizontal resolution of $6^\circ \times 4^\circ$ or $3^\circ \times 2^\circ$. Some of the two-dimensional meteorological fields (such as convective precipitation or surface latent heat flux) are transformed by the pre-processing onto an intermediate high resolution regular $1^\circ \times 1^\circ$ grid. The ERA-40 data is available for the years 1957 to 2002. It contains more meteorological fields than most other data sets : it includes vertical diffusion coefficients, convective mass fluxes, and convective detrainment rates that have not been archived before by ECMWF.

For advection of the tracers, the TM4 model uses the slopes scheme developed by Russell and Lerner [1981]. The diffusion is calculated with a non-local diffusion scheme based on Holtslag and Boville [1993], Voegelezung and Holtslag [1996], and Beljaars and Viterbo [1999]. To describe the convection, we can either use the archived convective mass fluxes, or use the off-line diagnosed convective mass fluxes.

TM4 contains a CBM-4 scheme [Howeling *et al.*, 1998] modified for tropospheric chemistry. It includes full HO_x-NO_x-SO_x-CO-CH₄-NMHC chemistry. In total 38 gaseous constituents are considered, of which 23 tracers are transported. 110 gas phase reactions and 24 photolysis reactions are taken into account. Dry deposition is accounted for by a resistance chain-based parameterisation [Ganzeveld *et al.*, 1998]. The wet deposition is based on a parameterisation of Junge and Gustafson [1957], and Langner and Rodhe [1991]. The heterogeneous removal of N₂O₅ on sulphate aerosols has been accounted for by using a parameterisation by Dentener and Crutzen [1993]. The annual totals and spatial distributions of the emissions of anthropogenic NMHC, anthropogenic CO, isoprene, soil and industrial NO_x are based on $1^\circ \times 1^\circ$ GEIA, POET and EDGAR-V2.0 emission inventories [Olivier *et al.*, 2003; Benkovitz *et al.*, 1996; Olivier, 1996; Guenther, 1995; Yienger and Levy, 1995]. Since the chemical scheme does not include sufficient stratospheric chemistry, a zonally and monthly mean O₃ climatology [Fortuin and Kelder, 1998] scaled with TOMS total O₃ measurements is prescribed above 50 hPa. HNO₃ transport from the stratosphere into the upper level of the TM4 model is accounted for by fixing the O₃/HNO₃ ratio in the model top layer, based on UARS derived O₃/HNO₃ ratios at 10 hPa.

4.2.2 Convection

The off-line parameterisation of the convection is based on Tiedtke [1989]. Based on the evaporation (surface latent heat flux), the moisture convergence, and profiles of temperature, humidity, and vertical wind, an updraft plume of rising air, and a downdraft plume of sinking air are calculated. The parameterisation distinguishes three types of convection : shallow, deep, and mid-level convection. In each column, only one type of convection can be present.

A model cloud (see left panel of Figure 4.1) has a cloud base, a cloud top and a level of free sinking. In the updraft air is taken from the layers below the cloud base and transported to the top of the cloud where it is detrained in the top one or two layers of the cloud. Between the cloud base and cloud top, there is turbulent mixing from the updraft plume with the environmental air at the sides of the updraft plume. This mixing is described with a turbulent entrainment and detrainment rate. In the downdraft air is transported from the level of free sinking downward and detrained

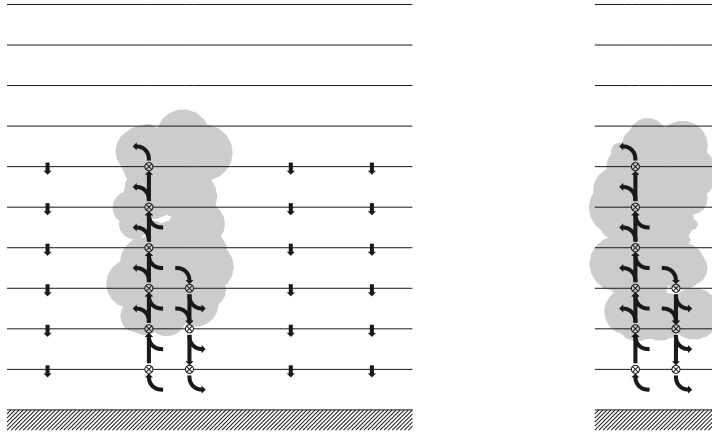


Figure 4.1: Left : the large-scale effect of convection on horizontal homogeneous distributed tracers in a grid box is modelled as a kind of pumping (updrafts, downdrafts, and subsidence). Right : to simulate the transport effect on LNO_x , all the convective activity of updrafts and downdrafts is assumed to act only on a small fraction of the grid box.

below the cloud base. Between the level of free sinking and the cloud base mixing occurs with environmental air described via turbulent entrainment and detrainment. In addition to the updraft and downdraft, there is also compensating subsidence to account for mass balance

Within the ERA-40 project, the ECMWF for the first time archived convective up- and downward mass fluxes, as 3 or 6-hourly averages. The convective parameterisation in the ECMWF model is more advanced than the convective parameterisation in the TM4 model. As a consequence, the ECMWF model has updrafts that reach higher, and the detrainment at the top of the cloud is not restricted to 1 or 2 model layers. The downdrafts in the archived data are much less intense than in the off-line diagnosed case. More detailed differences are described in *Gregory et al.* [2000] and *Olivié et al.* [2004b]. Importantly, the archived convective mass fluxes are also more consistent with other meteorological fields such as the convective precipitation or cloud cover.

4.2.3 LNO_x distribution

Horizontal distribution

The LNO_x production rate is calculated at the resolution of the 3-dimensional meteorological data, i.e. at a $3^\circ \times 2^\circ$ horizontal resolution and 60 layers in the vertical. The standard version of the TM model uses a parameterisation where the lightning frequency f [$1/(\text{m}^2 \text{s})$] is proportional to the convective precipitation [*Meijer et al.*, 2001],

$$f \sim P_c, \quad (4.1)$$

with P_c [mm/s] the intensity of convective precipitation. We will compare this to the parameterisation of *Grewe et al.* [2001] where the lightning frequency is proportional with the cloud thickness d [km] and the mean updraft velocity w [m/s],

$$f \sim (w d^{0.5})^{4.9}, \quad (4.2)$$

which can be regarded as a refinement of the relation between cloud top height and flash frequency over land, formulated by *Price and Rind* [1992],

$$f \sim h^{4.9}, \quad (4.3)$$

with h [km] the cloud top height. Instead of Equation (4.2) we will use a slightly modified version,

$$f \sim \begin{cases} (w d^{0.5})^{4.9} & \text{if } w d^{0.5} \leq (w d^{0.5})_c \\ (w d^{0.5})_c^{4.9} & \text{if } w d^{0.5} > (w d^{0.5})_c, \end{cases} \quad (4.4)$$

where $(w d^{0.5})_c$ is some fixed value. Such an upper limit is necessary for obtaining a realistic probability density function of flash frequencies.

In order to distinguish between cloud-to-ground (CG) flashes and intra-cloud (IC) flashes, *Price and Rind* [1993] determined the fraction p of CG flashes in an individual thunderstorm :

$$p = \frac{1}{0.021 d_c^4 - 0.648 d_c^3 + 7.49 d_c^2 - 36.54 d_c + 64.09} \quad (4.5)$$

where d_c [km] is the thickness of the cold cloud sector (0°C to cloud top). *Price and Rind* [1993] developed this formulation only for cold cloud thicknesses greater than 5.5 km and less than 14 km. Therefore, it is assumed that when convective clouds in the model have cold sectors less than 5.5 km in thickness, no CG flashes occur.

Price et al. [1997] derived a production efficiency of 6.7×10^{26} molecules NO per CG flash and 6.7×10^{25} molecules NO per IC flash. They combined their estimates of energy per flash with a selected best estimate of NO production per unit energy to obtain the NO production per flash for CG and IC flashes. The ratio IC/CG and the NO production per flash is the same in our implementations of the *Meijer et al.* [2001] and the *Grewe et al.* [2001] parameterisation.

The lightning frequency above sea is taken to be only 10% of the lightning frequency above land.

Vertical distribution

For the vertical distribution of LNO_x we used two different set-ups. In the standard formulation of the TM model, prescribed profiles are used based on *Pickering et al.* [1998]. With a cloud resolving model they derived 3 different profiles for LNO_x emissions, extending from the surface up to 16 km altitude, with the largest amount [kg[N]/(m³ s)] in the lowest kilometre and between 7 and 16 km, resulting in a C-shaped profile. Inspired on these profiles, the LNO_x is distributed in the TM model as follows : all the IC LNO_x and 70% of the CG LNO_x is distributed between the -15°C-isotherm and the cloud top; 10% of the CG LNO_x is distributed between the earth

surface and the -15°C -isotherm; the remaining 20% of the CG LNO_x is distributed in the boundary layer. The fact that 70% of the CG LNO_x is distributed in the upper part of the cloud, represents the effect of the updrafts transporting the produced LNO_x upward. Similarly, the 20% of CG LNO_x in the boundary layer accounts for downward transport by the downdrafts. We will refer to this parameterisation as PP (Prescribed Profiles).

In the second set-up, the convective mass fluxes themselves redistribute the produced LNO_x . We now explicitly use the convective mass flux profile for the generation of the LNO_x profile. The convective fluxes occupy only a fraction of the grid box, and the lightning flashes and LNO_x production is assumed to take place near and within the updrafts and downdrafts. An initial LNO_x profile is generated as above, with all the IC LNO_x distributed between the -15°C -isotherm and the cloud top, but the CG LNO_x is now distributed between the surface and the -15°C -isotherm. This initial LNO_x profile is then transformed into a final LNO_x profile by applying the convective transport parameterisation. To do this, we inject the initial LNO_x profile in the column above the (usually small) convectively active fraction of the grid cell area. All the convective transport is thus concentrated in only a small fraction of the grid cell where the updrafts and downdrafts are applied. Because we only describe the cloud and its nearest environment, subsidence is assumed not to affect the resulting LNO_x profiles. Two parameters, which are however not independent, are of importance, namely the duration of the convective redistribution of LNO_x and the area fraction of the cell area over which the convective redistribution takes place. Decreasing the area fraction has the same effect as increasing the duration of convective redistribution.

We have chosen to apply separately the updrafts and the downdrafts in this reduced part of the grid box, because the result of the downdraft is often not affected by the updrafts. The updrafts and downdrafts are responsible for creating respectively the upper and lower part of the LNO_x C-profile. This parameterisation will be referred to as C1, C2, and C3, where the number refers to the duration of convective redistribution (later see Table 4.1).

4.2.4 Observations

NO and NO_x observations from four measurement campaigns that are suitable for the evaluation of lightning parameterisations are used. The LINOX campaign (lightning-produced NO_x) was performed in July 1996 over Germany and Switzerland [Huntrieser *et al.*, 1998]. We will only use the data from the flights performed on July 23rd and 24th 1996. Both these flights were made in the vicinity of one of the most pronounced thunderstorms encountered during this campaign.

We also used data from the flights made during the PEM-TROPICS A campaign in 1996 [Hoell *et al.*, 1999]. We have used the data from the flights on August 15th and 20th, and September 1st, 3rd, 5th, 7th, 10th, 11th, 14th, 18th, 22nd, 23rd, 25th, and 26th 1996. We did not use data from other flight because either no NO was measured, or we suspected the flight tracking data not to be correct.

The Subsonic Assessment Ozone and Nitrogen Oxide Experiment (SONEX) was performed in October and November 1997 [Thompson *et al.*, 2000] over the North Atlantic. We used all flights from SONEX for which NO measurements were available.

These were performed on October 7th, 9th, 13th, 15th, 18th, 20th, 23rd, 25th, 28th, 29th, 30th, and on November 3rd, 5th, 9th, 10th, and 12th 1997.

The European Lightning Nitrogen Oxides Project (EULINOX) was performed in July 1998 [Höller and Schumann, 2000] over Europe. Flights were made on July 1st, 3rd, 7th, 10th, 14th, 17th, 20th, and 21st 1998.

4.2.5 Experimental set-up

Table 4.1: Overview of the different parameterisations for lightning.

| Convective mass flux | | |
|-----------------------|--------------------------------|--------------------------|
| ARC | archived mass fluxes | |
| OFF | off-line diagnosed mass fluxes | |
| Flash frequency | | |
| | Flash frequency | Cut-off |
| CP | $f \sim P_c$ | |
| WD0 | $f \sim (w d^{0.5})^{4.9}$ | $(w d^{0.5})_c = \infty$ |
| WD1 | $f \sim (w d^{0.5})^{4.9}$ | $(w d^{0.5})_c = 0.5$ |
| WD2 | $f \sim (w d^{0.5})^{4.9}$ | $(w d^{0.5})_c = 0.2$ |
| WD3 | $f \sim (w d^{0.5})^{4.9}$ | $(w d^{0.5})_c = 0.05$ |
| Vertical distribution | | |
| | Vertical distribution | Convective duration |
| PP | prescribed profiles | |
| C1 | convective redistribution | $\Delta t = 1000$ s |
| C2 | convective redistribution | $\Delta t = 3600$ s |
| C3 | convective redistribution | $\Delta t = 10000$ s |

We have performed simulations with the TM4 model separately for the two available sets of convective mass fluxes, and separately for the different lightning parameterisations described above. An overview of the different simulations is given in Table 4.1. The used convective mass fluxes are either the archived ones (ARC), or the off-line diagnosed ones (OFF). The flash frequency is either based on the convective precipitation (CP), either on a combination of mean updraft velocity and cloud top (WD). For the vertical distribution either prescribed profiles (PP), or convective redistribution (C) is used. As a reference, we also made simulations without lightning emissions. Details of the table will be clarified further in the next section.

The model is used with a horizontal resolution of $3^\circ \times 2^\circ$ and 31 layers up to 10 hPa. For comparison with the NO and NO_x observations made during the aircraft campaigns, model simulations were performed from January 1996 until July 1998.

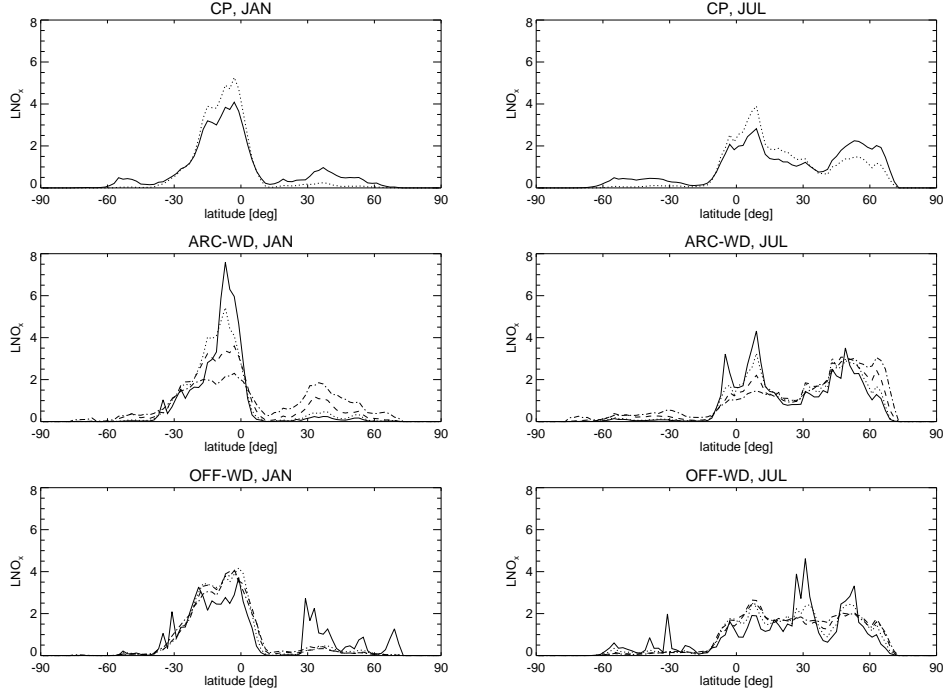


Figure 4.2: Zonal mean distribution of the LNO_x production in January (left) and July (right) 1998 for various lightning parameterisations. Upper panels : the lightning flash frequency depends on the convective precipitation in ARC-CP (solid) and OFF-CP (dotted). Middle panels : the lightning flash frequency depends on the updraft velocity and updraft top, using archived convective mass fluxes, and using different cut-off values, respectively ∞ (ARC-WD0, solid), 0.5 (ARC-WD1, dotted), 0.2 (ARC-WD2, dashed) and 0.05 (ARC-WD3, dot-dashed). Lower panels : as middle panel but using off-line diagnosed mass fluxes with cut-off values ∞ (OFF-WD0, solid), 0.5 (OFF-WD1, dotted), 0.2 (OFF-WD2, dashed) and 0.05 (OFF-WD3, dot-dashed). For the meaning of the abbreviations, see Table 4.1.

4.3 Results

4.3.1 Horizontal and seasonal variation

The CP parameterisation can be driven by either archived or off-line diagnosed convective mass fluxes. However, this does not influence the lightning flash frequency as this only depends on the convective precipitation. Differences in the LNO_x profiles are merely caused by the difference in cloud tops between the 2 data sets. The cloud top must be colder than -24°C to produce flashes, and the cloud top height determines the ratio between the IC and CG flashes, which have a different efficiency in LNO_x production. The upper panels of Figure 4.2 show the latitudinal distribution, and the first panel of Figure 4.3 shows the seasonal variation.

We found that the WD-parameterisation is very sensitive to the mean vertical velocity in the updraft. Due to the very strong dependence on the updraft velocity,

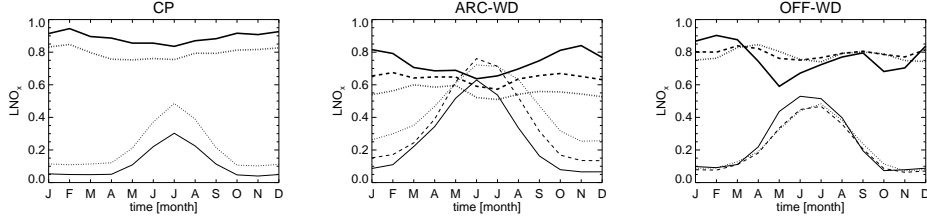


Figure 4.3: Seasonal cycle of the LNO_x production in 1996 in the tropics (thick line) and the extra-tropics (thin line). Left panel : the lightning frequency depends on the convective precipitation for ARC-CP (solid) and OFF-CP (dotted). Middle panel : the lightning frequency depends on the updraft velocity and updraft top for different values of the cut-off value in ARC-WD1 (solid), ARC-WD2 (dotted), and ARC-WD3 (dashed). Right panel : as middle panel but for off-line diagnosed mass fluxes for OFF-WD1 (solid), OFF-WD2 (dotted), and OFF-WD3 (dashed).

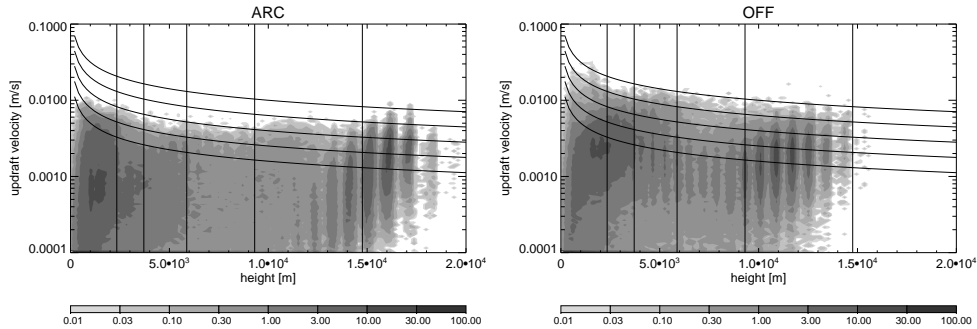


Figure 4.4: Distribution of the cloud top height versus updraft velocity over the period 1-8 July 1998. The vertical and curved lines are lines of constant flash frequency according to the $f \sim h^{4.9}$ and $f \sim (w d^{0.5})^{4.9}$ parameterisation respectively. For this comparison we assumed that $h \simeq d$.

only a very limited amount of events dominates the LNO_x production. This can be seen in Figure 4.4 where a probability density function is shown of the cloud top height versus the updraft velocity. In the same plot we have also indicated lines of equal flash frequency, following the $f \sim (w d^{0.5})^{4.9}$ parameterisation from *Grewe et al.* [2001] (curved lines), and for a parameterisation where the flash frequency is proportional to $f \sim h^{4.9}$ (vertical lines) [*Price and Rind*, 1992]. First of all, this illustrates the large difference between these parameterisations. Furthermore, one can note that the gradient along the updraft velocity axis in the flash production in the $f \sim (w d^{0.5})^{4.9}$ parameterisation is very strong, which illustrates the sensitivity to a few intense events. This high sensitivity is also reflected in the zonal distribution in the middle and lower panels of Figure 4.2, where localised spikes of high LNO_x appear. This sensitivity would seem to make this parameterisation less suitable. Note that the reason for formulating the original TM parameterisation in terms of convective

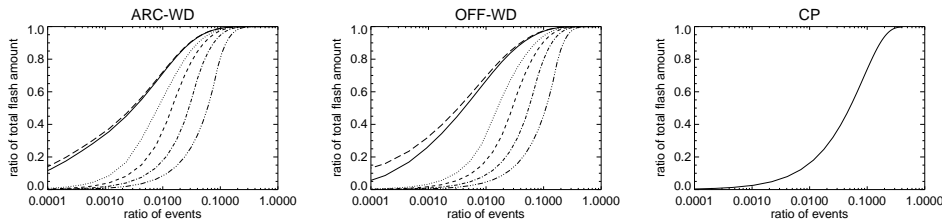


Figure 4.5: Cumulative distribution of the number of events versus the flash frequency over the period 1-8 July 1998, showing which fraction of events contributes to which fraction of the flash frequency. The two first panels represent the WD-parameterisation using archived (left) and off-line diagnosed fluxes (middle) for different values of the cut-off value of $(w d^{0.5})_c$: ∞ (long-dashed), 1 (solid), 0.5 (dotted), 0.4 (short dashed), 0.3 (dot-dashed), and 0.2 (dot-dot-dot-dashed). The right panel represents the CP-parameterisation.

precipitation instead of cloud top height as *Price and Rind* [1992] was to circumvent such sensitivities.

To circumvent this problem, we have introduced a maximum (cut-off) for the value of the product $w d^{0.5}$, accompanied by a normalisation to maintain the same total LNO_x production per year. By introducing a maximum value $(w d^{0.5})_c$, more events contribute significantly to the LNO_x production. This can be seen in Figure 4.5 where the cumulative distribution of the number of events (normalized to 1) versus the lightning flash frequency (normalized to 1), for different choices of the maximum value $(w d^{0.5})_c$ is shown. For comparison, we also show this distribution for the CP parameterisation. Due to the normalisation, imposing an upper bound on the maximum value of $w d^{0.5}$, also leads to a zonal (seasonal) redistribution in the LNO_x source. The introduction of the cut-off removes the spiky behaviour of the latitudinal distributions (middle and lower panels of Figure 4.2).

Global maps of the LNO_x production in July 1998 are shown in Figure 4.6. For comparison, we also show the lightning flash density as it is observed by the Optical Transient Detector (OTD) (from <http://thunder.msfc.nasa.gov/data/OTDsummaries>) in Figure 4.7. Comparison of ARC-CP and OFF-CP shows that ARC-CP puts more LNO_x at higher latitudes, while OFF-CP gives higher values in the tropics. For the WD-cases, going from weak to stronger cut-offs (from WD1 over WD2 to WD3) results in more homogeneous distributions. The ARC-WD1 simulates best the distribution over North America compared with OTD. The OFF-WD simulations reproduce the observed maximum in Southeast Asia best, while the ARC-WD simulation seems to miss this feature. The ARC parameterisation reproduces the distribution over Europe and Northwest Asia better than the OFF parameterisation.

4.3.2 Vertical distribution

In this section we compare the vertical distribution generated by the prescribed profile technique (PP) and the distribution generated by convective redistribution (C). For the horizontal distribution, we use here the CP-parameterisation (the results obtained for the WD parameterisation were similar).

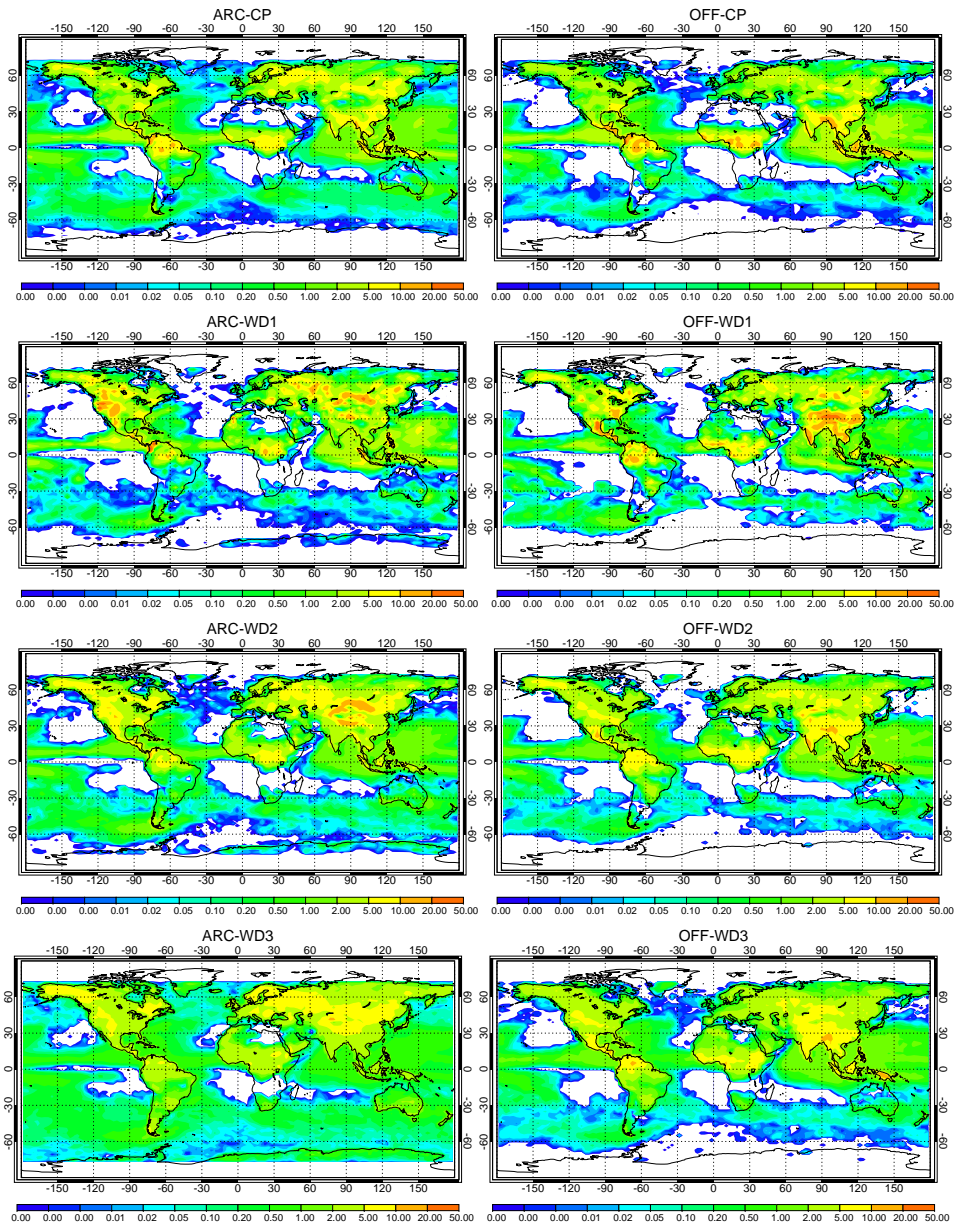


Figure 4.6: LNO_x production during July 1998, using archived mass fluxes (left), and off-line diagnosed mass fluxes (right). The first row uses the CP-parameterisation, the second till fourth row use the WD-parameterisation with different cut-off values $(w d^{0.5})_c$, respectively 0.5, 0.2, and 0.05.

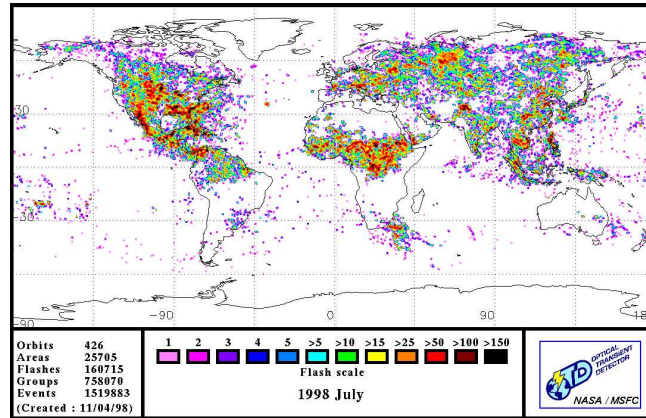


Figure 4.7: The lightning flash distribution as observed by OTD during July 1998 (courtesy of NASA-MSFC).

Prescribed LNO_x profiles

In Figure 4.8 zonal mean LNO_x profiles are shown for July 1998. Using the archived cloud tops (solid line), which are higher than the off-line diagnosed ones, leads to more production higher up in the troposphere. During summer at high latitudes there is also more LNO_x production when using the archived updraft tops. These profiles are rather similar to the profiles shown by *Pickering et al.* [1998], although there are some distinct differences : here the production in the lowest layers is a bit more spread out in the vertical; the ratio between the highest production rate (around 10 km) to the lowest production rate (around 5 km) is here also larger than in *Pickering et al.* [1998].

Convective redistribution of LNO_x production

The convective redistribution requires choices concerning the area fraction and the duration over which convection redistributes the initial LNO_x profile. For the area fraction of the grid box that is influenced by the thundercloud, we assumed a fraction of 0.01. This corresponds approximately to the fact that the updraft region is typically of the order of 10-30% (P. Siebesma, personal communication), assuming at the same time that the cloud cover at the altitude of strongest ascent for these high clouds is around 10%. For the convection duration, we have tested different values. In Figure 4.9 zonal mean LNO_x profiles are shown. The initial profiles are shown, but also profiles after convection has been acting on it for different durations : 100 s, 1000 s, and 10000 s.

There are distinct differences between the results for the archived and off-line diagnosed convective mass fluxes. Due to the higher tops of the archived convective mass fluxes, there are more IC-flashes, leading in the initial profile to more LNO_x at upper levels. Therefore different durations should be used for the archived and off-line diagnosed convective mass fluxes to obtain the best agreement with the profile shapes

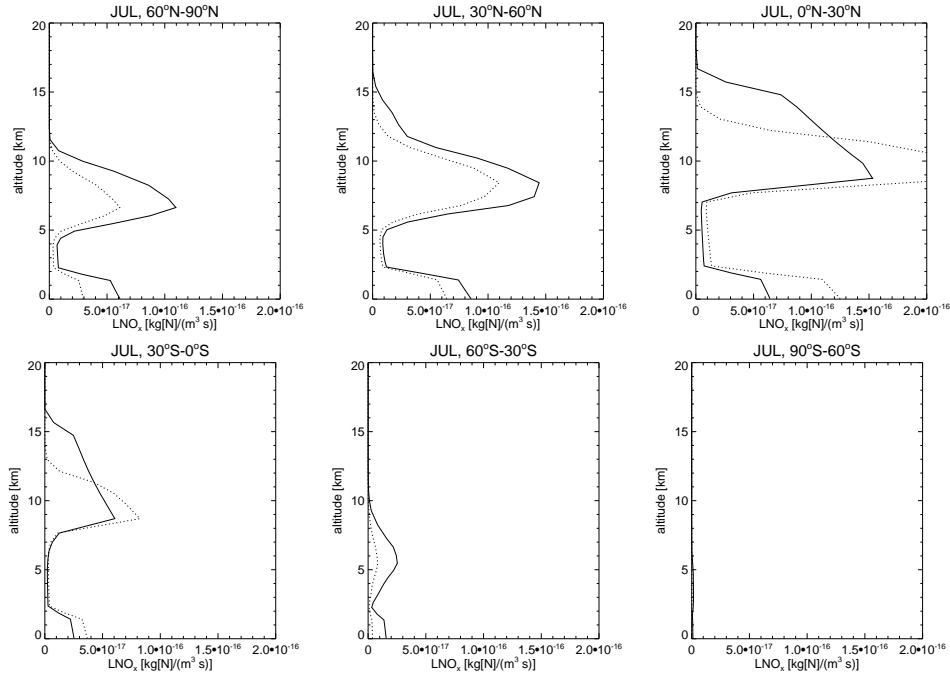


Figure 4.8: Zonal mean profiles of the LNO_x distribution when using prescribed profiles for July 1998 : using archived (solid line) and off-line diagnosed (dotted line) convective mass fluxes. The flash frequency is based on the CP-parameterisation.

of *Pickering et al.* [1998]. The archived profiles already lead to C-shaped profiles for durations of 1000 s, while an unrealistically large time of 10000 s is needed in the case of off-line diagnosed convection. This may be partially attributed to the mismatch between the convective precipitation (an archived quantity) and the off-line diagnosed convective mass fluxes. The higher top of the convective updrafts leads in the archived case also to much higher final profiles. In the off-line case, the detrainment zone is thinner than in the archived case. Off-line profiles detrain by definition only in the upper 1 or 2 layers, while the archived profiles detrain over more layers.

The influence of the downdrafts can also be observed. One finds strong enhancements of NO_x concentrations in the lower layers, especially for the longer durations. They are however smaller in vertical extent than in the prescribed profiles (where they are around 2 km deep). In the archived case they are also much smaller than in the off-line diagnosed case. This is consistent with the fact that the downdrafts are relatively weaker in the archived case (cfr. [*Olivié et al.*, 2004b]).

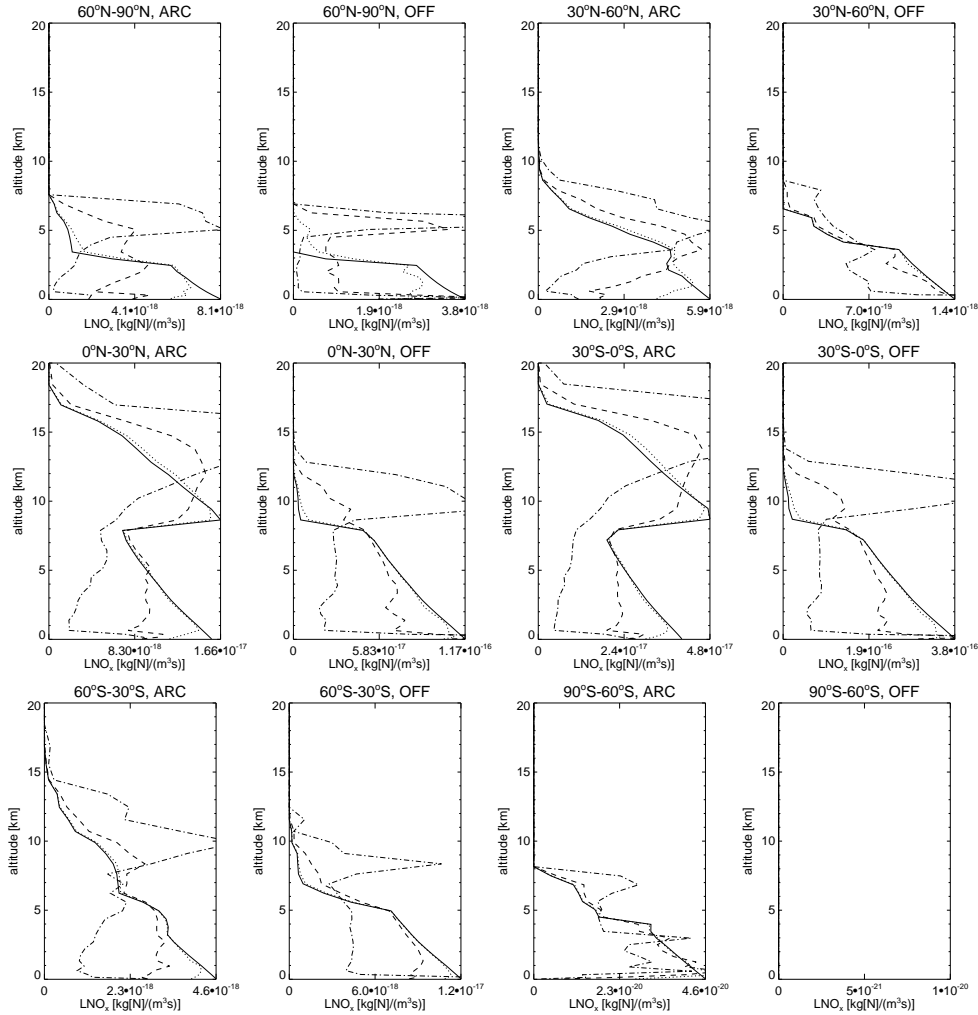


Figure 4.9: Zonal mean profiles of the LNO_x distribution for the explicit convective description on January 1st 1998 at 6h00 GMT. Profiles are shown for different convection durations: $\Delta t = 0$ s (solid), $\Delta t = 100$ s (dotted), $\Delta t = 1000$ s (dashed), and $\Delta t = 10000$ s (dot-dashed). For each latitude band the left panels are based on archived convective mass fluxes, the right panels are based on off-line diagnosed mass fluxes. The flash frequency was based on the CP-parameterisation.

4.4 Comparison of the model results with observations

We have compared the model simulations with the observations from the LINOX, PEM-TROPICS A, SONEX, and EULINOX campaigns described in Section 4.2.4. We have performed simulations with different choices for the convective mass fluxes,

flash-frequency parameterisation, and vertical distribution (as mentioned in Section 4.2.5). As a reference we have also made model simulations without any lightning production, as well with the archived convective mass fluxes (ARC-nolighting) as with the off-line diagnosed ones (OFF-nolighting). (Although the difference in NO_x concentration between a base simulation and a simulation without lightning does not represent the exact contribution of lightning due to the non-linearity of the chemistry, it is good indication for it.)

4.4.1 LINOX flights of July 23rd and 24th 1996

Figure 4.10 shows a comparison of the observed and simulated NO_x profiles on July 23rd and 24th 1996. The observations on these consecutive days were made in the same air mass before and after a prominent thunderstorm. A distinct NO_x increase around 300 hPa is visible in the observations on July 24th, i.e. 1 day after the passage of a thunderstorm front line. On July 23rd, the profile is well simulated and the correspondence is reasonably good for most simulations. Only ARC-WD3-PP and OFF-WD[1-3]-PP overestimate the "background" concentration. As discussed in Section 4.3.1 and illustrated in Figure 4.2 these parameterisations yield a relatively high lightning frequency in the extra-tropics relative to the tropics. The profiles on July 24th show significant differences. Comparison of the ARC-CP-PP and OFF-CP-PP case shows that the ARC-CP-PP reproduces the overall vertical gradient in LNO_x best, but the source still seems a bit too small. All the OFF-WD runs seem to inject the LNO_x at too low altitudes (below 350 hPa). Probably the off-line diagnosed downdrafts are too strong in this case. They were smaller for the archived ERA-40 data. The profiles are sometimes not sensitive to changes in the parameterisations, like for OFF-CP-C[2-3] or for ARC-WD1-C[1-3]. For ARC-WD1-C[1-3] the lightning production is probably too small (other events probably strongly dominate the global annual production). Note that the ARC-CP-C[1-3] are performing well, with a clear sensitivity to the assumed duration of convective redistribution. Still, the source (at upper levels) is slightly underestimated. In short, the ARC-CP parameterisation is performing best for this case.

4.4.2 EULINOX flight of July 1st 1998

Time series of the observed and model simulated NO concentration for the EULINOX flight on July 1st 1998 are shown in Figure 4.11. During this flight, the aircraft sampled the outflow of a thunderstorm over Spain that occurred the previous day. The simulations are grouped per panel to show the sensitivities to the different parameterisations. The last panel shows the flight altitude. The simulations can be judged as to how close they get from the no-lightning case (blue) towards the observations (black). The OFF cases and the PP cases (in the panels a and c) are not able to reproduce the high observed NO concentration in the middle part of the flight. The OFF-WD1-C3 (panel g) gives a significant, albeit too small, lightning contribution. The ARC-CP-C[2-3] (panel d) and ARC-WD1-C[2-3] (panel f) cases do simulate the observed NO-concentration reasonably well.

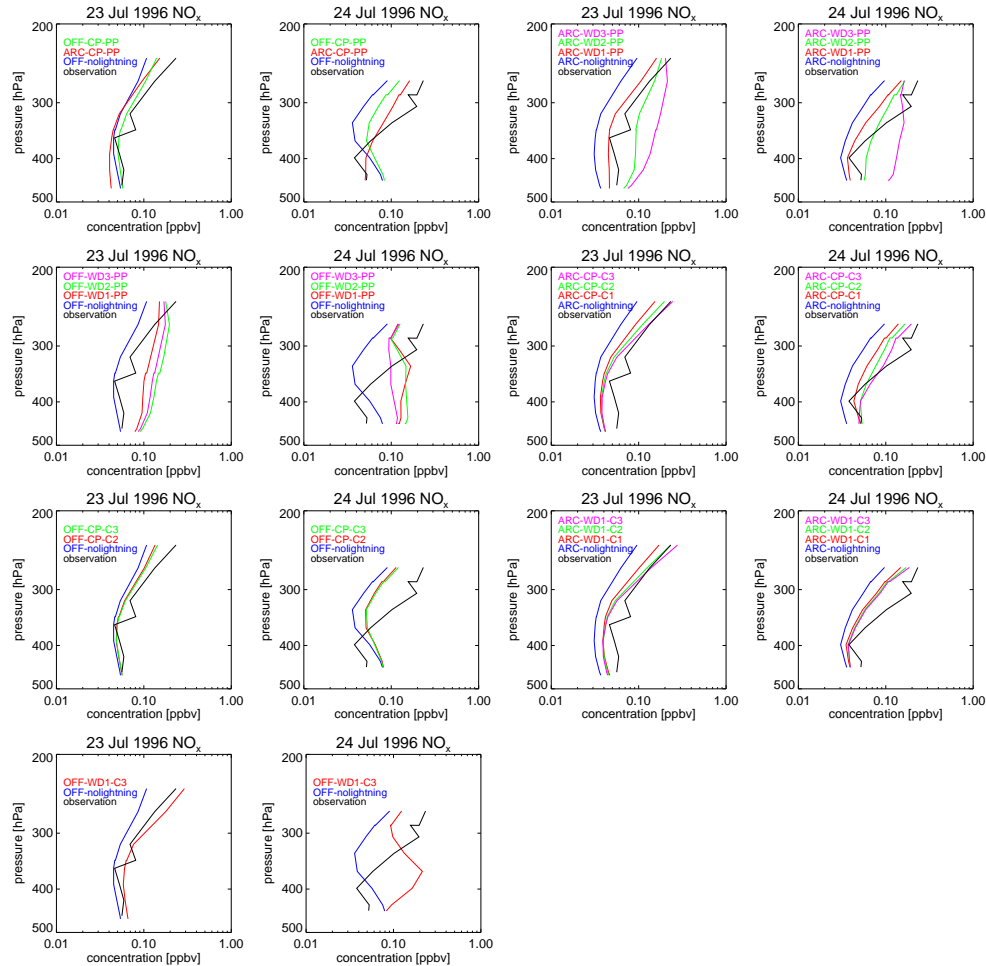


Figure 4.10: Observed and model simulated NO_x concentration during the LINOX flights on July 23rd (left) and 24th (right) 1996. The same air mass was sampled before and after a very prominent thunderstorm over central Europe. The observational data is the same as in *Huntrieser et al.* [1998], but averaged over 1-minute time intervals.

4.4.3 EULINOX flight of July 3rd 1998

For the EULINOX flight on July 3rd 1998, we compare the results of the different parameterisations in Figure 4.12. During this flight the aircraft penetrated a thunderstorm embedded in a large convective system over Switzerland. The model simulations that perform reasonably well for this case are the archived simulations ARC-CP-PP (red curve in panel a), ARC-WD2-PP (green curve in panel b), and ARC-CP-C2 (green curve in panel d), as well as the off-line diagnosed OFF-WD2-PP (green curve in panel c) and OFF-WD1-C3 (red curve in panel g). During the last part of the flight, measurements were made between 300 and 200 hPa (where the

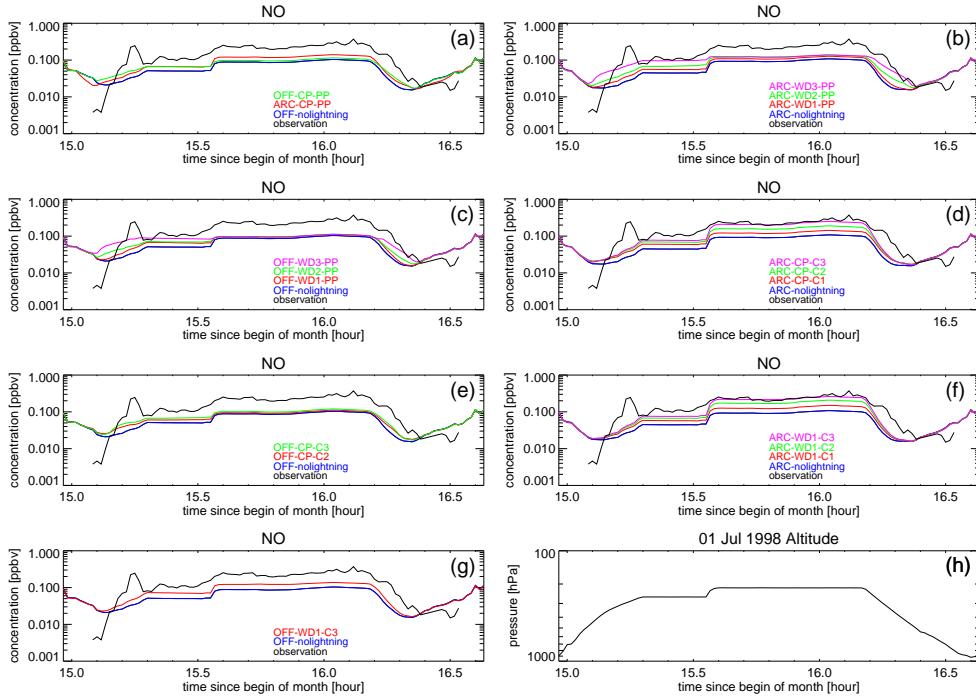


Figure 4.11: Observed (black) and model simulated NO concentration for the EULINOX flight on July 1st 1998. The flight altitude is shown in the last panel.

time coordinate equals about 65 hours). One sees that in the no-lightning case, the increase in altitude leads to an increase in simulated NO. However the observations show a sudden dip in the NO-concentration. This signature is pretty well captured by some of the model simulations (OFF-WD3-PP in panel c and OFF-WD1-C3 in panel g).

4.4.4 Overview of all flights

The upper panel of Figure 4.13 gives an overview for each flight of the mean NO concentration for the observations and 3 model simulations : OFF-nolightning, ARC-CP-PP, and OFF-CP-PP. The ARC-CP-PP and OFF-CP-PP give a better agreement than OFF-nolightning which underestimates in almost every flight the observed NO concentration. The ARC-CP-PP performs better than the OFF-CP-PP indicated in the flights with high observed NO-concentrations, although big discrepancies remain. We tentatively conclude that the archived convective mass fluxes give a better representation of convective clouds than the off-line diagnosed ones. Evidence for this was also presented in Chapter 2 (cfr. [Olivié *et al.*, 2004b]). The big differences for flights with high observed NO concentration can be partially attributed to the low resolution of the TM4 model. High peaks of NO generated by lightning cannot be expected to

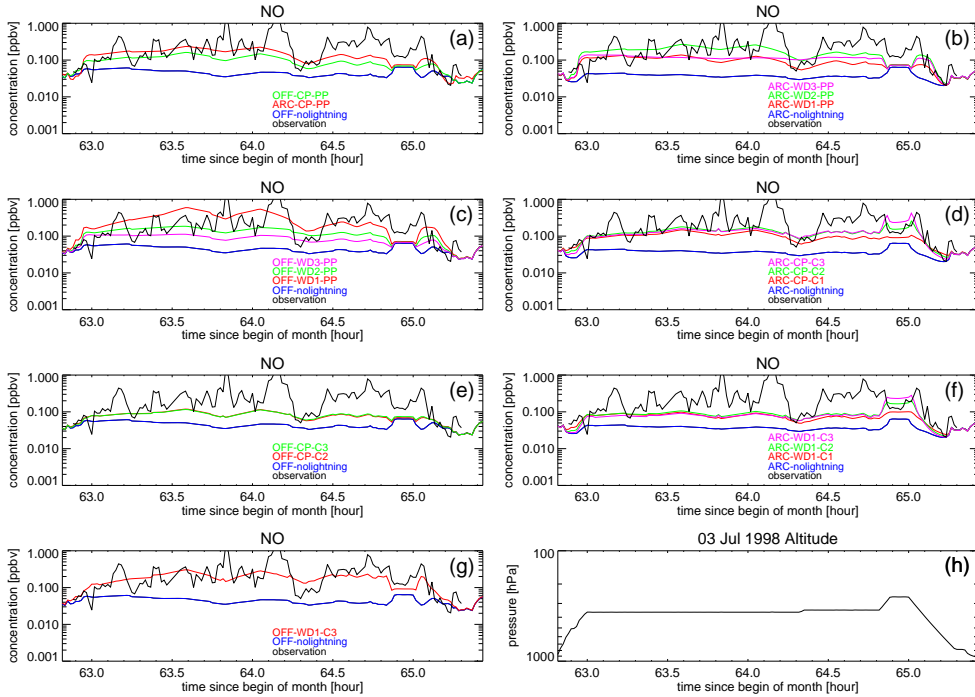


Figure 4.12: Observed (black line) and model simulated NO concentration for the EULL-NOX flight on July 3rd 1998. The flight altitude is shown in the last panel.

be modelled accurately in coarse resolution models. Additionally, TM4 produces only effective LNO_x profiles and cannot simulate instantaneous NO_x concentrations inside active thunderstorms.

In the other panels of Figure 4.13 we show for a range of parameterisations the mean bias per flight between the model simulation and the observation. For each parameterisation we have ordered the mean biases for all flights and have plotted from left to right the flight with the most negative up to the flight with the most positive bias.

Here again one can observe that the ARC-CP-PP parameterisation gives fewer underestimates of the observed NO concentration than the OFF-CP-PP one. In the remaining panels, we have always included either ARC-CP-PP or OFF-CP-PP for comparison. The ARC-WD[1-3]-PP cases are found to be quite similar to the ARC-CP-PP. Only the ARC-WD3-PP case performs slightly worse : for a few flights it overestimates the observed NO concentrations resulting in a positive mean bias. Considering both ARC-CP-C[1-3] and ARC-WD1-C[1-3], one can note that the ARC-CP-C[2-3] and ARC-WD1-C[2-3] are able to reduce some of the negative biases (underestimates) : this demonstrates the positive impact of the convective redistribution. At the same time ARC-CP-C3 and ARC-WD1-C3 strengthen the positive biases (overestimates), showing that a convective redistribution duration of $\Delta t = 10000$ s is clearly

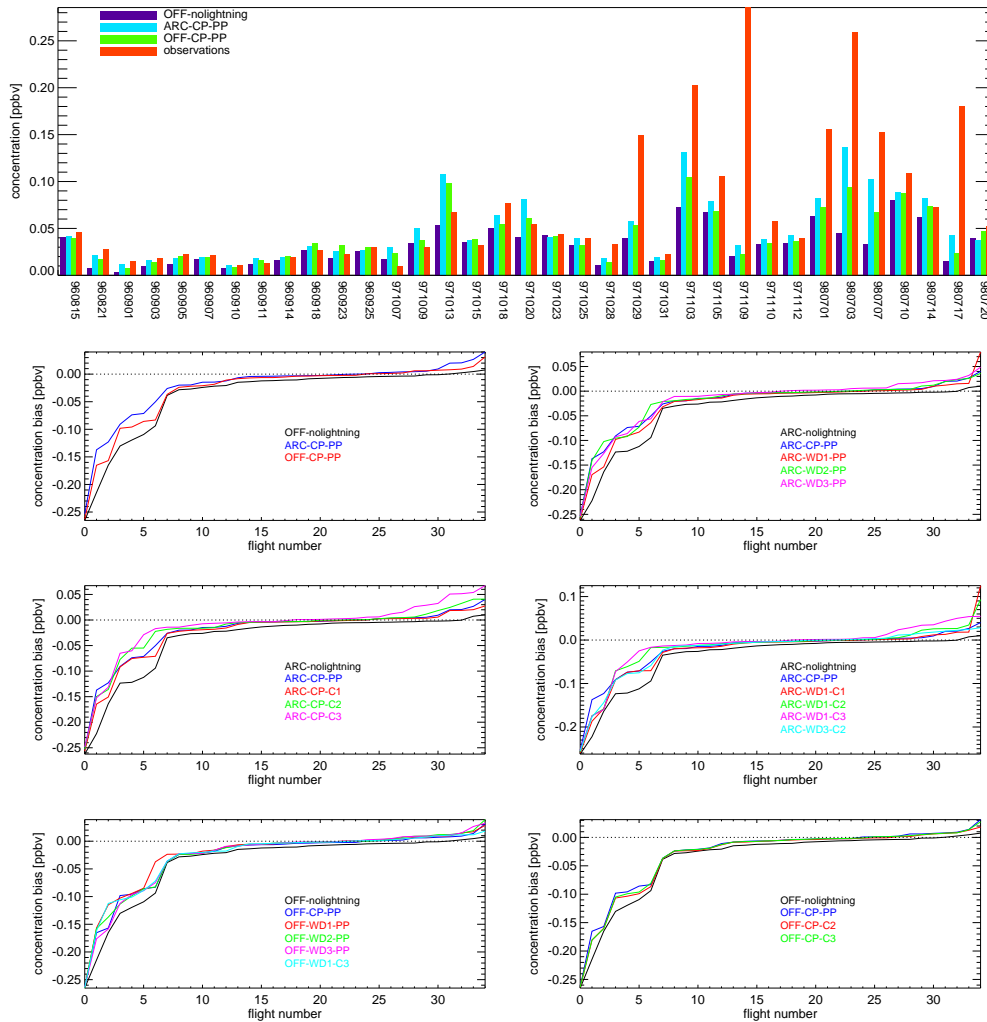


Figure 4.13: Upper panel : Mean NO concentration per flight for the observations and 3 simulations (OFF-nolightning, ARC-CP-PP, and OFF-CP-PP). Other panels : ordered mean bias in NO concentration per flight between the model simulations and the observations.

too long.

If we consider the OFF simulations in the bottom panels, we observe that the sensitivity to the parameterisations is smaller. In most cases, also their positive biases are smaller. However, the improvement of the negative biases relative to the no-lightning case is smaller than for the ARC-CP and ARC-WD parameterisations.

4.5 Conclusions and discussion

We have studied the influence of different aspects of lightning parameterisations. The higher updraft top in the ARC-case than the OFF-case leads to different partitioning between IC and CG flashes, resulting in a different horizontal distribution, seasonal cycle and vertical distribution. The unmodified WD-parameterisation gives much too spiky lightning production, where a very few intense events dominate the lightning production. To avoid this we have introduced a maximum value (cut-off) for the product $w d^{0.5}$. The WD horizontal distribution performs better than the CP horizontal distribution, and distinctly optimal cut-off frequencies exist for the ARC-case and the OFF-case. The choice of the cut-off value has a strong effect on the latitudinal distribution of LNO_x.

The explicit convective redistribution is able to generate the observed C-shaped profiles for physically meaningful values of the area fraction and the duration of convective redistribution. Due to the different cloud top heights between the ARC- and OFF-case their initial profiles of LNO_x before vertical redistribution differ. This results in different optimal durations of convective redistribution. However, the small downdrafts in the ARC-case and the simple convective mass flux profiles in the OFF-case, might limit the applicability of this new redistribution approach.

We have made a comparison to a comprehensive set of observations. The differences between some of the simulations and the observed NO concentrations are often small. All parameterisations yield significant mean biases and discrepancies for individual flights. The comparison with the observations therefore does not allow firm conclusions. The archived convective mass fluxes apparently perform better than the off-line diagnosed. Also the convective redistribution frequently leads to good results and seems therefore a valuable alternative to using prescribed profiles.

Further efforts should be done to improve the agreement with observations. Observations from the recent TROCCINOX measurement campaigns performed over Brazil in 2004/2005 may provide a useful complementary data set for evaluation of the parameterisations in the tropics.

Since ERA-40 data is only available until 2002, and operational data from the ECMWF does not contain archived convective mass fluxes, it may be interesting to either implement a more advanced scheme for the off-line diagnosis of convective mass fluxes in the TM4 model, or to archive also the convective mass fluxes in the operational ECMWF model forecasts.

Because the horizontal resolution in the global TM4 model is much coarser than the original meteorological fields, and because the time step of the original ECMWF model is much shorter than 3 hours, the profiles of convective mass fluxes are averages in space as well as in time. One should keep this in mind when using them for this C[1-3] parameterisation. Because lightning is a small-scale process, one also expects that increasing the model resolution may improve the agreement between observations and model simulations.

Convective redistribution of LNO_x is modelled as if the up- and downdrafts influence a fixed fraction of 1% of the area of a grid box where convection is active. Instead of using a fixed fraction, it might be interesting to make this fraction depending on the cloud cover e.g. at 400 hPa.

For the distinction between IC and CG flashes, we assumed that when the cold

cloud thickness is smaller than 5.5 km, all flashes appear as IC-flashes. This is based on *Price and Rind* [1994]. As a consequence, almost all the LNO_x is injected into a rather small portion of the cloud, leading to locally very high and unrealistic LNO_x concentrations. Instead, the approach from *Allen et al.* [2000], who assumed that in thin clouds all flashes are CG-flashes, might be evaluated.

Acknowledgements

The ECMWF ERA-40 data used in this study have been kindly archived and provided by ECMWF. This work was supported by the Netherlands Organization for Scientific Research (NWO) and by the European Union under contract number EVK2-CT-2002-00170 (RETRO). We thank H. Huntrieser of DLR for the LINOX and EULINOX data.

5

Conclusions and outlook

5.1 Introduction

Chemistry transport models are widely used to assess the impact of anthropogenic emissions on the atmospheric composition and climate. A good description of the (small-scale) transport is essential for understanding the present distribution of ozone and its precursors. The quality of these assessments thus strongly depends on the quality of the description of some key processes in the chemistry transport models. The investigation of the sensitivity of the chemistry transport model TM3/4 to different descriptions of the convection, the turbulence, and the production of nitrogen oxides by lightning was the main topic in this thesis. The availability of the ERA-40 data set has allowed us to investigate these sensitivities in CTM-modelling. By comparing model results with observations, an attempt has been made to quantify the differences between the different meteorological data sets and parameterisations.

5.2 Summary and conclusions

An overview of the work with the main conclusions is presented here. The conclusions are formulated as answers to the questions formulated in the introduction :

1. How large is the sensitivity of the (model simulated) distribution of ozone and nitrogen oxides on (the) convection (parameterisation)?

This question has been addressed in Chapter 2. We have performed model simulations with the TM3 model for the years 1991 until 1996. We have used two different data sets for describing the convective transport : archived convective mass fluxes during the ERA-40 project, and off-line diagnosed convective mass fluxes. Comparison with observations of ^{222}Rn in the upper troposphere showed that the archived convective mass fluxes perform better. Large differences in tracer concentrations resulted from switching the convective data sets. In the archived case, NO_x concentrations were found to be larger in the middle troposphere and substantially smaller in the upper troposphere and lower stratosphere than in the diagnosed case. For ozone rather strong differences were found, with for the archived case enhanced concentrations in the middle troposphere and lower values in the upper troposphere and lower stratosphere. In summary, the modelled NO_x and O_3 distributions for the two convective data sets differ substantially. This large sensitivity of the model results, also shows that convection is a key process in the distribution for ozone and its precursors.

2. What requirements should be fulfilled by diffusive transport parameterisations in order to simulate the diurnal cycle in trace gas concentrations?

This question has been addressed in Chapter 3. We have performed model simulations with the TM3 model for the years 1959 until 1962, and for 1993, using 4 different sets of vertical diffusion coefficients. We have compared the model simulated ^{222}Rn concentration with observations at four surface stations. We have also compared model simulated and observed atmospheric boundary layer heights at 2 northern hemispheric mid-latitude locations. Using a time resolution of 3 hours for the diffusion coefficients, resulted in a reasonable representation of the daily cycle of the ^{222}Rn concentration. Because the daily evolution of the diffusion coefficient is characterized by strong increases and decreases in the turbulence, instantaneous diffusion coefficients were better suited to simulate the observed ^{222}Rn than averaged/accumulated ones. The comparison has also shown that non-local diffusion schemes perform better than local diffusion schemes.

The ^{222}Rn concentration at one of the surface stations which lies on top of a hill, was not well represented. Because of the rather coarse model resolution at the top of the boundary layer, strong gradients that may exist there, are not represented accurately by the model. Therefore an increased model resolution might be necessary to simulate well the daily cycle higher up in the ABL or lower free troposphere.

3. How large are the differences in concentrations between simulations with archived and off-line diagnosed physical parameterisations?

This question refers to Chapters 2 and 3. In these chapters, we compared the effect of using archived data from an NWP model for describing subgrid-scale transport instead of off-line diagnosis of subgrid-scale transport. *Rasch et al.* [1997] also studied this effect and suggested that using 6 hourly diagnosed meteorological fields would be sufficient for a reasonable representation. We must admit that our comparison is slightly biased. The parameterisation for the off-line diagnosis of the transport is not completely identical to the parameterisation applied in the NWP. It reflects however the realistic situation where changes in NWP are incorporated with a delay in the off-line parameterisations in CTMs. Although there are some apparent differences between the parameterisations, some of the offline parameterisations are quite well able to reproduce the archived fields : for instance the profiles of convective mass fluxes, as well as the profiles of the diffusion coefficients.

The differences in the concentrations of tracers such as ^{222}Rn , NO_x and O_3 are related to their lifetime and to the magnitude of the gradient in the tracer concentration at the location where the diffusive or convective processes are active. Due to the sensitivity to convection, in the upper troposphere the difference in zonal mean concentration for ^{222}Rn , and NO_x amounted to more than 50%, while for ozone they were still up to 20%. Also in the middle troposphere, the differences were substantial, but mainly so in the tropics.

The effect of using different turbulent transport data on the concentration of ^{222}Rn was smaller. In the middle and upper troposphere, zonal mean differences in ^{222}Rn concentration were less than 10%. However, in the ABL, instantaneous differences amounted locally up to 20%.

4. How do the results of different parameterisations of nitrogen oxide production by lightning compare?

This question was addressed in Chapter 4. The current standard TM lightning parameterisation [Meijer *et al.*, 2001] has been compared with the lightning parameterisation of Grewe *et al.* [2001]. The implementation of the latter parameterisation, which depends non-linearly on the updraft velocity, appeared to be very sensitive to updraft intensity in the TM model. Therefore a slightly modified formulation has been applied, which mitigates the over-intense events. We found significant differences in the zonal distribution and seasonal cycle between the different parameterisations. The comparison with airborne observations from measurement campaigns did not allow to decide which parameterisation performs best.

5. What is the effect of an explicit description of the effect of convective redistribution on the vertical distribution of lightning produced NO_x ?

This question has also been addressed in Chapter 4. With an explicit description of the vertical redistribution of LNO_x by convection, we were able to reproduce the C-shaped emission profiles suggested by Pickering *et al.* [1998]. Large differences were again found between the use of archived and off-line diagnosed convective mass fluxes. The difference in convective mass flux profiles resulted in characteristic features. The off-line diagnosed mass fluxes have organized detrainment only close to the top of the updraft. This results in rather thin outflow layers. The archived convection, having organized detrainment over a somewhat larger extent of the cloud, showed thicker outflow layers, which is probably more realistic. The downdrafts were however not able to realise enough explicit downward transport to the lowest model layers. The comparison with aircraft measurements showed some improvement for the flights where the model in previous versions exhibited an underestimate of the NO_x concentrations. It can be concluded that the convective mass fluxes are a promising tool to improve the vertical distribution of lightning emissions.

5.3 Outlook

Changes in the atmospheric composition are highly relevant for the quality of life of mankind. The increasing amount of available measurements and the continuous model improvements should lead to a better assessment of the changes in the atmospheric composition, and enable us to improve our understanding of tropospheric chemistry. The TM model has contributed in many studies to better understand the past changes in the atmospheric composition. The planned rerun of parts of the ERA-40 period (1957-2002) will produce even more valuable data sets. Better simulations of past changes increase our faith in projections of future changes caused by anthropogenic emissions.

The results presented in this thesis have contributed to a better understanding of the impact of certain processes on the composition of the troposphere. As is usual, closely investigating certain questions about the subject, leads to the emergence of new (small and big) questions.

5.3.1 Radiative forcing

The sensitivity of the model simulated ozone distributions to the description of convection appeared to be rather large (see Chapter 2), especially in the upper tropical troposphere. Because the radiative forcing by ozone also has a strong height dependence near the tropical tropopause, the combined effect of these sensitivities should be investigated.

5.3.2 Convection

Different paths can be identified to further improve the convective transport in the TM chemistry transport model. Because the ERA-40 data set also contains 3-hourly convective mass fluxes, it would be interesting to investigate how this would further improve the comparison with observations. Using 3-hourly convective data may be important for short-lived trace gases, or for species with a highly varying emission rate (gases emitted by vegetation in relation to photo synthesis). It would be interesting to perform a purer evaluation of the performance difference between archived and off-line diagnosed convective transport data by using more similar parameterisations in the ECMWF model and off-line. Such an evaluation was not so urgent to us, because we preferred to investigate first the current parameterisations applied in the TM model (which are not completely identical to the parameterisations in the ECMWF model). Even if this test is performed for only a short time period, it could offer us quite valuable information. It would be really instructive to run the identical model archived and off-line to study the exact differences.

Because the ERA-40 data sets ends in 2002, and because of limitations in the representation of the Brewer-Dobson circulation in this set, it might be interesting to update the off-line parameterisation in the TM-model itself. Therefore one could use the description of the convection as it was used during ERA-40, or even more recent adaptations as already implemented in the ECMWF model [*Jakob and Siebesma, 2003*].

The better the description of convection becomes, the more the emphasis shifts towards accurately describing the actual tracer transport by the convection. Also the dependence of the compensating subsidence on the horizontal grid size should be considered. One could investigate whether subsidence should be spread over more grid boxes in the TM model. The averaging of profiles from the high resolution of the meteorological data to the TM resolution might also lead to unforeseen consequences.

Also the direct observations of radiatively active trace gases as NO_2 by satellite instruments, such as SCIAMACHY and OMI, might in the future contribute to a better understanding of convection [*Boersma et al., 2005*].

5.3.3 Atmospheric boundary layer turbulence

In Chapter 3 we only compared the 6-hourly ERA-40 archived ABL heights to observations. In a first follow-up step, it would be interesting to compare the 3-hourly archived ABL heights with observations and with the off-line diagnosed ABL height. In Chapter 3 the comparison of the ABL heights was also limited to a short period. For the ERA-15 data set, an extensive study has in the past been performed of the

modelled and observed surface fluxes and parameters relevant for the structure of the ABL at Cabauw (the Netherlands) [Bosveld *et al.*, 1999]. A similar extensive study is presently being done for ERA-40 (Fred Bosveld, personal communication). This could sustain and further increase the confidence in and understanding of the archived ABL heights from ERA-40. The ERA-40 data will thus probably become a good reference for testing future off-line parameterisations. It would also be interesting to extend the set of parameters measured at the Cabauw tower with a few more or less passive tracers, e.g. to measure ^{222}Rn at several heights. It would be even more interesting to measure tracer profiles with a tethered balloon at Cabauw. The large set of observed parameters measured at Cabauw will then allow a thorough analysis of the performance of boundary layer turbulence schemes for tracer transport.

Currently, ABL transport is intensively studied, e.g. within the GEWEX Atmospheric Boundary Layer Study (GABLS). Its overall objective is to improve the understanding and the representation of the atmospheric boundary layer in regional and large-scale climate models. Results from these studies will also be relevant for transport in atmospheric chemistry transport model. GABLS concentrates on meteorological parameters, including water vapour. It would be interesting to extend these studies with a tracer transport component.

In Chapter 3, we only studied the effect of the different turbulent diffusion coefficient data sets on the representation of the ABL height and the distribution of ^{222}Rn . It would be interesting to further investigate its effect on O_3 and its precursors. It will furthermore be interesting to study the effect of including a counter gradient term in the description of the turbulent transport in the convective ABL.

Although ^{222}Rn has a well-known global mean emission rate, there are large regional variations. One could improve this by describing more accurately the emission (Conen and Robertson [2002] published a new latitudinal distribution), and by better describing the dependence on local meteorological circumstances (snow cover, soil temperature, surface pressure, precipitation history, etc.). The sources of some anthropogenically emitted tracers are also quite well known, which would allow them to be used in a similar way as tracers of small-scale transport. Especially SF_6 could highlight deficiencies in the modelling of the small-scale vertical transport in models [Peters *et al.*, 2004].

5.3.4 Lightning parameterisation

Lightning parameterisations will continue to be an important topic of research. Based on our findings, we think it would be interesting to further investigate some aspects of the convective redistribution technique. One might focus on the influence of the initial distribution of the LNO_x (which has a large effect on the final distribution), the possible dependence of the area fraction on e.g. the cloud cover at 400 hPa, and the use of available 3-hourly convective mass fluxes. Imposing some diffusive redistribution on the final LNO_x profile, and better treating the convective mass fluxes which are area and time-averages might further improve the results.

Furthermore we think it would be good to investigate other points in detail, for instance the assumption that lightning flashes have a much lower frequency of occurrence over oceans than over land for the same convective precipitation rate and the assumed constant factor between the efficiency of IC/CG flashes in producing NO_x .

5.3.5 Effect of climate change on convection and lightning

Apart from studying and understanding the processes and atmospheric composition in the current climate, it will be important to understand the processes in possible future climates. The expected global warming in this century will have important effects on the distribution of tropospheric ozone because of the enhanced temperature and water vapour concentration. The two major climate-chemistry feedback mechanisms are the change of chemical reaction rates with the average increase in tropospheric temperature, and the enhanced photochemical destruction of tropospheric ozone with the increase in water vapour [Johnson *et al.*, 1999; Stevenson *et al.*, 2000; Houghton *et al.*, 2001]. In these studies the role of changes in the circulation and convection seems to play a lesser role. Our results show that the description of convection itself has strong impact on the distribution and its precursors. Hence also changes in convective intensity might have an important effect that needs to be assessed. Finally, the link of lightning with deep convection suggests the possibility that this source of NO_x would vary strongly with climate change [Houghton *et al.*, 2001].

Bibliography

- Allen, D., K. Pickering, G. Stenchikov, A. Thompson, and Y. Kondo, A three-dimensional total odd nitrogen (NO_y) simulation during SONEX using a stretched-grid chemical transport model, *J. Geophys. Res. D3*, 105, 3851–3876, 2000.
- Allen, D. J., R. B. Rood, A. M. Thompson, and R. D. Hudson, Three-dimensional radon 222 calculations using assimilated meteorological data and a convective mixing algorithm, *J. Geophys. Res. D3*, 101, 6871–6881, 1996.
- Balkanski, Y. J., and D. J. Jacob, Transport of continental air to the subantarctic Indian Ocean, *Tellus B*, 42, 62–75, 1990.
- Balkanski, Y. J., D. J. Jacob, R. Arimoto, and M. A. Kritz, Long-range transport of radon-222 over the North Pacific Ocean : Implications for continental influence, *J. Atmos. Chem.*, 14, 353–374, 1992.
- Beljaars, A. C. M., and P. Viterbo, Role of the boundary layer in a numerical weather prediction model, in *Clear and cloudy boundary layers*, edited by A. A. M. Holtslag and P. G. Duynkerke, pp. 287–304, NH-publishers, 1999.
- Benkovitz, C. M., M. T. Scholtz, J. Pacyna, L. Tarrason, J. Dignon, E. C. Voldener, P. A. Spiro, J. A. Logan, and T. E. Graedel, Global gridded inventories of anthropogenic emissions of sulfur and nitrogen, *J. Geophys. Res.*, 101, 29,239–29,253, 1996.
- Boersma, K. F., H. J. Eskes, E. W. Meijer, and H. M. Kelder, Estimates of NO_2 production by lightning from GOME satellite observations, 2005, in preparation.
- Bosveld, F., A. van Ulden, and A. C. M. Beljaars, A comparison of ECMWF Re-Analysis data with fluxes and profiles observed in Cabauw, *ECMWF Re-Analysis Project Report Series 8*, ECMWF, Reading RG2 9AX, UK., 1999.
- Bregman, B., A. Segers, M. Krol, E. Meijer, and P. van Velthoven, On the use of mass-conserving wind fields in chemistry transport models, *Atmos. Chem. Phys.*, 3, 447–457, 2003, sRef-ID: 1680-7324/acp/2003-3-447.
- Broecker, W. S., Y. H. Li, and J. Cromwell, Radium-226 and radon-222 concentration in Atlantic and Pacific Oceans, *Science*, 158, 1307–1310, 1967.
- Brost, R. A., and R. B. Chatfield, Transport of radon in a three-dimensional, sub-hemispheric model, *J. Geophys. Res.*, 94, 5095–5119, 1989.

- Chapman, S., A theory of upper-atmospheric ozone, *Memoirs Roy. Meteorol. Soc.*, *103*, 1930.
- Conen, F., and L. B. Robertson, Latitudinal distribution of radon-222 flux from continents, *Tellus B*, *54*, 127–133, 2002.
- Dentener, F., J. Feichter, and A. Jeuken, Simulation of the transport of ^{222}Rn using on-line and off-line global models at different horizontal resolutions : a detailed comparison with measurements, *Tellus B*, *51*, 573–602, 1999.
- Dentener, F., W. Peters, M. Krol, M. van Weele, P. Bergamaschi, and J. Lelieveld, Interannual variability and trend of CH_4 lifetime as measure for OH changes in the 1979-1993 time period, *J. Geophys. Res.*, *108*, 4442, 2003a, doi:10.1029/2002JD002916.
- Dentener, F., M. van Weele, M. Krol, S. Houweling, and P. van Velthoven, Trends and inter-annual variability of methane emissions derived from 1979-1993 global CTM simulations, *Atmos. Chem. Phys.*, *3*, 73–88, 2003b, sRef-ID: 1680-7324/acp/2003-3-73.
- Dentener, F. J., and P. J. Crutzen, Reaction of N_2O_5 on tropospheric aerosols : impact on the global distributions of NO_x , O_3 , and OH, *J. Geophys. Res.*, *93*, 7149–7163, 1993.
- Eloranta, E. W., Boundary Layer Heights: LIDAR (FIFE). Data set., Available on-line [<http://www.daac.ornl.gov>] from Oak Ridge National Laboratory Distributed Active Archive Center, Oak Ridge, Tennessee, U.S.A., 1994, also published in D. E. Streb, D. R. Landis, K. F. Huemrich, and B. W. Meeson (eds.), Collected Data of the First ISLSCP Field Experiment, Vol. 1 : Surface Observations and Non-Image Data Sets. CD-ROM. National Aeronautics and Space Administration, Goddard Space Flight Center, Greenbelt, Maryland, U.S.A.
- Feichter, J., and P. J. Crutzen, Parameterization of vertical transport due to deep cumulus convection in a global transport model and its evaluation with ^{222}Rn measurements, *Tellus B*, *42*, 100–117, 1990.
- Fishman, J., and P. J. Crutzen, The origin of ozone in the troposphere, *Nature*, *274*, 855–857, 1978.
- Fortuin, J. P., and H. Kelder, An ozone climatology based on ozonesonde and satellite measurements, *J. Geophys. Res.*, *103*, 31,709–31,734, 1998.
- Ganzeveld, L., J. Lelieveld, and G.-J. Roelofs, A dry deposition parameterization for sulfur oxides in a chemistry and general circulation model, *J. Geophys. Res.*, *103*, 5679–5694, 1998.
- Gibson, J. K., P. Källberg, S. Uppala, A. Hernandez, A. Nomura, and E. Serrano, ERA-15 description, *ECMWF Re-Analysis Project Report Series 1*, ECMWF, Reading RG2 9AX, UK., 1997.

- Gold, S., H. W. Barkhau, B. Shleien, and B. Kahn, Measurements of naturally occurring radionucleides in air, in *The Natural Radiation Environment*, edited by J. A. S. Adams and W. M. Lowder, pp. 369–382, University of Chicago Press, Chicago, Ill., 1964.
- Goldenbaum, G. C., and R. R. Dickerson, Nitric oxide production by lightning discharges, *J. Geophys. Res.*, *98*, 18,333–18,338, 1993.
- Gregory, D., J.-J. Morcrette, C. Jakob, A. C. M. Beljaars, and T. Stockdale, Revision of convection, radiation and cloud schemes in the ECMWF Integrated Forecasting System, *Q. J. R. Meteor. Soc.*, *126*, 1685–1710, 2000.
- Grewe, V., D. Brunner, M. Dameris, J. L. Grenfell, R. Hein, D. Shindell, and J. Staelin, Origin and variability of upper tropospheric nitrogen oxides and ozone at northern mid-latitudes, *Atm. Environment*, *35*, 3421–3433, 2001.
- Guenther, A., A global model of natural volatile organic compound emissions, *J. Geophys. Res.*, *100*, 8873–8892, 1995.
- Hagemann, S., K. Arpe, L. Bengtsson, and I. Kirchner, Validation of precipitation from ERA-40 and an ECHAM 4.5 simulation nudged with ERA-40 data, *ERA-40 Project Report Series 3*, ECMWF, 2001.
- Heimann, M., The global atmospheric tracer model TM2, *Tech. Rep. 10*, Deutsches Klimarechenzentrum, Hamburg, Germany, 1995.
- Hoell, J. M., D. D. Davis, D. J. Jacob, M. O. Rodgers, R. E. Newell, H. E. Fuelberg, R. J. McNeal, J. L. Raper, and R. J. Bendura, Pacific Exploratory Mission in the tropical Pacific : PEM-Tropics A, August-September 1996, *J. Geophys. Res.*, *104*, 5567–5583, 1999.
- Höller, H., and U. Schumann, EULINOX - the European lightning nitrogen oxides project, *Dlr forschungsbericht 2000-28*, Deutsches Zentrum für Luft- und Raumfahrt (DLR), 2000.
- Holtlag, A. A. M., and B. A. Boville, Local versus nonlocal boundary-layer diffusion in a global climate model, *J. Climate*, *6*, 1825–1842, 1993.
- Holtlag, A. A. M., E. van Meijgaard, and W. C. de Rooy, A comparison of boundary layer diffusion schemes in unstable conditions over land, *Bound.-Layer Meteor.*, *76*, 69–95, 1995.
- Houghton, J. T., Y. Ding, D. J. Griggs, M. Noguer, P. J. van der Linden, X. Dai, K. Maskell, and C. A. Johnson (Eds.), *Climate change 2001 : the scientific basis. Contribution of working group I to the third assessment report of the intergovernmental panel on climate change*, Cambridge University Press, New York, 2001, 881 pp.
- Houweling, A., F. Dentener, and J. Lelieveld, The impact of nonmethane hydrocarbon compounds on tropospheric photochemistry, *J. Geophys. Res.* *D9*, *103*, 10,673–10,696, 1998.

- Huntrieser, H., H. Schlager, C. Feigl, and H. Höller, Transport and production of NO_x in electrified thunderstorms : survey of previous studies and new observations at midlatitudes, *J. Geophys. Res.*, *103*, 28,247–28,264, 1998.
- Jacob, D. J., and M. J. Prather, Radon-222 as a test of boundary layer convection in a general circulation model, *Tellus B*, *42*, 117–134, 1990.
- Jacob, D. J., et al., Evaluation and intercomparison of global transport models using ²²²Rn and other short-lived tracers, *J. Geophys. Res. D5*, *102*, 5953–5970, 1997.
- Jakob, C., and A. P. Siebesma, A new subcloud model for mass-flux convection schemes : influence on triggering, updraft properties, and model climate, *Mon. Weather Rev.*, *131*, 2765–2778, 2003.
- Jeuken, A., Evaluation of chemistry and climate models using measurements and data assimilation, Ph.D. thesis, University of Technology Eindhoven, Eindhoven, The Netherlands, 2000, available at <http://alexandria.tue.nl/extra2/200001283.pdf>.
- Jeuken, A., J. P. Veeffkind, F. Dentener, S. Metzger, and C. R. Gonzales, Simulation of the aerosol optical depth over Europe for August 1997 and a comparison with observations, *J. Geophys. Res. D22*, *106*, 28,295–28,311, 2001.
- Johnson, C. E., W. J. Collins, D. S. Stevenson, and R. G. Derwent, Relative role of climate and emission changes on future tropospheric oxidant concentrations, *J. Geophys. Res.*, *104*, 18,631–18,645, 1999.
- Junge, C. E., and P. E. Gustafson, On the distribution of sea salt over the United States and its removal by precipitation, *Tellus*, *9*, 164–173, 1957.
- Kley, D., P. J. Crutzen, H. G. Smit, H. Vömel, S. J. Oltmans, H. Grassl, and V. Ramanathan, Observations of near-zero ozone concentrations over the convective Pacific : effects on air chemistry, *Science*, *274*, 230–233, 1996.
- Kritz, M. A., J.-C. L. Roulley, and E. F. Danielsen, The China Clipper—fast advective transport of radon-rich air from the Asian boundary layer to the upper troposphere near California, *Tellus B*, *42*, 46–61, 1990.
- Kritz, M. A., S. W. Rosner, K. K. Kelly, M. Loewenstein, and K. Chan, Radon measurements in the lower tropical stratosphere : evidence for rapid vertical transport and dehydration of tropospheric air, *J. Geophys. Res. D5*, *98*, 8725–8736, 1993.
- Kritz, M. A., S. W. Rosner, and D. Z. Stockwell, Validation of an off-line three-dimensional chemical transport model using observed radon profiles 1. Observations, *J. Geophys. Res. D7*, *103*, 8425–8432, 1998.
- Lacis, A. W., D. J. Wuebbles, and J. A. Logan, Radiative forcing of climate by changes in the vertical distribution of ozone, *J. Geophys. Res.*, *95*, 9971–9981, 1990.
- Lambert, G., G. Polian, J. Sanak, B. Ardouin, A. Buisson, A. Jegou, and J. C. L. Roulley, Cycle du radon et de ses descendants : application à l'étude des échanges troposphère-stratosphère, *Ann. Géophys.* *4*, *38*, 497–531, 1982.

- Langner, J., and H. Rodhe, A global three-dimensional model of the tropospheric sulfur cycle, *J. Atmos. Chem.*, *12*, 229–267, 1991.
- Lee, H. N., and R. J. Larsen, Vertical diffusion in the lower atmosphere using aircraft measurements of ^{222}Rn , *J. Appl. Meteorol.*, *36*, 1262–1270, 1997.
- Lelieveld, J., and F. Dentener, What controls tropospheric ozone?, *J. Geophys. Res.* *D3*, *105*, 3531–3551, 2000.
- Lin, X., M. Trainer, and S. C. Liu, On the nonlinearity of tropospheric ozone production, *J. Geophys. Res.*, *93*, 15,879–15,888, 1988.
- Lin, X., F. Zaucker, E.-Y. Hsie, M. Trainer, and S. A. McKeen, Radon 222 simulations as a test of a three-dimensional regional transport model, *J. Geophys. Res.* *D22*, *101*, 29,165–29,177, 1996.
- Liu, S. C., J. R. McAfee, and R. J. Cicerone, Radon 222 and tropospheric vertical transport, *J. Geophys. Res.* *D5*, *89*, 7291–7297, 1984.
- Liu, S. C., M. Trainer, F. C. Fehsenfeld, D. D. Parrish, E. J. Williams, D. W. Fahey, G. Hübler, and P. C. Murphy, Ozone production in the rural troposphere and the implications for regional and global ozone distributions, *J. Geophys. Res.*, *92*, 4191–4207, 1987.
- Louis, J.-F., A parametric model of vertical eddy fluxes in the atmosphere, *Bound.-Layer Meteor.*, *17*, 187–202, 1979.
- Louis, J. F., M. Tiedtke, and J. F. Geleyn, A short history of the operational PBL-parameterization at ECMWF, in *Proceedings of ECMWF workshop on boundary layer parameterization, November 1981*, pp. 59–79, ECMWF, Reading, England, 1982.
- Mahowald, N. M., P. R. Rasch, and R. G. Prinn, Cumulus parameterizations in chemical transport models, *J. Geophys. Res.*, *100*, 26,173–26,189, 1995.
- Mahowald, N. M., P. J. Rasch, B. E. Eaton, S. Whittlestone, and R. Prinn, Transport of $^{222}\text{radon}$ to the remote troposphere using the Model of Atmospheric Transport and Chemistry and assimilated winds from ECMWF and the National Center for Environmental Prediction/NCAR, *J. Geophys. Res.* *D23*, *102*, 28,139–28,151, 1997.
- Meijer, E. W., P. F. J. van Velthoven, A. M. Thompson, L. Pfister, H. Schlager, P. Schulte, and H. Kelder, Model calculations of the impact of NO_x from air traffic, lightning, and surface emissions, compared with measurements, *J. Geophys. Res.* *D3*, *105*, 3833–3850, 2000.
- Meijer, E. W., P. F. J. van Velthoven, D. W. Brunner, H. Huntrieser, and H. Kelder, Improvement and evaluation of the parameterisation of nitrogen oxide production by lightning, *Phys. Chem. Earth. (C)*, *26*, 577–583, 2001.
- Nordeng, T. E., Extended versions of the convective parametrization scheme at ECMWF and their impact on the mean and transient activity of the model in the tropics, *Research Department Technical Memorandum 206*, ECMWF, Reading RG2 9AX, UK., 1994.

- Olivié, D. J. L., P. F. J. van Velthoven, and A. C. M. Beljaars, Evaluation of archived and off-line diagnosed vertical diffusion coefficients from ERA-40 with ^{222}Rn simulations, *Atmos. Chem. Phys.*, *4*, 2313–2336, 2004a, sRef-ID: 1680-7324/acp/2004-4-2313.
- Olivié, D. J. L., P. F. J. van Velthoven, A. C. M. Beljaars, and H. M. Kelder, Comparison between archived and off-line diagnosed convective mass fluxes in the chemistry transport model TM3, *J. Geophys. Res. D11*, *109*, D11,303, 2004b, doi:10.1029/2003JD004036.
- Olivier, J., J. Peters, C. Granier, G. Pétron, J. F. Müller, and S. Wallens, Present and future surface emissions of atmospheric compounds, *POET Report 2*, 2003, EU project EVK2-1999-00011.
- Olivier, J. G. L., Description of EDGAR version 2.0 : A set of global emission inventories of greenhouse gases and ozone depleting substances for all anthropogenic and most natural sources on a per country basis on $1^\circ \times 1^\circ$ grid, *Tech. rep.*, Natl. Inst. for Public Health and the Environ., 1996, RIVM rep. 771060 002/TNO MEP rep. R96/119.
- Peters, W., et al., Toward regional-scale modeling using the two-way nested global model TM5 : Characterization of transport using SF_6 , *J. Geophys. Res.*, *109*, D19,314, 2004, doi:10.1029/2004JD005020.
- Pickering, K. E., Y. Wang, W.-K. Tao, C. Price, and J.-F. Muller, Vertical distribution of lightning NO_x for use in regional and global chemical transport models, *J. Geophys. Res. D23*, *109*, 31,203–31,216, 1998.
- Polian, G., G. Lambert, B. Ardouin, and A. Jegou, Long-range transport of radon in subantarctic and antarctic areas, *Tellus B*, *38*, 178–189, 1986.
- Price, C., and D. Rind, A simple lightning parameterization for calculating global lightning distributions, *J. Geophys. Res. D9*, *97*, 9919–9933, 1992.
- Price, C., and D. Rind, What determines the cloud-to-ground lightning fraction in thunderstorms?, *Geophys. Res. Lett.*, *20*, 463–466, 1993.
- Price, C., and D. Rind, Modeling global lightning distributions in a general circulation model, *Mon. Weather Rev.*, *97*, 9919–9933, 1994.
- Price, C., J. Penner, and M. Prather, NO_x from lightning 1. Global distribution based on lightning physics, *J. Geophys. Res. D5*, *97*, 5929–5941, 1997.
- Ramanathan, V., and R. E. Dickinson, The role of stratospheric ozone in the zonal and seasonal radiative energy balance of the Earth-troposphere system, *J. Atmos. Sci.*, *36*, 1084–1104, 1979.
- Ramonet, M., J. C. L. Roulley, P. Bousquet, and P. Monfray, Radon-222 measurements during the Tropoz II campaign and comparison with a global atmospheric transport model, *J. Atmos. Chem.*, *23*, 107–136, 1996.

- Rasch, P. J., N. M. Mahowald, and B. E. Eaton, Representations of transport, convection, and the hydrological cycle in chemical transport models : Implications for the modeling of short-lived and soluble species, *J. Geophys. Res. D23*, 102, 28,127–28,138, 1997.
- Ridley, B., et al., Convective transport of reactive constituents to the tropical and mid-latitude topopause region : I. Observations, *Atm. Environment*, 38, 1259–1274, 2004.
- Ridley, B. A., J. E. Dye, J. G. Walega, J. Zheng, F. E. Grahek, and W. Rison, On the production of active nitrogen by thunderstorms over New Mexico, *J. Geophys. Res. D15*, 101, 20,985–21,005, 1996.
- Russell, G. L., and J. A. Lerner, A new finite-differencing scheme for the tracer transport equation, *J. Appl. Meteorol.*, 20, 1483–1498, 1981.
- Russell, P. B., L. Pfister, and H. B. Selkirk, The tropical experiment of the Stratosphere-Troposphere Exchange Project (STEP) : science objectives, operations, and summary findings, *J. Geophys. Res. D5*, 98, 8563–8589, 1993.
- Schery, S. D., S. Whittlestone, K. P. Hart, and S. E. Hill, The flux of radon and thoron from Australian soils, *J. Geophys. Res. D6*, 94, 8567–8576, 1989.
- Sellers, P. J., F. G. Hall, G. Asrar, D. E. Strebel, and R. E. Murphy, The First ISLSCP Field Experiment (FIFE), *Bull. Am. Meteor. Soc.*, 69, 22–27, 1988.
- Simmons, A. J., and D. M. Burridge, An energy and angular-momentum conserving vertical finite-difference scheme and hybrid vertical coordinates, *Mon. Weather Rev.*, 109, 758–766, 1981.
- Simmons, A. J., and J. K. Gibson, The ERA-40 project plan, *ERA-40 Project Report Series 1*, ECMWF, Reading RG2 9AX, UK., 2000.
- Stevenson, D. S., C. E. Johnson, W. J. Collins, R. G. Derwent, and J. M. Edwards, Future estimates of tropospheric ozone radiative forcing and methane turnover - the impact climate change, *Geophys. Res. Lett.*, 27, 2073–2076, 2000.
- Stockwell, D. Z., and M. P. Chipperfield, A tropospheric chemical-transport model : development and validation of the model transport schemes, *Q. J. R. Meteorol. Soc.*, 125, 1747–1783, 1999.
- Stockwell, D. Z., M. A. Kritz, M. P. Chipperfield, and J. A. Pyle, Validation of an off-line three-dimensional chemical transport model using observed radon profiles 2. Model results, *J. Geophys. Res. D7*, 103, 8433–8445, 1998.
- Thompson, A. M., H. B. Singh, and H. Schlager, Introduction to special section : Subsonic Assessment Ozone and Nitrogen Oxide Experiment (SONEX) and Pollution From Aircraft Emissions in the North Atlantic Flight Corridor (POLINAT 2), *J. Geophys. Res. D3*, 105, 3595–3603, 2000.
- Tiedtke, M., A comprehensive mass flux scheme for cumulus parameterization in large-scale models, *Mon. Weather Rev.*, 117, 1779–1800, 1989.

- Tiedtke, M., Representation of clouds in large-scale models, *Mon. Weather Rev.*, *121*, 3040–3061, 1993.
- Troen, I., and L. Mahrt, A simple model of the atmospheric boundary layer; sensitivity to surface evaporation, *Bound.-Layer Meteor.*, *37*, 129–148, 1986.
- Turekian, K. K., Y. Nozaki, and L. K. Benninger, Geochemistry of atmospheric radon and radon products, *Ann. Rev. Earth Planet. Sci.*, *5*, 227–255, 1977.
- van Leer, B., Towards the ultimate conservative difference scheme. IV. A new approach to numerical convection, *J. Computational Phys.*, *23*, 276–299, 1977.
- van Noije, T. P. C., H. J. Eskes, M. van Weele, and P. F. J. van Velthoven, Implications of the enhanced Brewer-Dobson circulation in European Centre for Medium-Range Weather Forecasts reanalysis ERA-40 for the stratosphere-troposphere exchange of ozone in global chemistry transport models, *J. Geophys. Res.*, *109*, D19,308, 2004, doi:10.1029/2004JD004586.
- van Velthoven, P. F. J., and H. Kelder, Estimates of stratosphere-troposphere exchange : Sensitivity to model formulation and horizontal resolution, *J. Geophys. Res. D1*, *101*, 1429–1434, 1996.
- Viterbo, P., A. Beljaars, J.-F. Mahfouf, and J. Teixeira, The representation of soil moisture freezing and its impact on the stable boundary layer, *Q. J. R. Meteor. Soc.*, *125*, 2401–2426, 1999.
- Vogelezang, D. H. P., and A. A. M. Holtslag, Evaluation and model impacts of alternative boundary-layer height formulations, *Bound.-Layer Meteor.*, *81*, 245–269, 1996.
- Wang, K.-Y., J. A. Pyle, M. G. Sanderson, and C. Bridgeman, Implementation of a convective atmospheric boundary layer scheme in a tropospheric chemistry transport model, *J. Geophys. Res. D19*, *104*, 23,729–23,745, 1999.
- Wesely, M. L., Boundary Layer Heights: SODAR (FIFE). Data set., Available online [<http://www.daac.ornl.gov>] from Oak Ridge National Laboratory Distributed Active Archive Center, Oak Ridge, Tennessee, U.S.A., 1994, also published in D. E. Strebler, D. R. Landis, K. F. Huemrich, and B. W. Meeson (eds.), Collected Data of the First ISLSCP Field Experiment, Vol. 1: Surface Observations and Non-Image Data Sets. CD-ROM. National Aeronautics and Space Administration, Goddard Space Flight Center, Greenbelt, Maryland, U.S.A.
- Wilkening, M. H., Daily and annual courses of natural atmospheric radioactivity, *J. Geophys. Res.*, *64*, 521–526, 1959.
- Wilkening, M. H., and W. E. Clements, Radon 222 from the ocean surface, *J. Geophys. Res.*, *80*, 3828–3830, 1975.
- Williams, E. R., Large-scale charge separation in thunderclouds, *J. Geophys. Res.*, *90*, 6013–6025, 1985.

- Williamson, D. L., J. T. Kiehl, V. Ramanathan, R. E. Dickinson, and J. J. Hack, Description of NCAR Community Climate Model (CCM1), *NCAR Technical Note 285*, NCAR, 1987.
- Yienger, J. J., and H. Levy, Empirical model of global soil-biogenic NO_x emissions, *J. Geophys. Res.*, *100*, 11,447–11,464, 1995.
- Zaucker, F., P. H. Daum, U. Wetterauer, C. Berkowitz, B. Kromer, and W. S. Broecker, Atmospheric ²²²Rn measurements during the 1993 NARE Intensive, *J. Geophys. Res. D22*, *101*, 29,149–29,164, 1996.
- Zhang, X., J. H. Helsdon, and R. D. Farley, Numerical modeling of lightning-produced NO_x using an explicit lightning scheme : 1. Two dimensional simulation as a "proof of concept", *J. Geophys. Res.*, *108*, 4579, 2003, doi:10.1029/2003JD003224.

Dankwoord

Toen ik eind 2000 de mogelijkheid kreeg om te gaan werken bij het KNMI, heb ik niet lang getwijfeld. Een onderzoeksdomein dat me aansprak, vlot bereikbaar met de trein vanuit België en dezelfde taal (dat dacht ik althans). Mijn meteorologische kennis en kunde reikten toen niet veel verder dan het observeren van contrailvorming door vliegtuigen boven België en het in elkaar knutselen van wat bovenmaatse meetinstrumenten. Ik heb de sprong gewaagd en het is me goed bevallen.

Gaan werken in het KNMI betekende niet alleen een nieuwe werkomgeving, maar ook een nieuw land. Voor ik naar Nederland verhuisde, kende ik het land een beetje. Nederland was nooit ver : 8 kilometer fietsen vanaf mijn ouders hun huis en je was in Zeeuws-Vlaanderen. Ik hield van de eindeloze dijken, populierenrijen en kreken. Maar het was toch steeds een beetje buitenland. Dat is het nu niet meer, denk ik.

Ik herinner mij hoe slecht ik aanvankelijk mijn nieuwe collega's kon verstaan en hoe verbaasd ik soms was wanneer zij mij niet verstonden. Ik probeerde me een beetje aan te passen maar werd af en toe toch nog hard met mijn neus op de feiten gedrukt. Wanneer ik in de supermarkt in het Nederlands uitleg vroeg, kreeg ik wel eens antwoord in het Engels. Langzaamaan echter leerde ik wat een dubbeltje en een stuiver zijn, dat lopen eerder gaan en hardlopen eerder joggen is, dat Europa hier Brussel wordt genoemd, hoe het leven in een eentalig land is, wat een lage 32-er is, dat alles leuk kan zijn en wanneer nu ook weer de slag bij Nieuwpoort was geweest. Toen ik op een keer weer in Vlaanderen was en als enige door het rode licht fietste, besepte ik dat het assimileren misschien verder was gegaan dan goed voor me was.

De voorbije jaren heb ik de reis tussen België en Utrecht bijna 200 keer met de trein gemaakt. Van de lijn Antwerpen-Roosendaal-Rotterdam-Utrecht ken ik nu bijna elk plekje. Ondanks een staking omwille van het 'rondje rond de kerk', uitval van treinen door blaadjes op het spoor, ontregelde treinen na de storm van 27 oktober 2002, tijdelijk gebrek aan zitplaatsen op de lijn naar Antwerpen door materieelvernieuwing, een blauw oog, en een boete voor het fout parkeren van mijn fiets op het perron, vond ik het reizen met de trein erg leuk. Het was de ideale plaats om de bouw van de nieuwe Moerdijkbrug over het Hollands Diep of het graven van de Noord-Zuid verbinding onder Antwerpen te volgen of om knus naar 'Met het oog op morgen' te luisteren.

Ik vond het KNMI een inspirerende en aangename plaats om te werken. Ik heb er veel geleerd en kreeg er de tijd om me in te werken, om de code van het TM-model te doorgronden, om zomerscholen te volgen en om naar conferenties te gaan. Het onderzoek dat ik er deed, werd mogelijk gemaakt door de Nederlandse Organisatie voor Wetenschappelijk Onderzoek (NWO). Vooral de mensen in het KNMI ben ik

erg dankbaar. Bij het tot stand komen van dit proefschrift heb ik steun van velen gehad. Allereerst wil ik Hennie Kelder, mijn promotor, bedanken. Hij heeft vanaf afstand maar met interesse mijn onderzoek gevolgd. Verder wil ik vooral Peter van Velthoven, mijn copromotor, hartelijk bedanken voor de dagelijkse begeleiding, al de hulp, de ideeën, het creëren van de goede omstandigheden om onderzoek te doen, het signaleren van relevante publicaties, het grondig nalezen en zorgvuldig verbeteren van mijn teksten en zeker ook voor het motiveren. Anton Beljaars van het ECMWF ben ik erkentelijk voor zijn bijdrage tot het archiveren van extra data tijdens het ERA-40 project en voor zijn nuttige opmerkingen over mijn onderzoek. Verder wil ik Michiel bedanken voor zijn bereidheid steeds opnieuw in de TM-code te duiken en voor het leveren van nuttig commentaar op mijn teksten. Ernst ben ik erg dankbaar voor zijn hulp en ideeën bij het onderzoeken van de bliksemparаметrisaties. Ook Bas, met wie ik bijna 3 jaar een kamer heb gedeeld, ben ik dankbaar. Hij hield van discussie, was erg open, vertelde me af en toe wat over het echte leven, en was verdraagzaam jegens mijn onverbeterlijke neiging om mijn bureau en onze kamer er te laten uitzien alsof er net een windhoos door was gewaaid. Ik wil Peter en Michiel ook danken voor hun gastvrijheid de eerste twee maanden dat ik in Nederland verbleef, en voor de hulp bij het vinden van een kamer. Ik wil ook al mijn andere collega's van de afdeling atmosferische samenstelling bedanken. Zij zorgden er mede voor dat ik vrijwel elke morgen fluitend naar het KNMI fietste. Het was ook via mijn collega's dat ik in contact kwam met voetbal en badminton – sporten waar ik wat verborgen talent voor hoopte te ontdekken. Ik ben ze fanatieker en met veel plezier gaan beoefenen, maar ik bleek toch vooral veel inzet en wat minder aanleg te hebben.

Tot slot wil ik mijn ouders bedanken. Ze gaven me uitgebreid de mogelijkheid om te studeren en waren steeds gastvrij wanneer ik de voorbije jaren op de meest onmogelijke uren bij hen aanklopte.

Curriculum vitae

Dirk Olivié werd geboren op 26 december 1972 in Sint-Niklaas. Van 1978 tot 1984 ging hij naar de gemeentelijke basisschool in Vrasene. Van 1984 tot 1990 volgde hij middelbaar onderwijs in het Sint-Jozef-Klein-Seminarie in Sint-Niklaas in de richting latijn-wiskunde. In 1990 ging hij studeren aan de Katholieke Universiteit Leuven en rondde daar in 1995 de studie burgerlijk bouwkundig ingenieur en in 1997 de studie natuurkunde af. Van oktober 1997 tot oktober 2000 werkte hij aan de Katholieke Universiteit Leuven. Hij deed er onderzoek naar ikinvariantie en pointsplitting in de quantumelectrodynamica.

Eind 2000 verhuisde hij naar Nederland. Van december 2000 tot november 2004 was hij verbonden aan de Technische Universiteit Eindhoven. Het onderzoek werd uitgevoerd aan het Koninklijk Nederlands Meteorologisch Instituut.